Medical Image Processing and Analysis

Medical Imaging Modalities

- Three orthogonal directions of the medical imaging of the human body

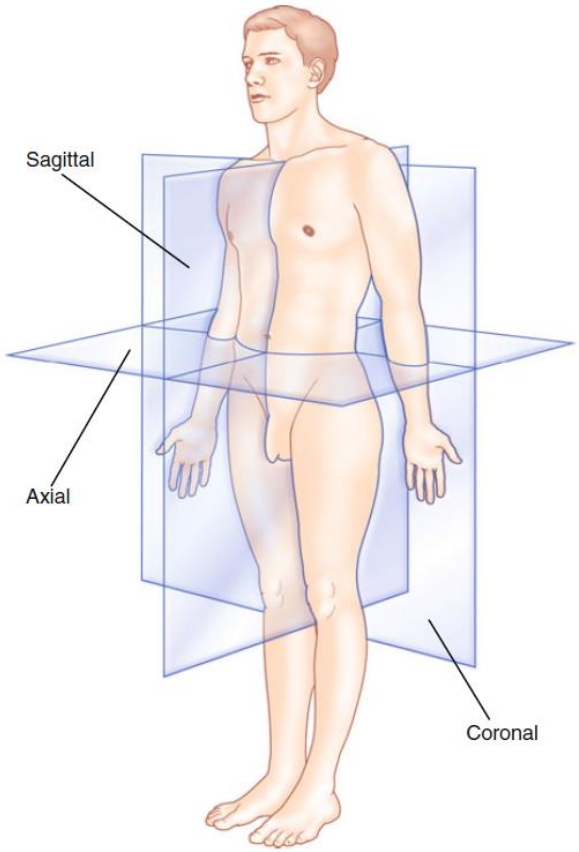

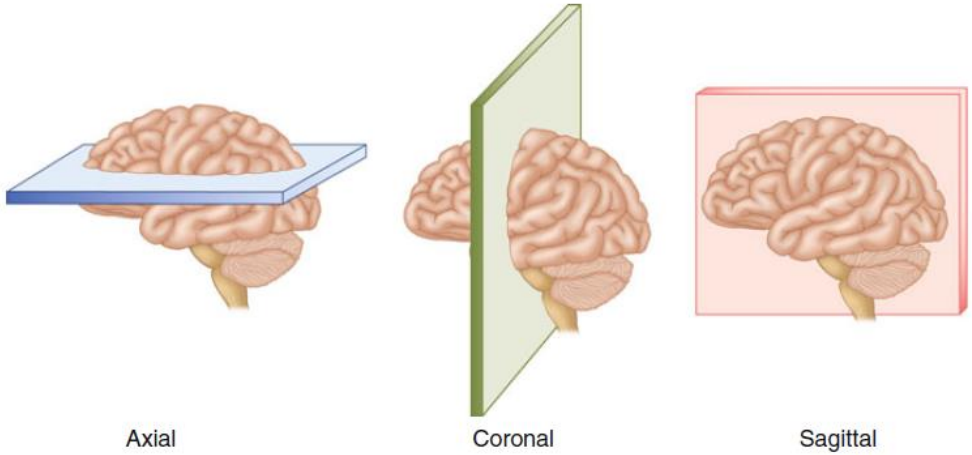

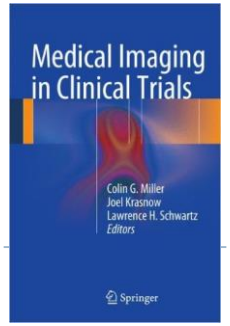

Medical Imaging in Clinical Trials
Chapter 1. Medical Imaging Modalities

Computed Tomography (CT)

Fig. 1.3 Computed tomography (CT) of the chest in axial view (Used with kind permission of Springer Science+Business Media from Levine et al. [17])

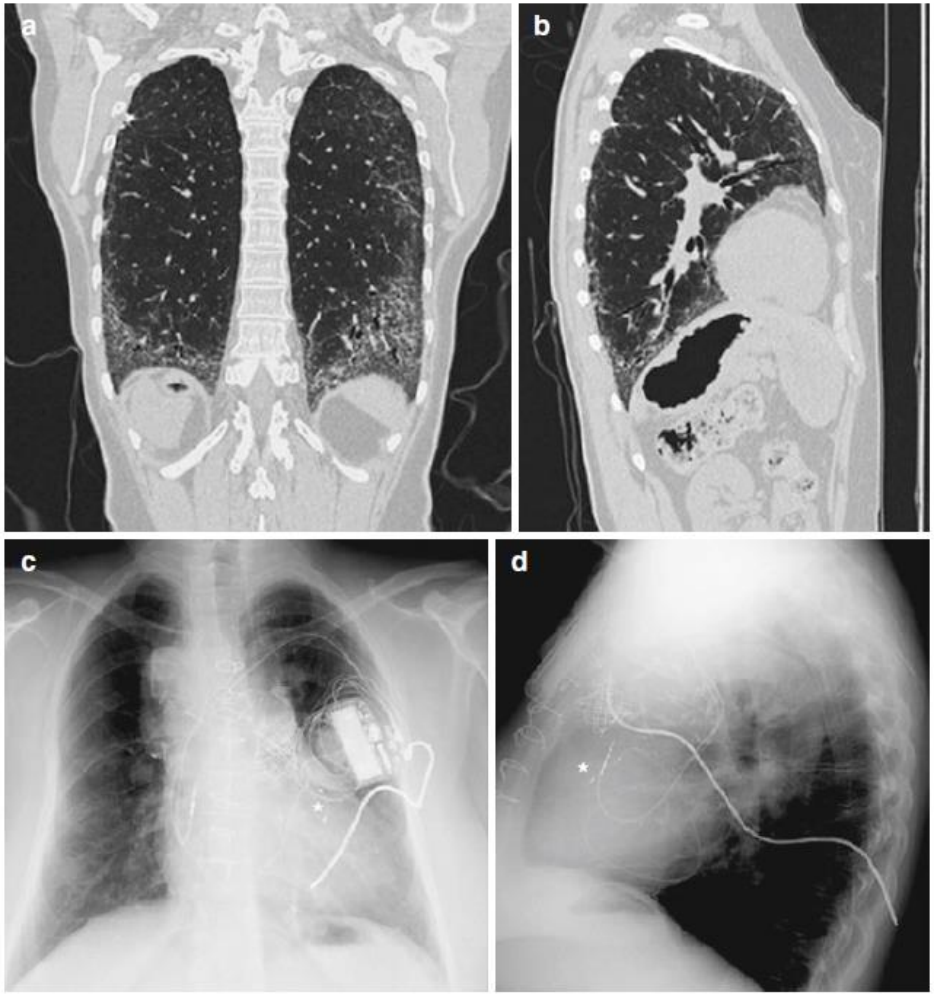

Fig. 1.4 Chest CT in coronal (**a**) and sagittal (**b**) view. Chest radiograph in a posterior-anterior (**c**) and lateral view with heart indicated by * (**d**) (c, d: Used with permission of Springer Science+Business Media from Gupta et al. [18])

Radiography/X-Ray

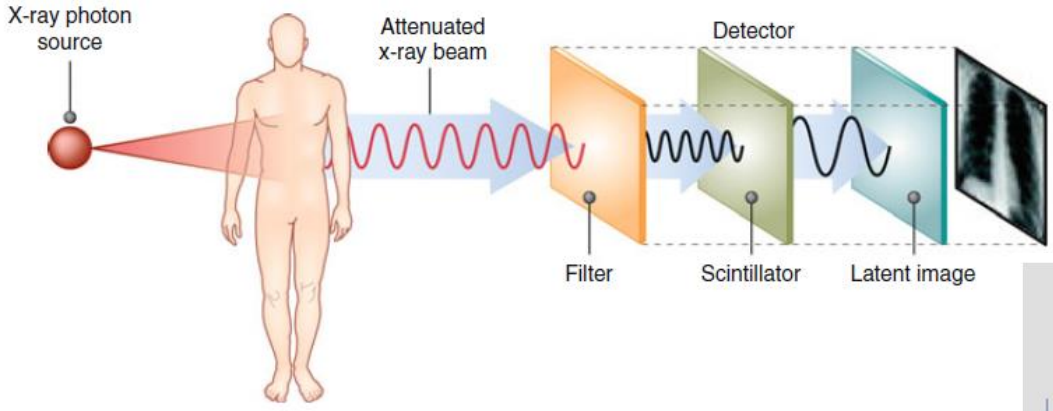

Fig. 1.5 X-ray from source to image (Modified with kind permission of Springer Science + Busin Media from Aberle et al. [19])

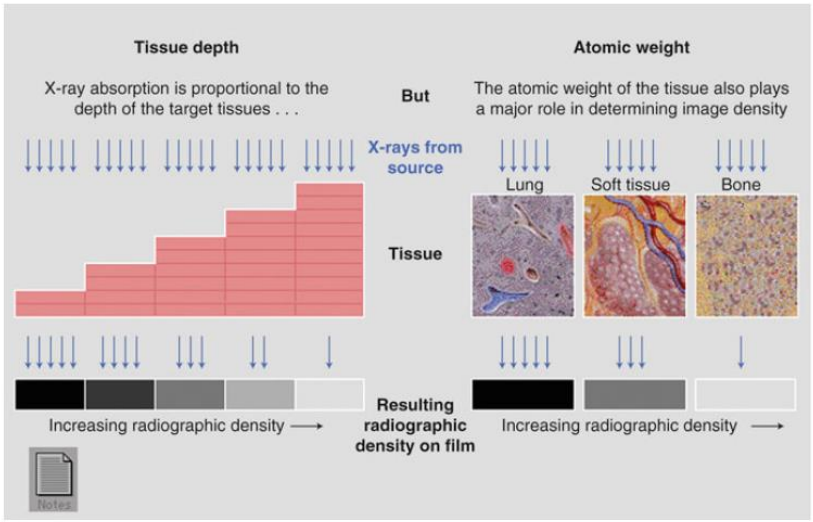

Fig. 1.6 Relationship of radiographic density as a gray scale verses atomic weight (Modified with permission of Patrick Lynch, Yale University, from http://www.yale.edu/imaging/techniques/radiographic_density/index.html)

Table 1.1 Radiography: applications, advantages, and disadvantages

Applications	Fractures, bone diseases, pneumonia, pulmonary edema, intestinal obstructions, renal or gallbladder stones
Advantages	Low cost, widely available, portable, bedside
Disadvantages	Radiation, limited color spectrum, 2D information

Computed Tomography

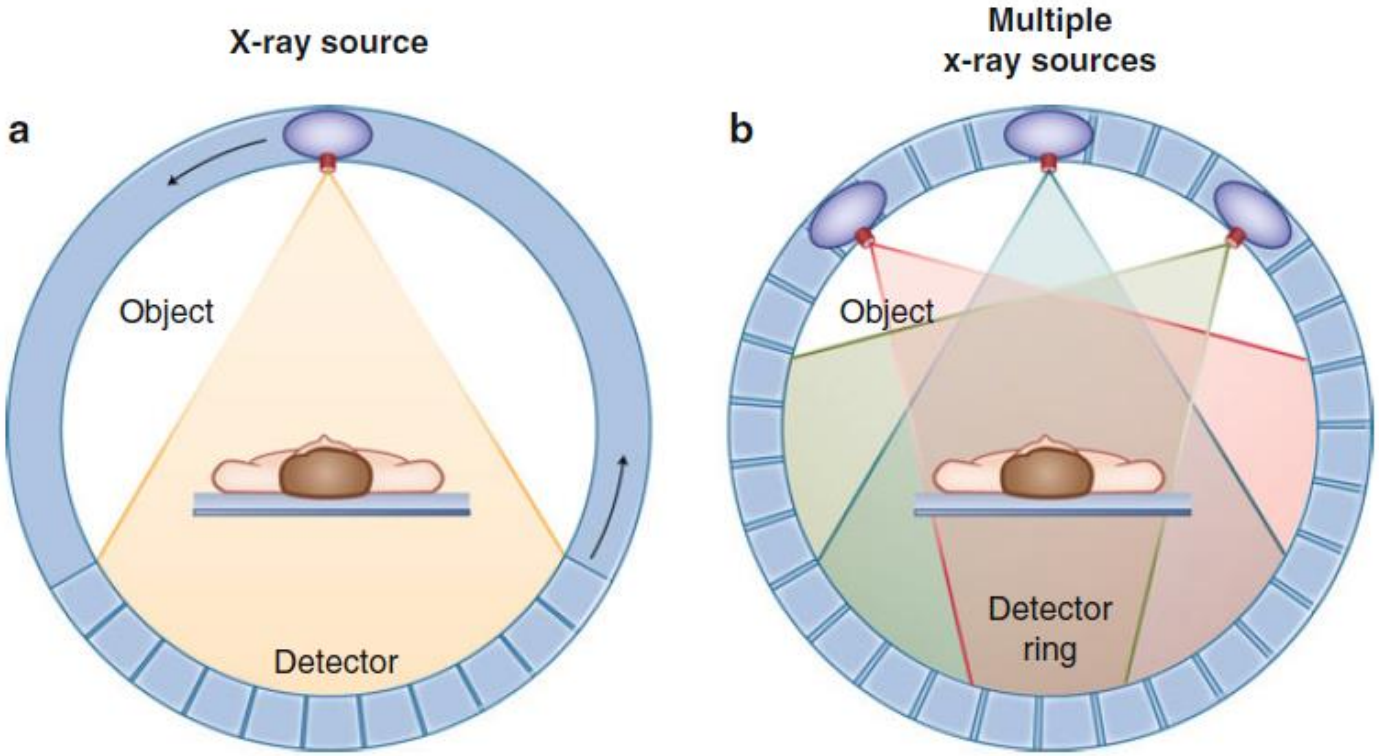

Fig. 1.7 (a, b) Multiple X-ray sources (b) arranged in a configuration to produce a CT scan (Modified with permission from Zhang et al. [20])

Table 1.2 Computed tomography: applications, advantages, and disadvantages

Applications	Lesion assessment, trauma evaluation, evaluation of nearly all organ systems (gastrointestinal, neurologic, bone, vascular etc.)
Advantages	Cross-sectional view, tissue contrast, rapid acquisition
Disadvantages	Radiation, contrast allergy, cost

Magnetic Resonance Imaging

Fig. 1.8 Picture of a MRI scanner (Used with kind permission of Springer Science+Business Media from Semrud-Clikeman et al. [21])

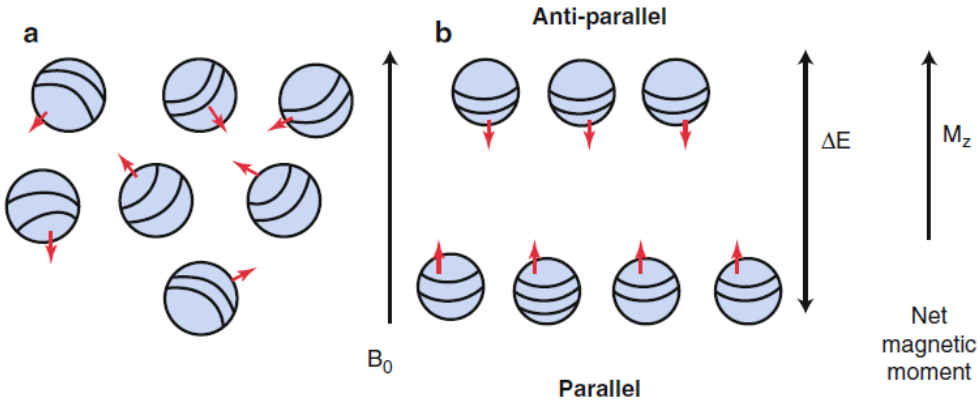

Fig. 1.9 (**a**, **b**) Alignment of protons with the magnetic field (Used with kind permission of Springer Science+Business Media from Saha [22])

Positron Emission Tomography (PET)

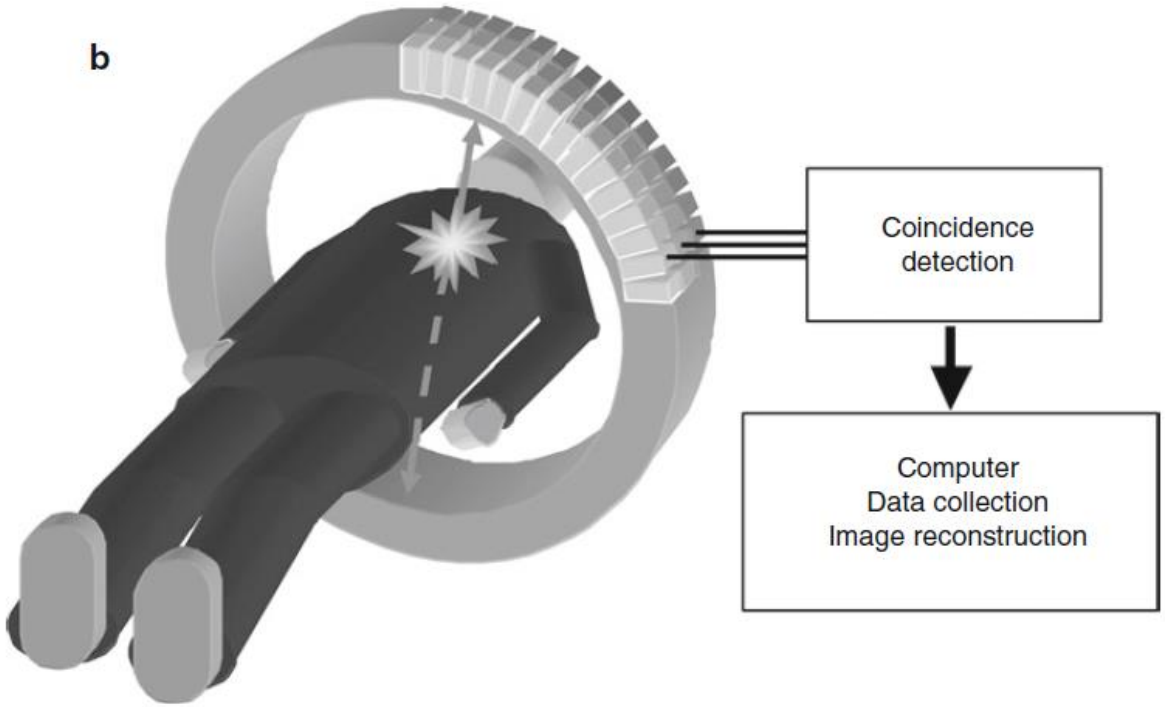

PET/CT scanner

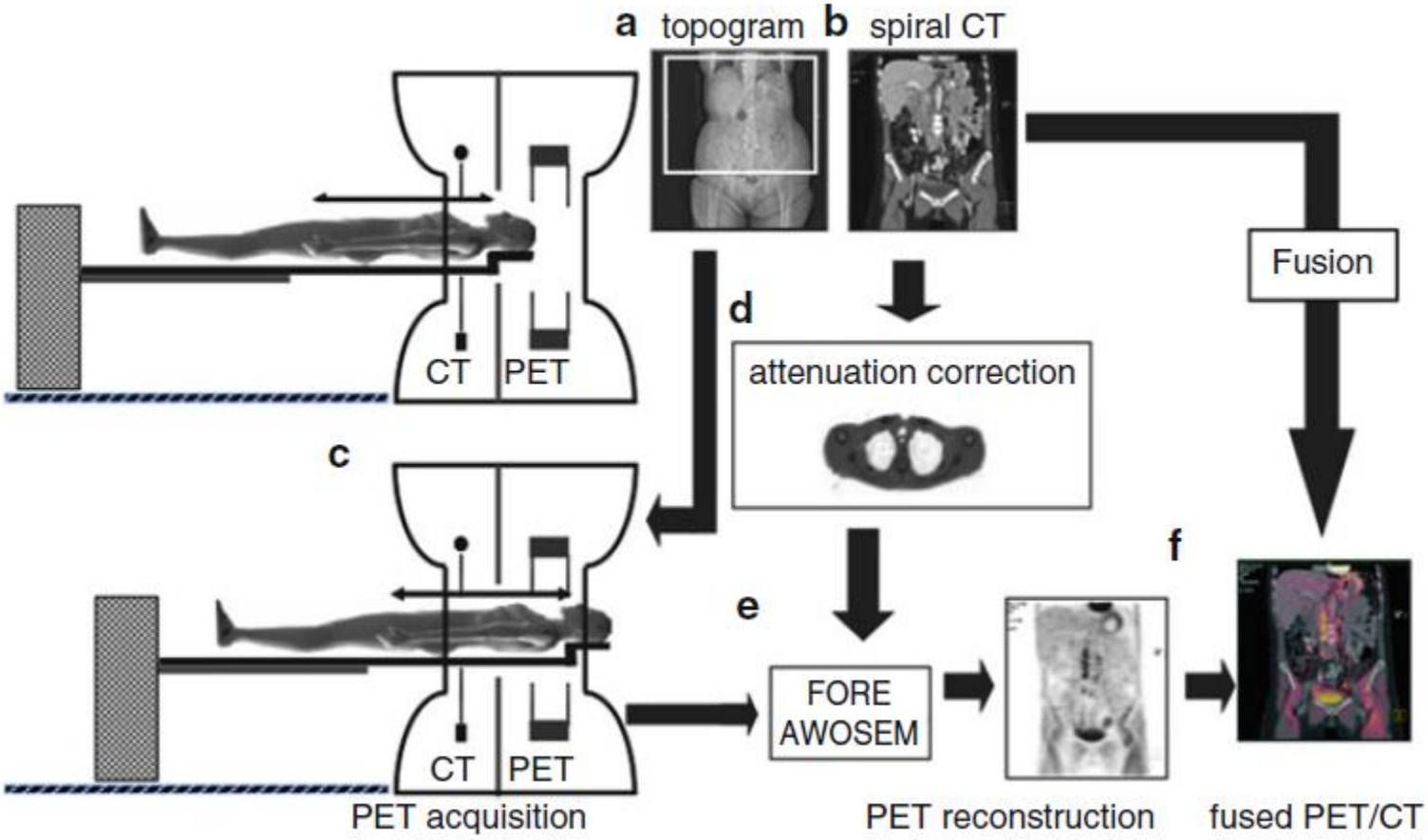

Ultrasound Techniques

- ***Grayscale Ultrasound***
- ***Doppler Ultrasound***

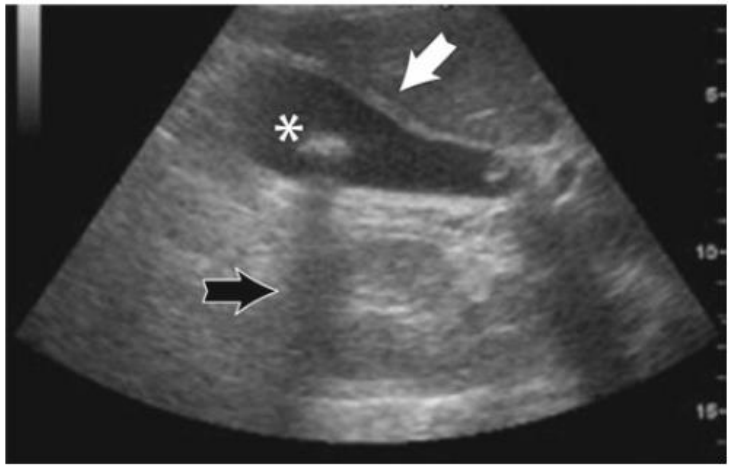

Table 1.4 Applications, advantages, and disadvantages of grayscale and Doppler ultrasound

Applications	Cholecystitis, appendicitis, pancreatitis, ectopic pregnancy, pelvic masses, aortic aneurysms, deep vein thrombosis
Advantages	Avoids use of ionizing radiation and therefore no biological damage, portable, mobile use; can be performed at bedside, less expensive than CT or MRI, can depict bodily organs in motion (i.e., heart), flexible imaging orientation view (transaxial, oblique, sagittal), no contraindications to use, real-time images
Disadvantages	Operator dependent, poor resolution, interpretation requires specialist, requires use of unpleasant gel on patient body

Subsampling

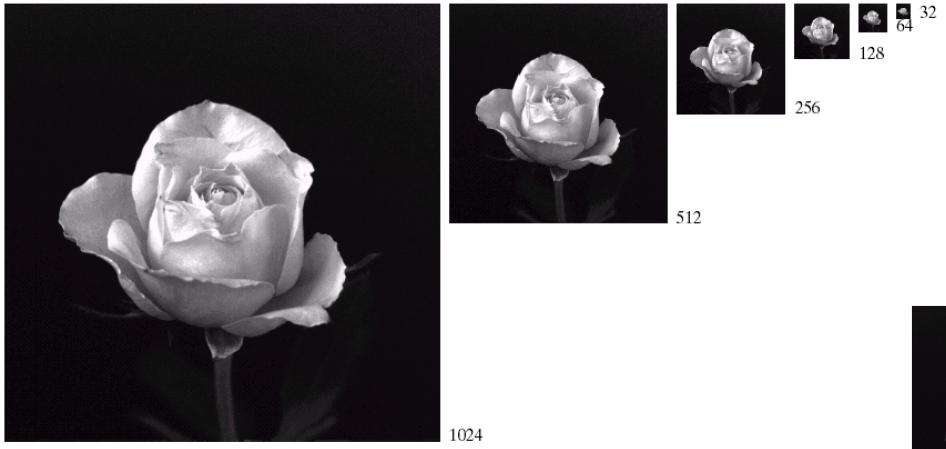

FIGURE 2.19 A 1024 × 1024, 8-bit image subsampled down to size 32 × 32 pixels. The number of allowa gray levels was kept at 256.

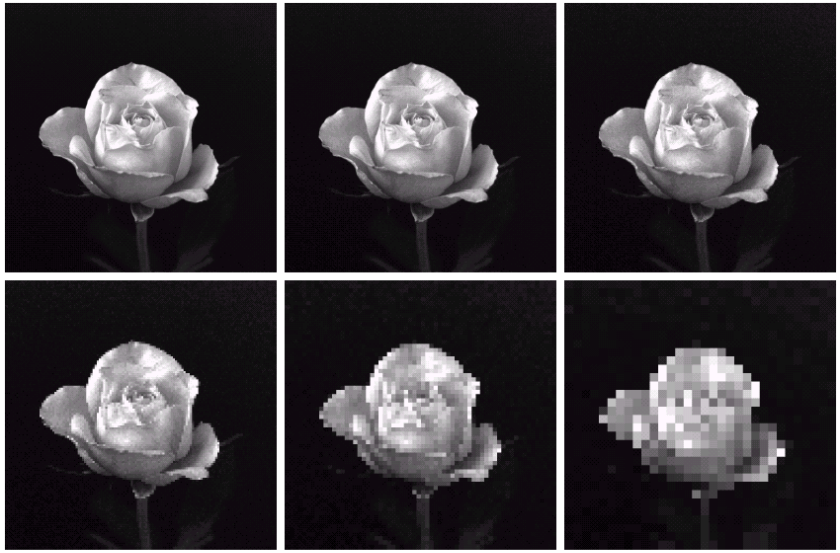

a b c
d e f

FIGURE 2.20 (a) 1024 × 1024, 8-bit image. (b) 512 × 512 image resampled into 1024 × 1024 pixels by row and column duplication. (c) through (f) 256 × 256, 128 × 128, 64 × 64, and 32 × 32 images resampled into 1024 × 1024 pixels.

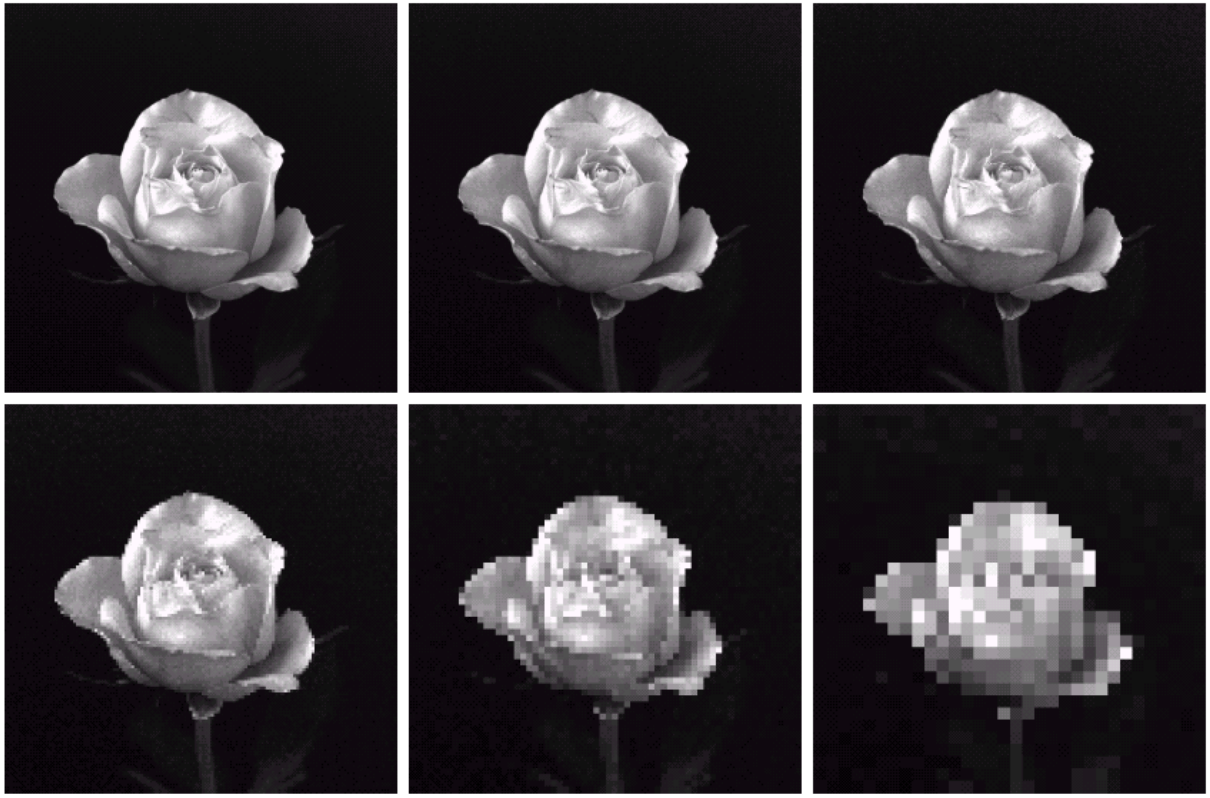

a b c
d e f

FIGURE 2.20 (a) 1024 × 1024, 8-bit image. (b) 512 × 512 image resampled into 1024 × 1024 pixels by row and column duplication. (c) through (f) 256 × 256, 128 × 128, 64 × 64, and 32 × 32 images resampled into 1024 × 1024 pixels.

The number of gray levels

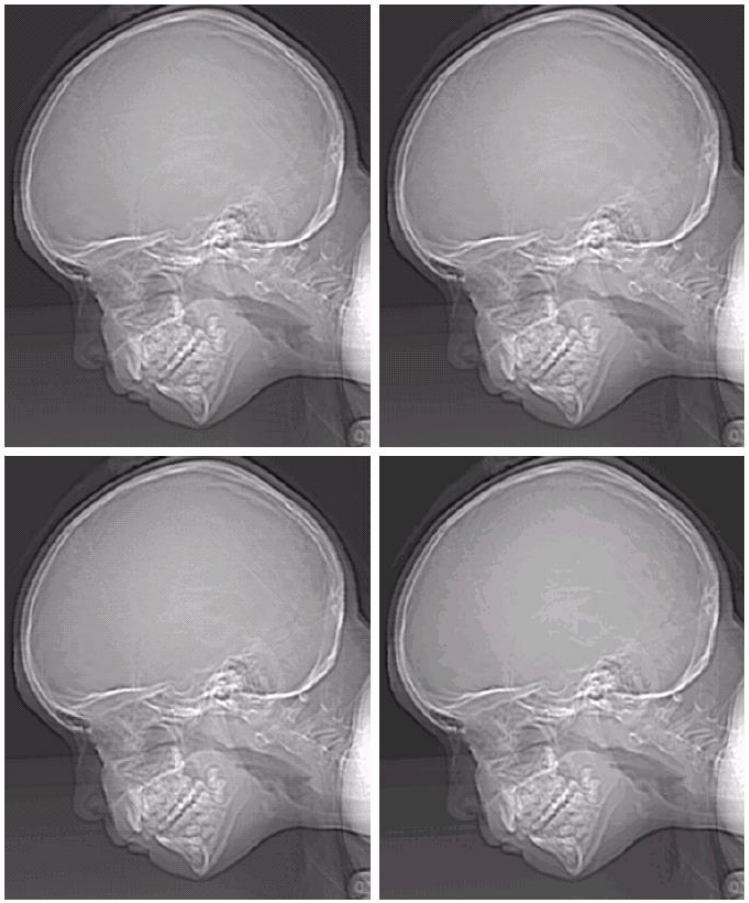

a b
c d

FIGURE 2.21
(a) 452 × 374, 256-level image. (b)–(d) Image displayed in 128, 64, and 32 gray levels, while keeping the spatial resolution constant.

e f
g h

FIGURE 2.21
(Continued)
(e)–(h) Image displayed in 16, 8, 4, and 2 gray levels. (Original courtesy of Dr. David R. Pickens, Department of Radiology & Radiological Sciences, Vanderbilt University Medical Center.)

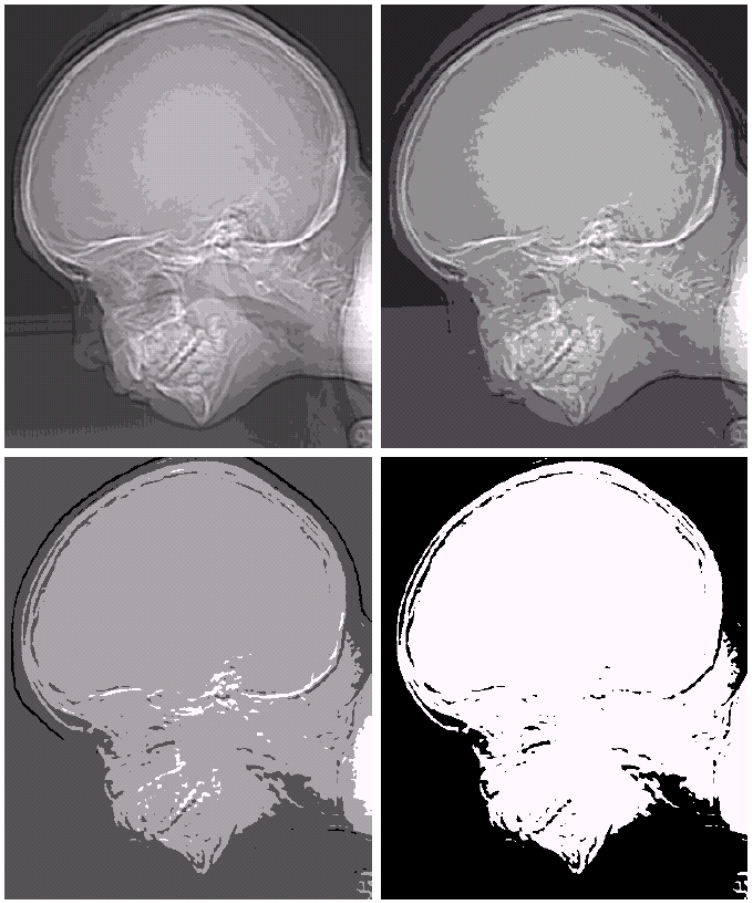

An Image Processing Pipeline

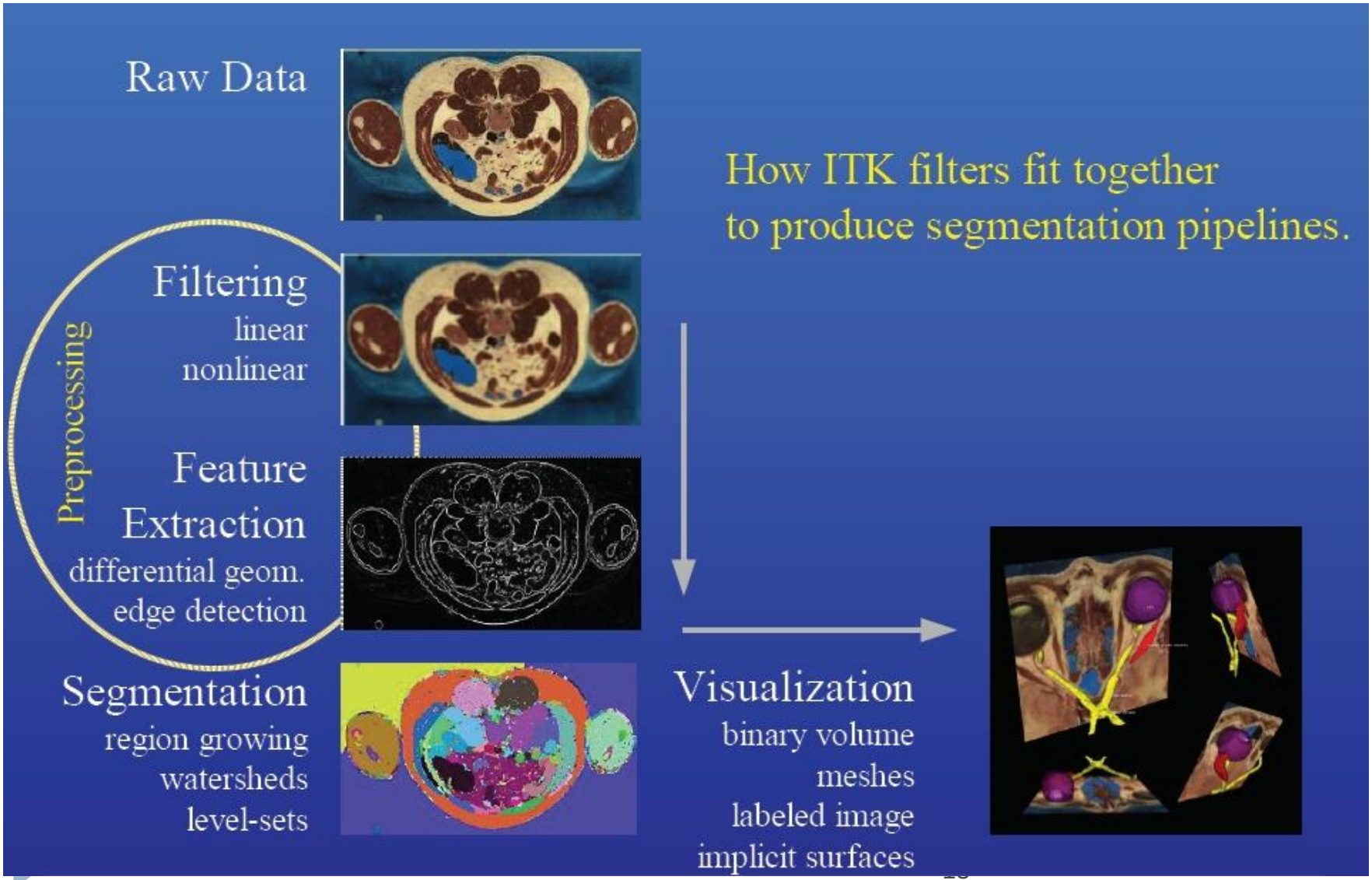

Linear Diffusion

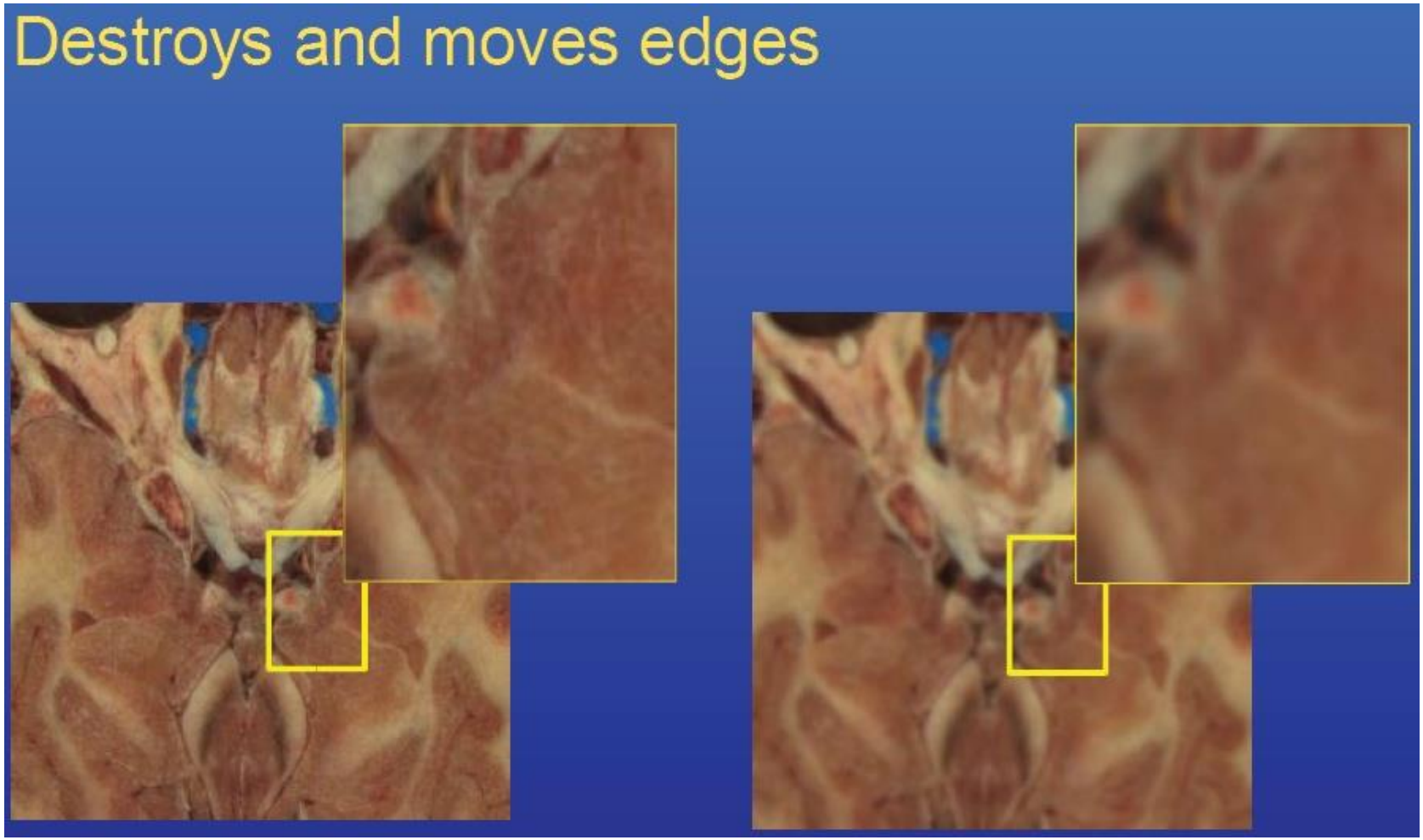

Nonlinear Diffusion

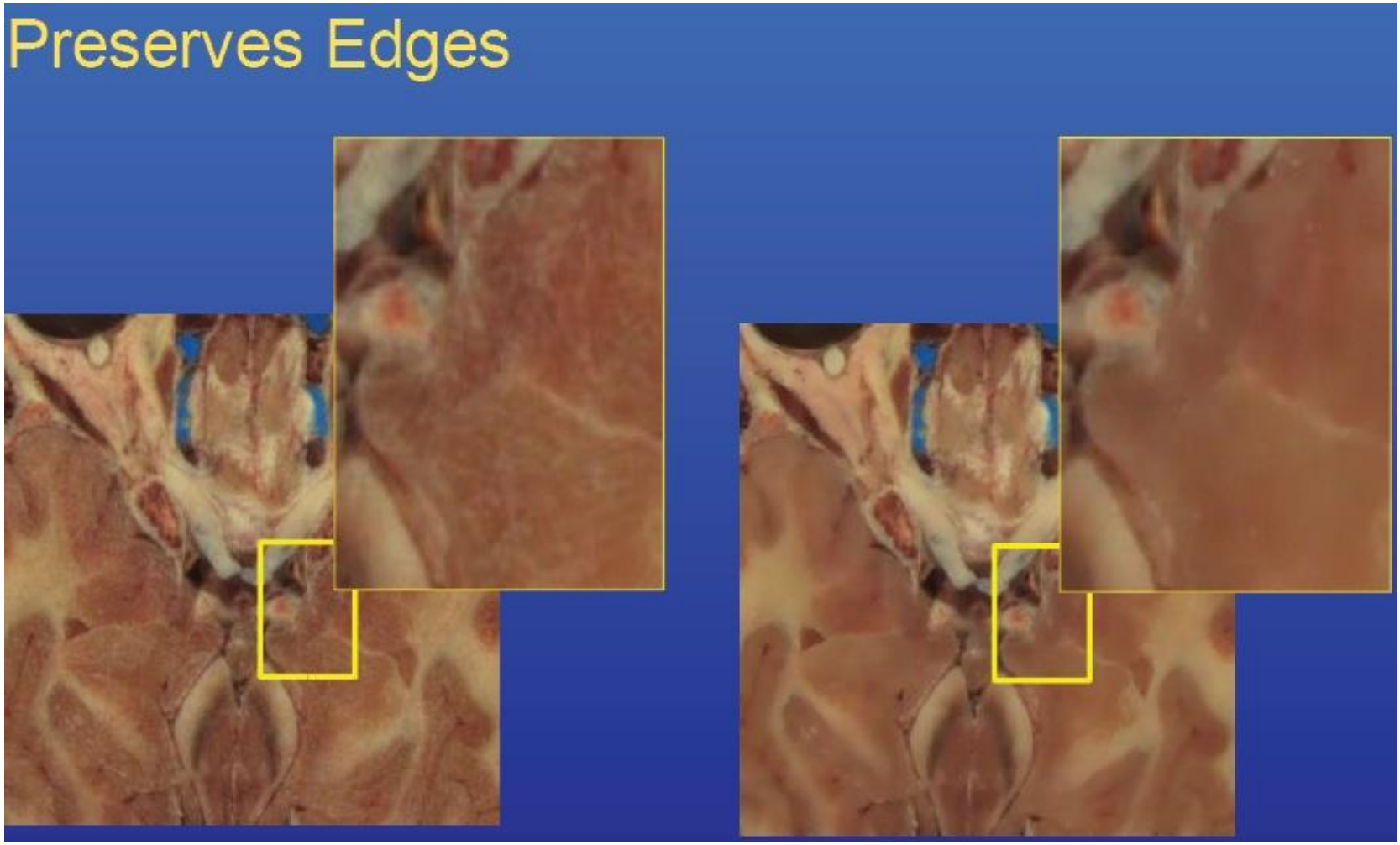

Image Enhancement in the Spatial Domain

- *Spatial domain*
  - refers to the image plane itself, and approaches in this category are based on direct manipulation of pixels in an image.
- *Frequency domain*
  - based on modifying the Fourier transform of an image.

Some Basic Gray Level Transformations

FIGURE 3.3 Some basic gray-level transformation functions used for image enhancement.

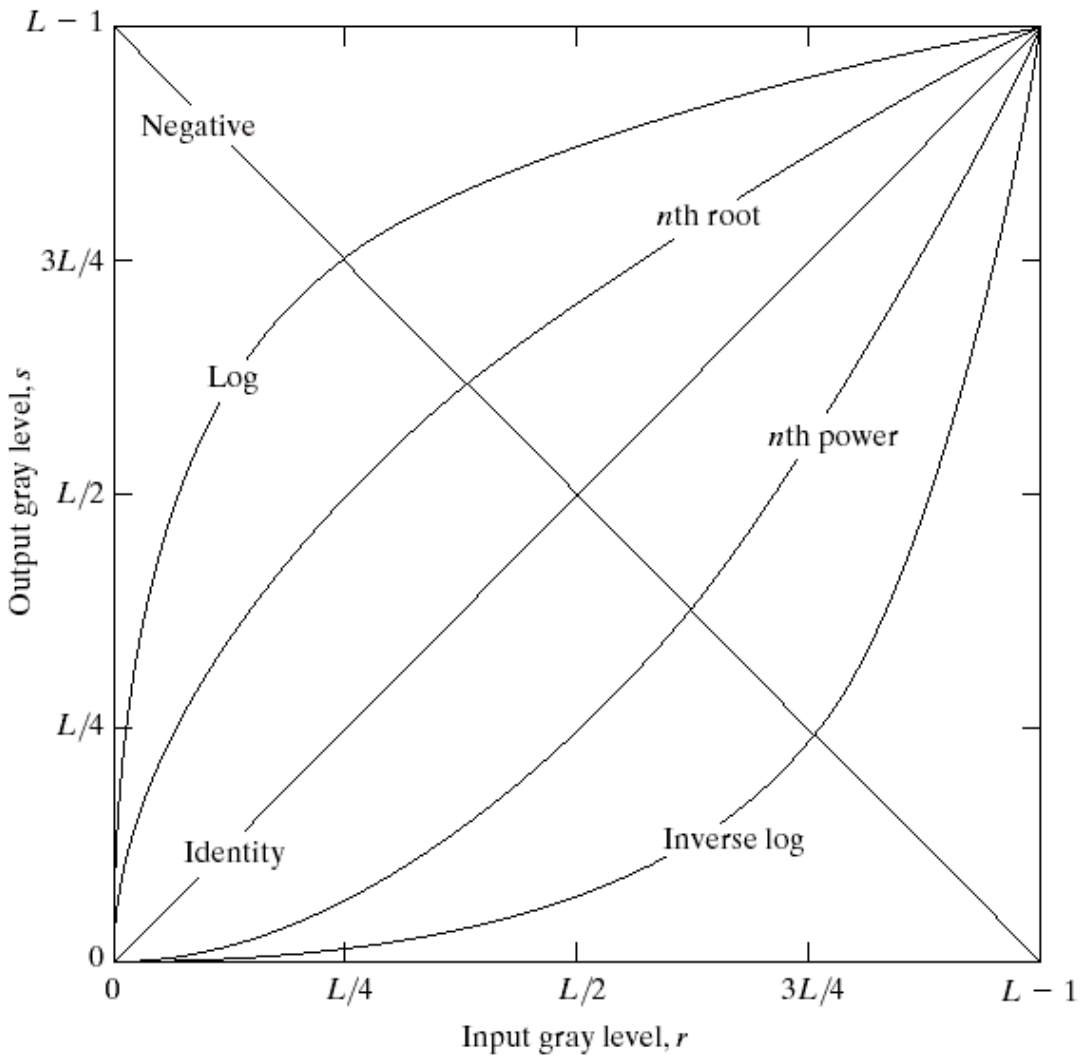

Image Negatives

a b

FIGURE 3.4 (a) Original digital mammogram. (b) Negative image obtained using the negative transformation in Eq. (3.2-1). (Courtesy of G.E. Medical Systems.)

Log Transformation

a b

FIGURE 3.5
(a) Fourier spectrum.
(b) Result of applying the log transformation given in Eq. (3.2-2) with $c = 1$.

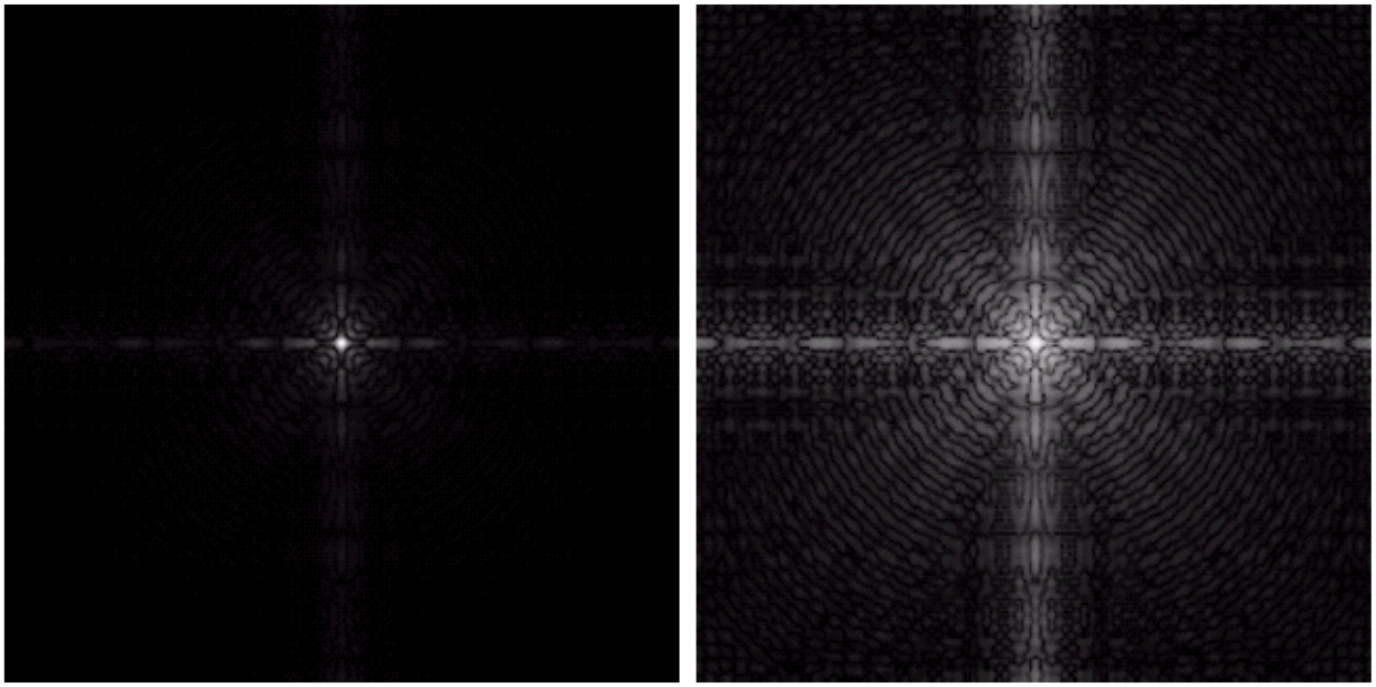

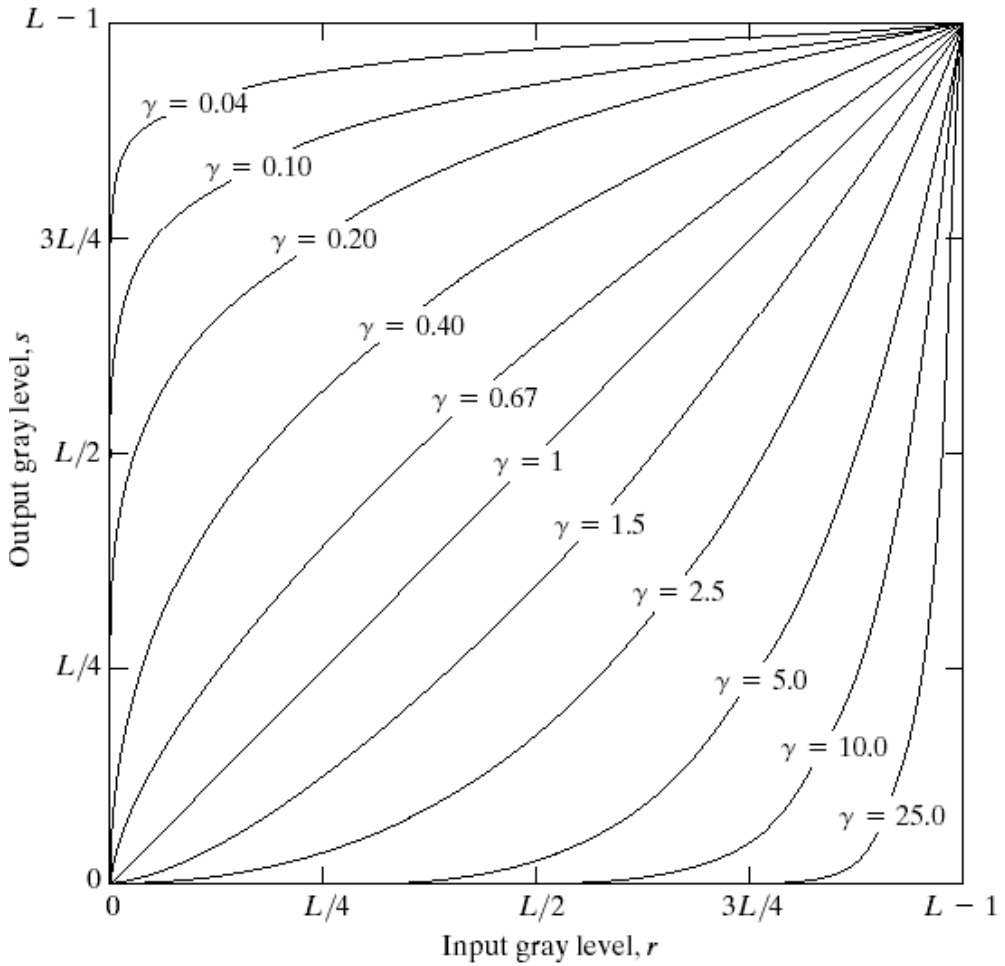

FIGURE 3.6 Plots of the equation $s = cr^{\gamma}$ for various values of γ ($c = 1$ in all cases).

Gamma Correction

a b
c d

FIGURE 3.7
(a) Linear-wedge gray-scale image. (b) Response of monitor to linear wedge. (c) Gamma-corrected wedge. (d) Output of monitor.

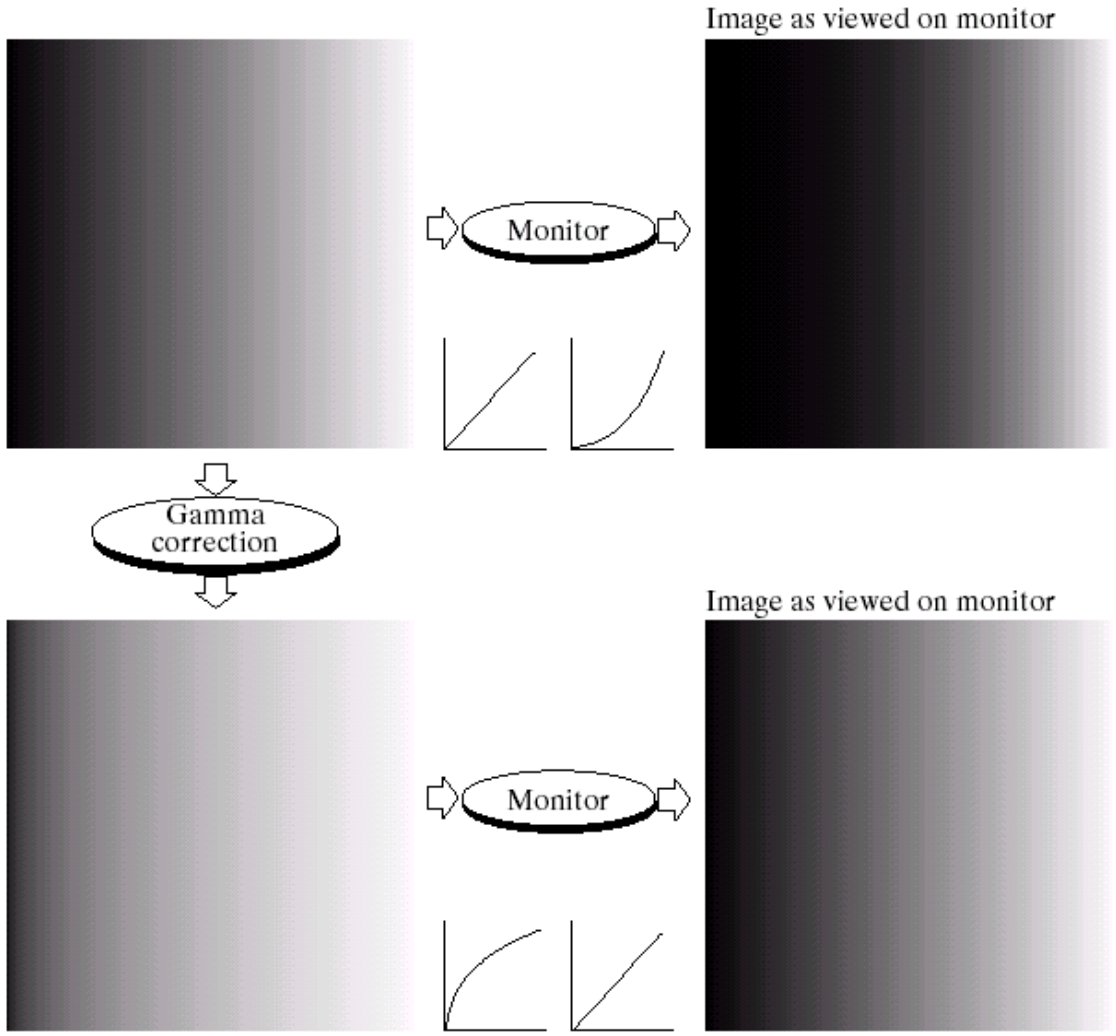

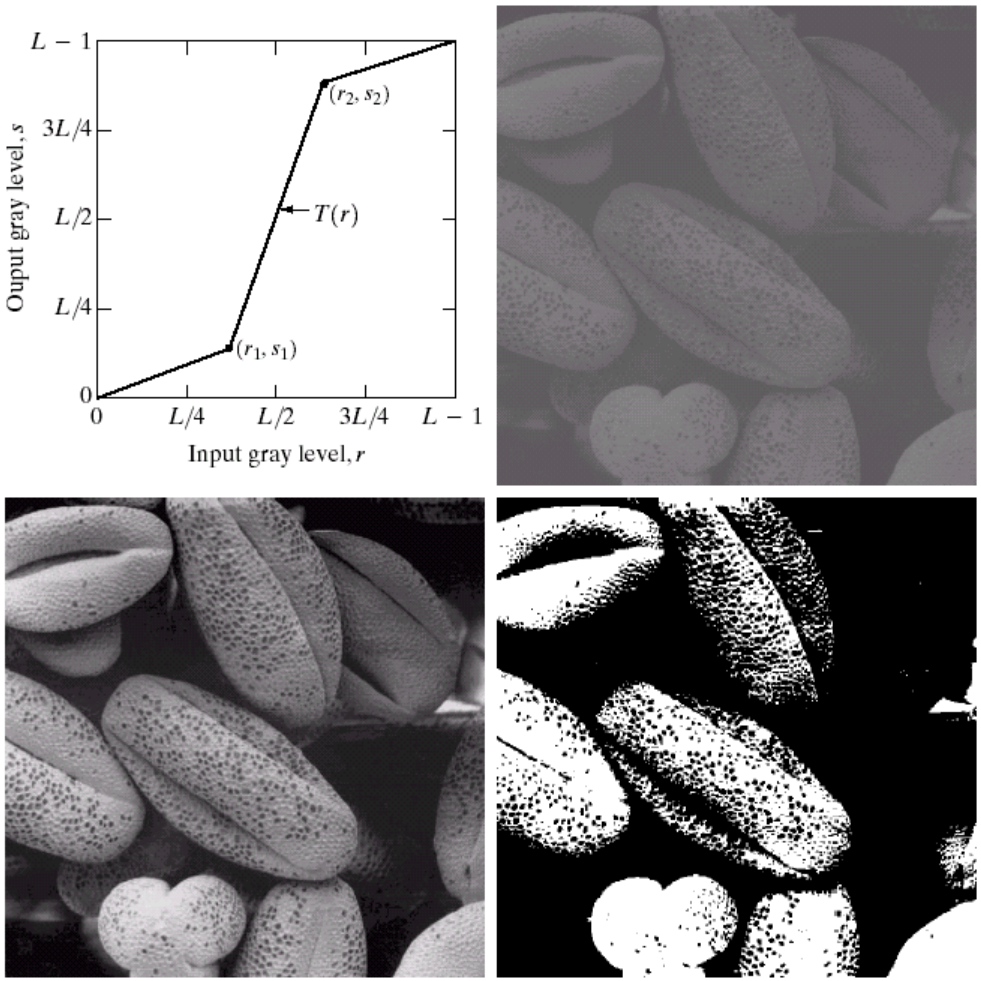

a b
c d

FIGURE 3.10 Contrast stretching. (a) Form of transformation function. (b) A low-contrast image. (c) Result of contrast stretching. (d) Result of thresholding. (Original image courtesy of Dr. Roger Heady, Research School of Biological Sciences, Australian National University, Canberra, Australia.)

Histogram Processing

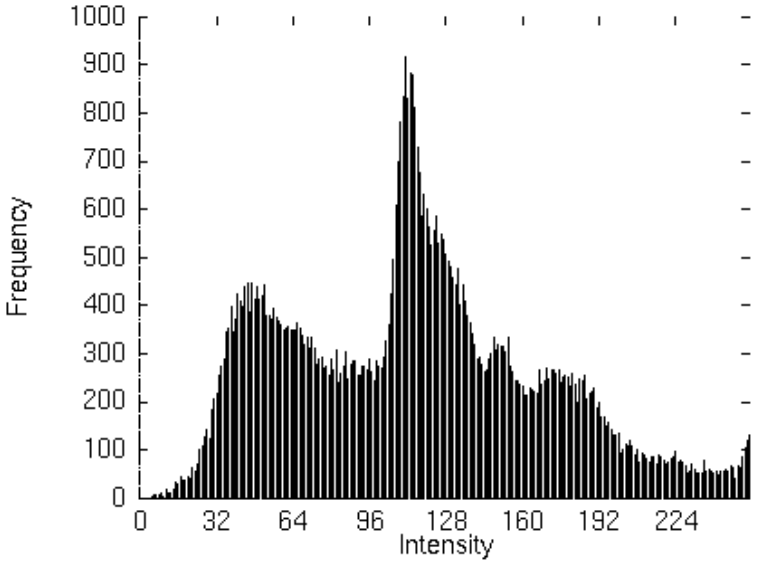

Figure 2.11 *A brightness histogram.*

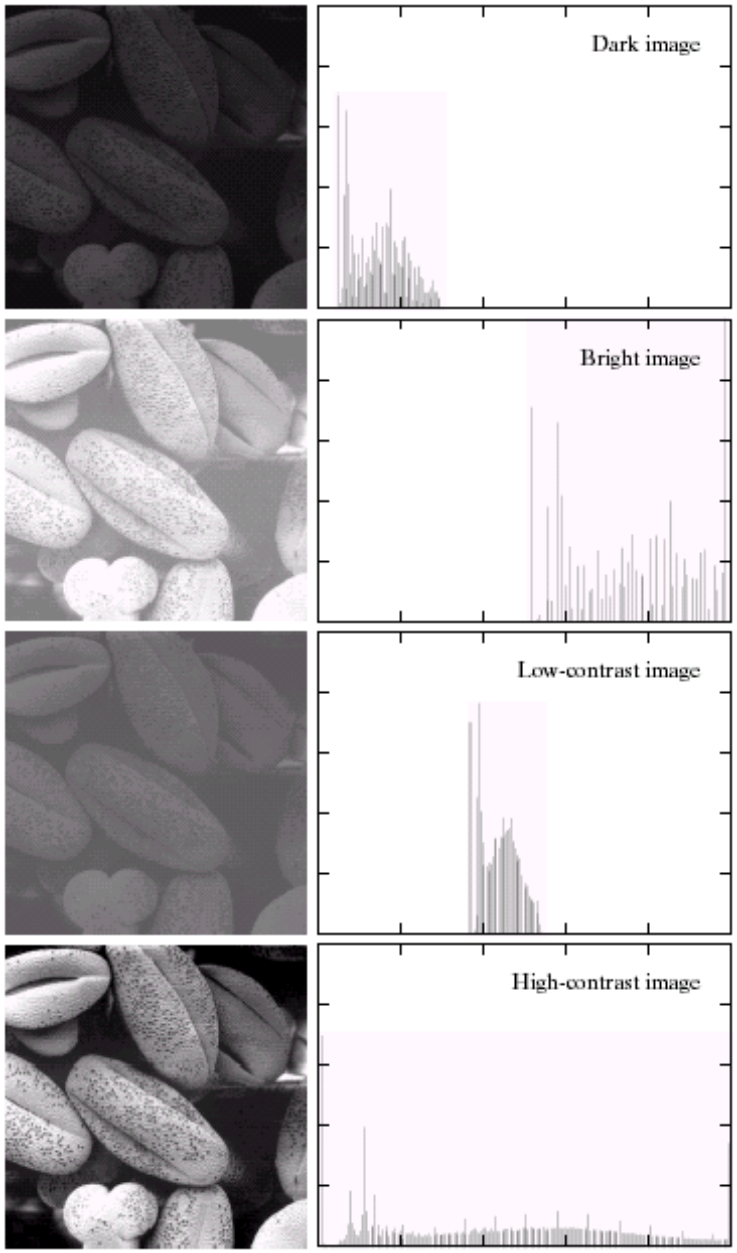

Histogram Equalization

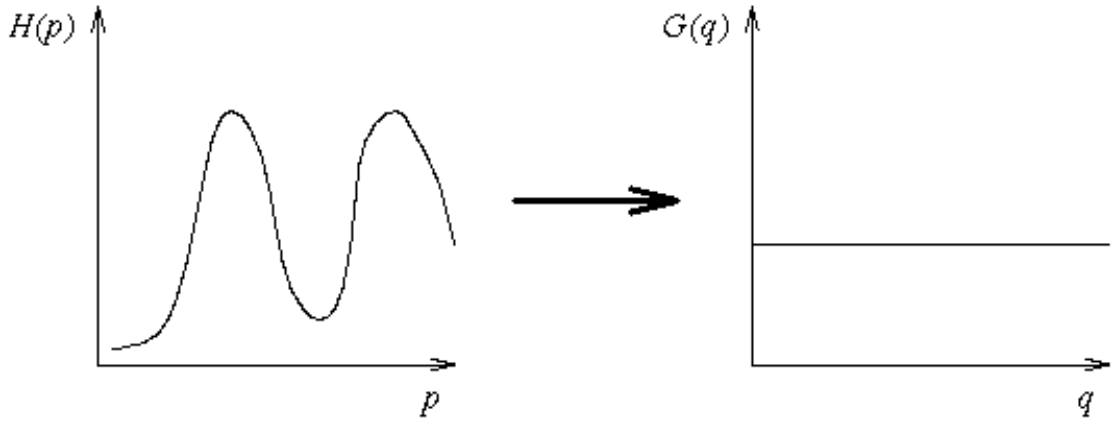

Figure 4.2 Histogram equalization.

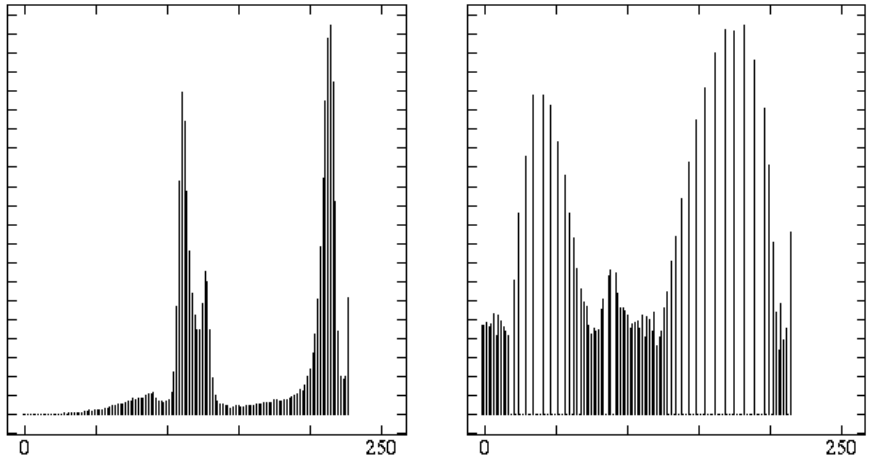

Figure 4.4 Histogram equalization: Original and equalized histograms.

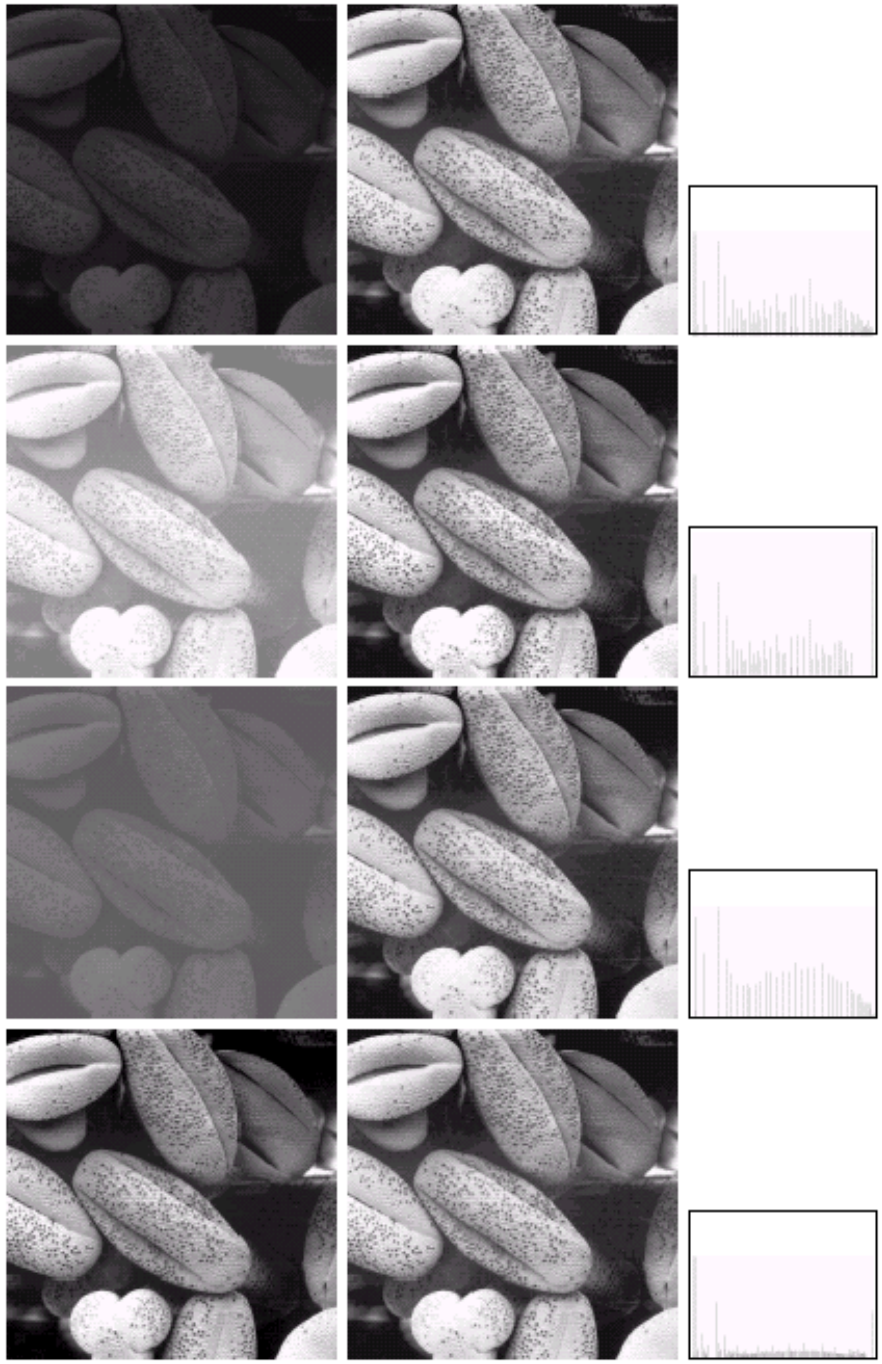

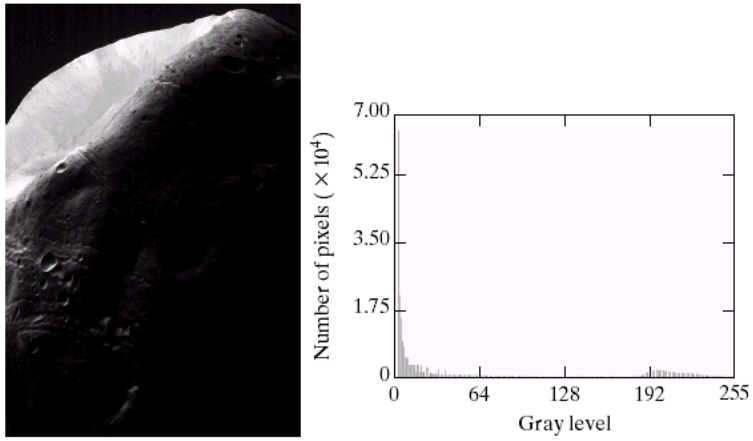

a b

FIGURE 3.20 (a) Image of the Mars moon Photos taken by NASA's *Mars Global Surveyor.* (b) Histogram. (Original image courtesy of NASA.)

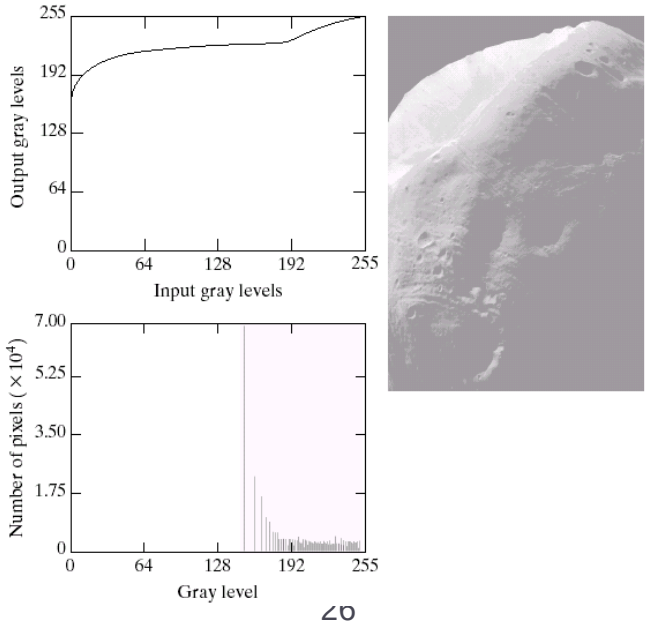

a b
c

FIGURE 3.21
(a) Transformation function for histogram equalization. (b) Histogram-equalized image (note the washed-out appearance). (c) Histogram of (b).

Specified Histogram

a c
b
d

FIGURE 3.22
(a) Specified histogram.
(b) Curve (1) is from Eq. (3.3-14), using the histogram in (a); curve (2) was obtained using the iterative procedure in Eq. (3.3-17).
(c) Enhanced image using mappings from curve (2).
(d) Histogram of (c).

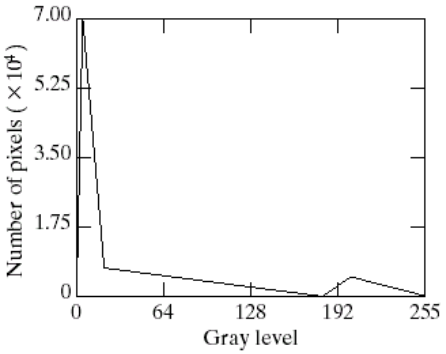

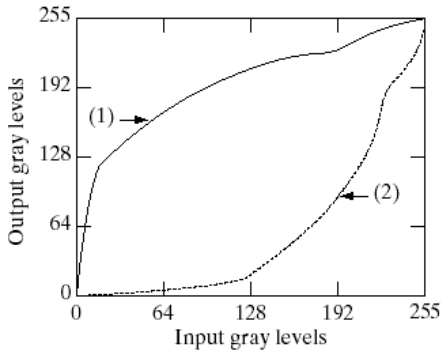

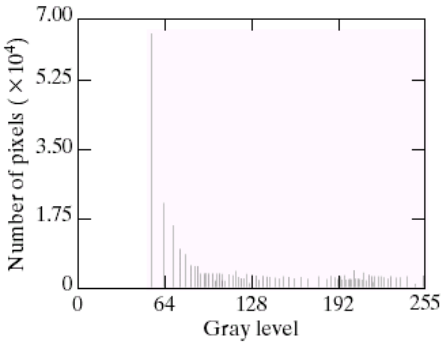

Image Subtraction

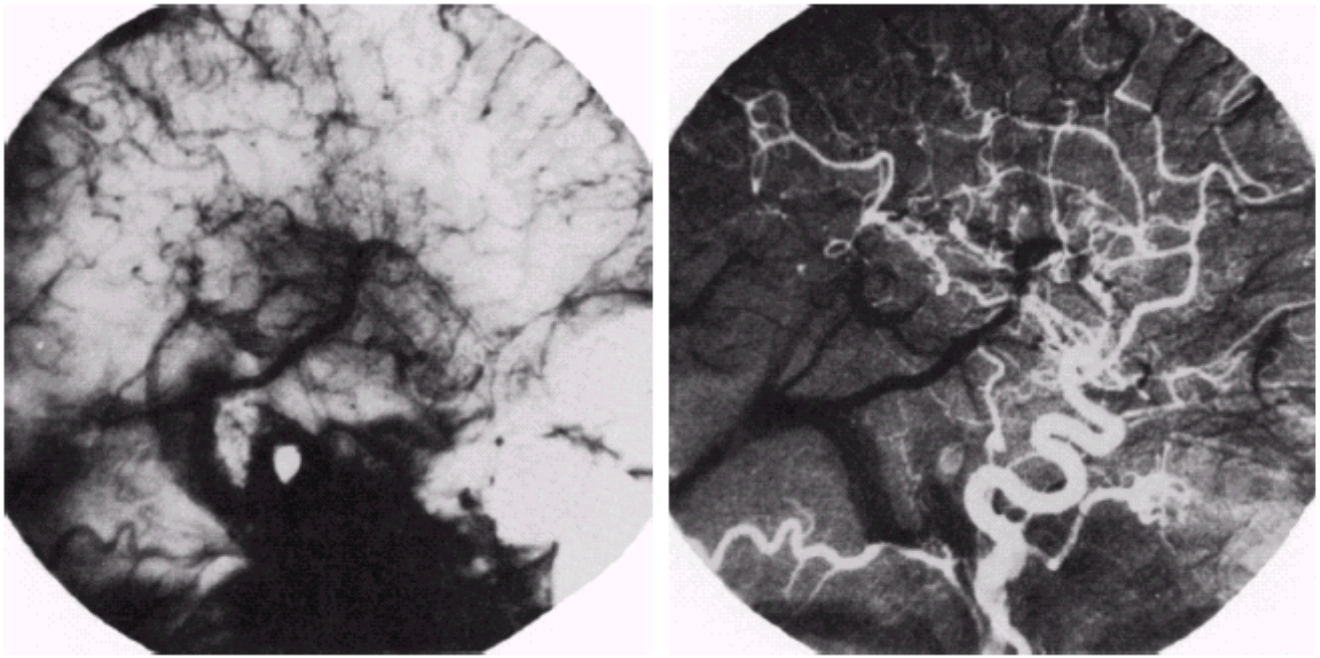

a b

FIGURE 3.29
Enhancement by image subtraction. (a) Mask image. (b) An image (taken after injection of a contrast medium into the bloodstream) with mask subtracted out.

Image Averaging

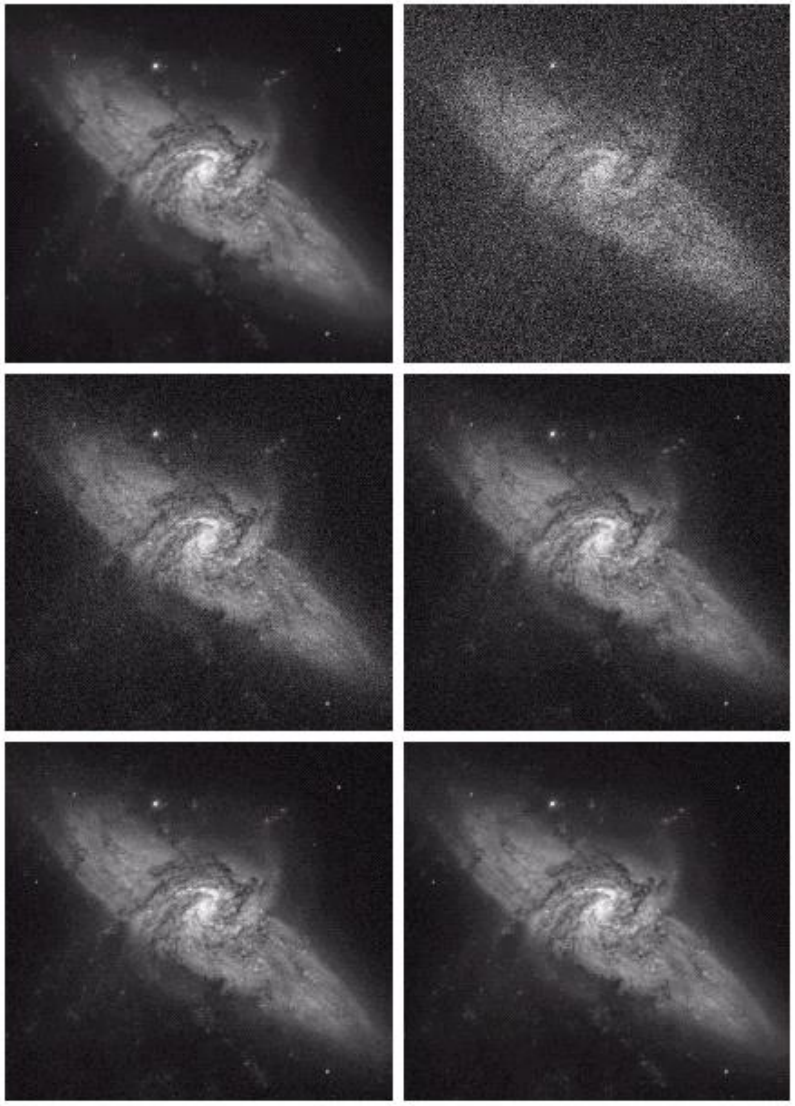

a b
c d
e f

FIGURE 3.30 (a) Image of Galaxy Pair NGC 3314. (b) Image corrupted by additive Gaussian noise with zero mean and a standard deviation of 64 gray levels. (c)–(f) Results of averaging $K = 8, 16, 64$, and 128 noisy images. (Original image courtesy of NASA.)

Spatial Filtering

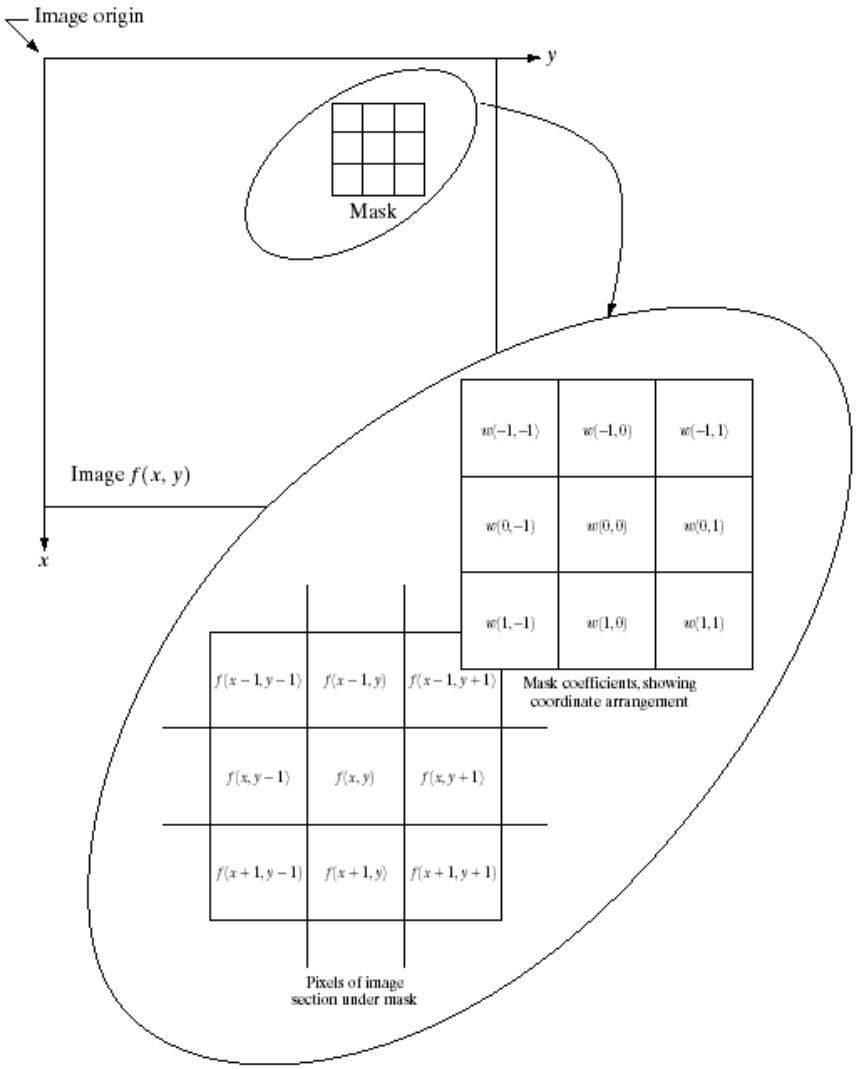

FIGURE 3.32 The mechanics of spatial filtering. The magnified drawing shows a 3×3 mask and the image section directly under it; the image section is shown displaced out from under the mask for ease of readability.

Image Averaging

$\frac{1}{9} \times$

1	1	1
1	1	1
1	1	1

$\frac{1}{16} \times$

1	2	1
2	4	2
1	2	1

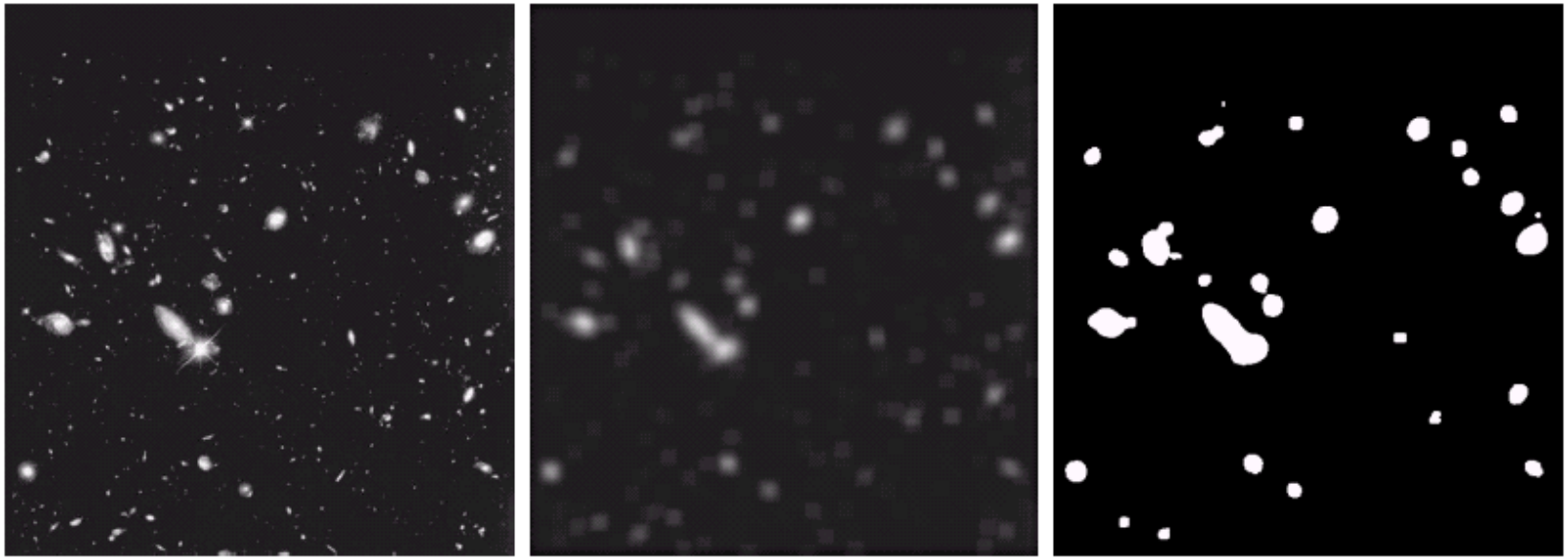

a b c

FIGURE 3.36 (a) Image from the Hubble Space Telescope. (b) Image processed by a 15 × 15 averaging mask. (c) Result of thresholding (b). (Original image courtesy of NASA.)

Median filters

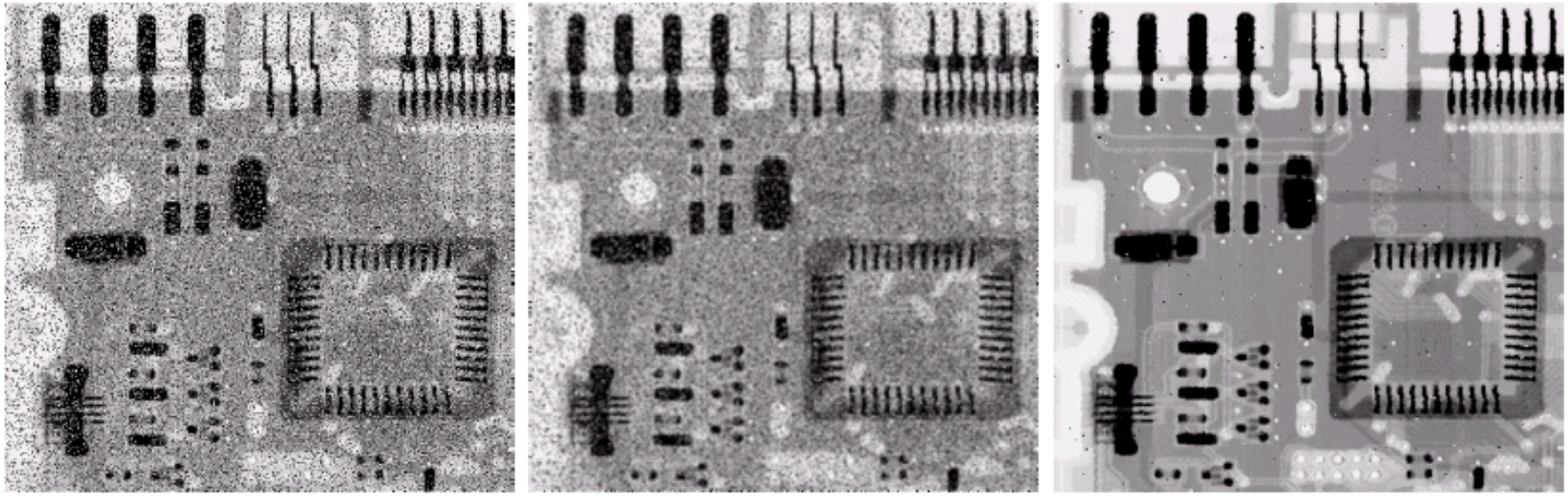

a b c

FIGURE 3.37 (a) X-ray image of circuit board corrupted by salt-and-pepper noise. (b) Noise reduction with a 3×3 averaging mask. (c) Noise reduction with a 3×3 median filter. (Original image courtesy of Mr. Joseph E. Pascente, Lixi, Inc.)

Sharpening Spatial Filters

0	1	0
1	−4	1
0	1	0

1	1	1
1	−8	1
1	1	1

0	−1	0
−1	4	−1
0	−1	0

−1	−1	−1
−1	8	−1
−1	−1	−1

a b
c d

FIGURE 3.39
(a) Filter mask used to implement the digital Laplacian, as defined in Eq. (3.7-4). (b) Mask used to implement an extension of this equation that includes the diagonal neighbors. (c) and (d) Two other implementations of the Laplacian.

a b
c d

FIGURE 3.40
(a) Image of the North Pole of the moon.
(b) Laplacian-filtered image.
(c) Laplacian image scaled for display purposes.
(d) Image enhanced by using Eq. (3.7-5).
(Original image courtesy of NASA.)

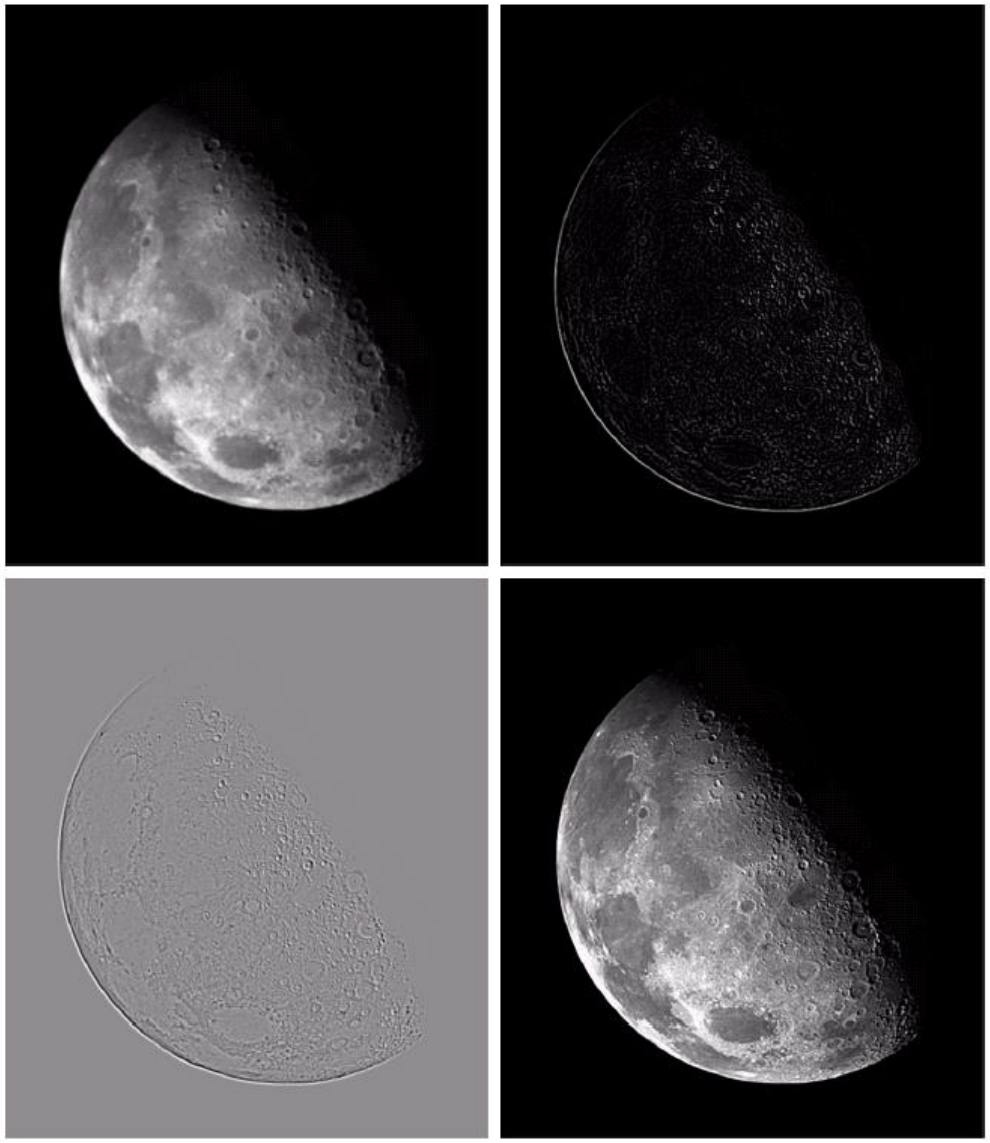

0	−1	0
−1	5	−1
0	−1	0

−1	−1	−1
−1	9	−1
−1	−1	−1

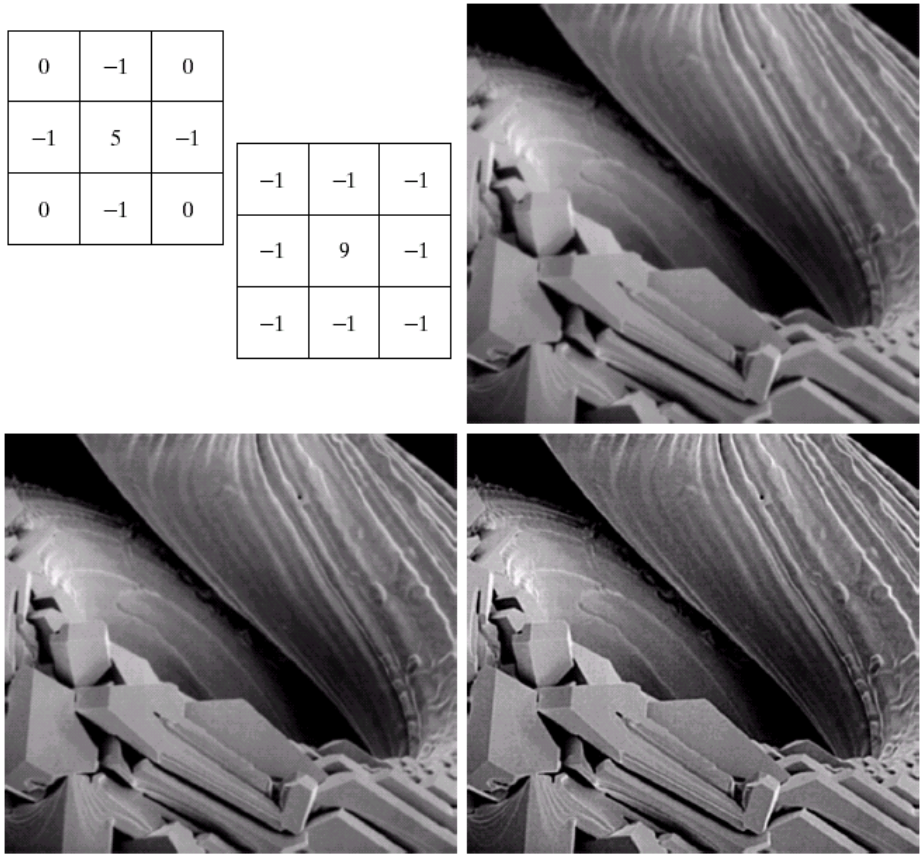

a b c
d e

FIGURE 3.41 (a) Composite Laplacian mask. (b) A second composite mask. (c) Scanning electron microscope image. (d) and (e) Results of filtering with the masks in (a) and (b), respectively. Note how much sharper (e) is than (d). (Original image courtesy of Mr. Michael Shaffer, Department of Geological Sciences, University of Oregon, Eugene.)

Gradient

a
b c
d e

FIGURE 3.44
A 3×3 region of an image (the z's are gray-level values) and masks used to compute the gradient at point labeled z_5. All masks coefficients sum to zero, as expected of a derivative operator.

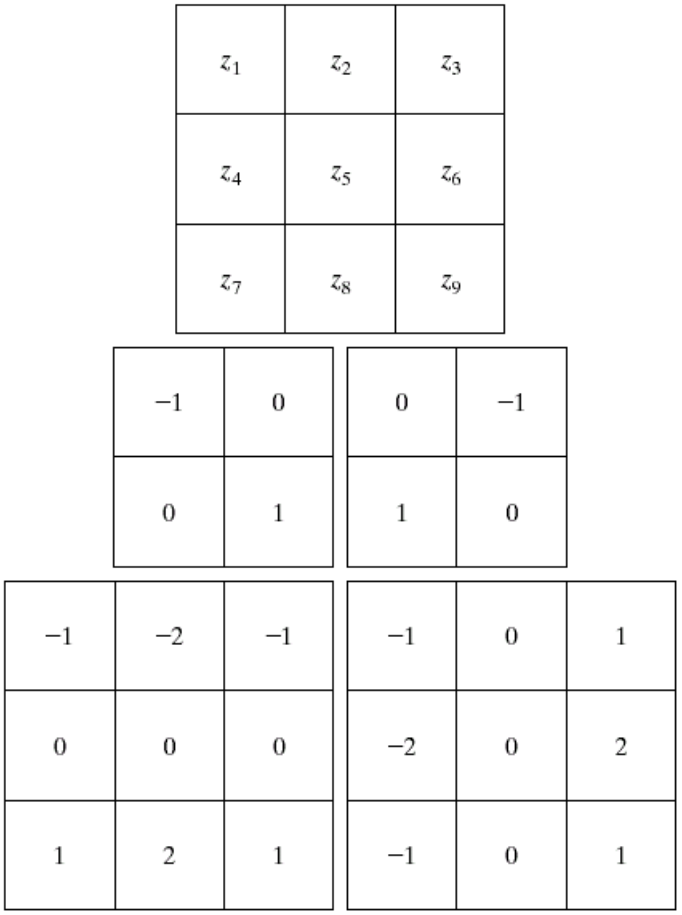

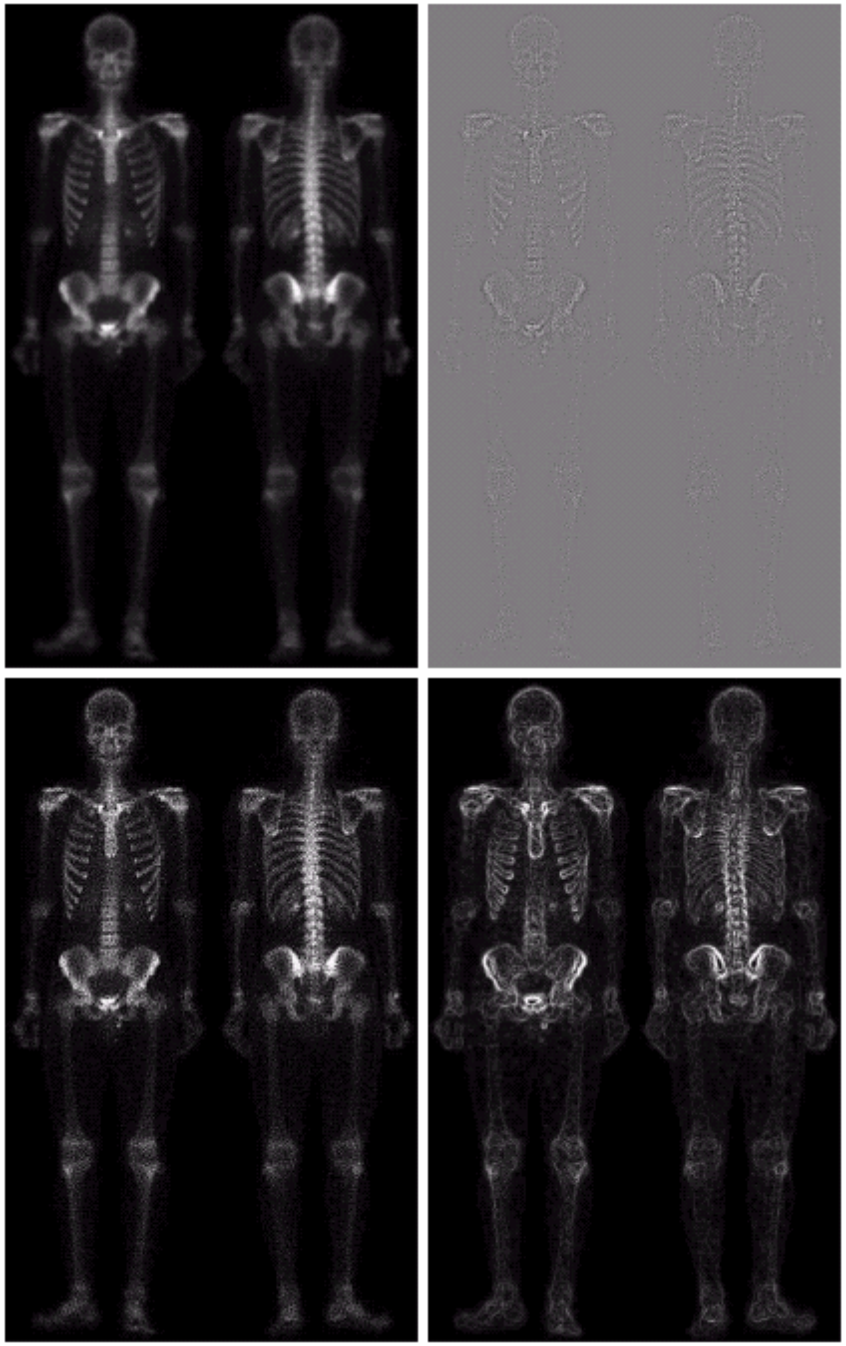

a b
c d

FIGURE 3.46
(a) Image of whole body bone scan.
(b) Laplacian of (a). (c) Sharpened image obtained by adding (a) and (b). (d) Sobel of (a).

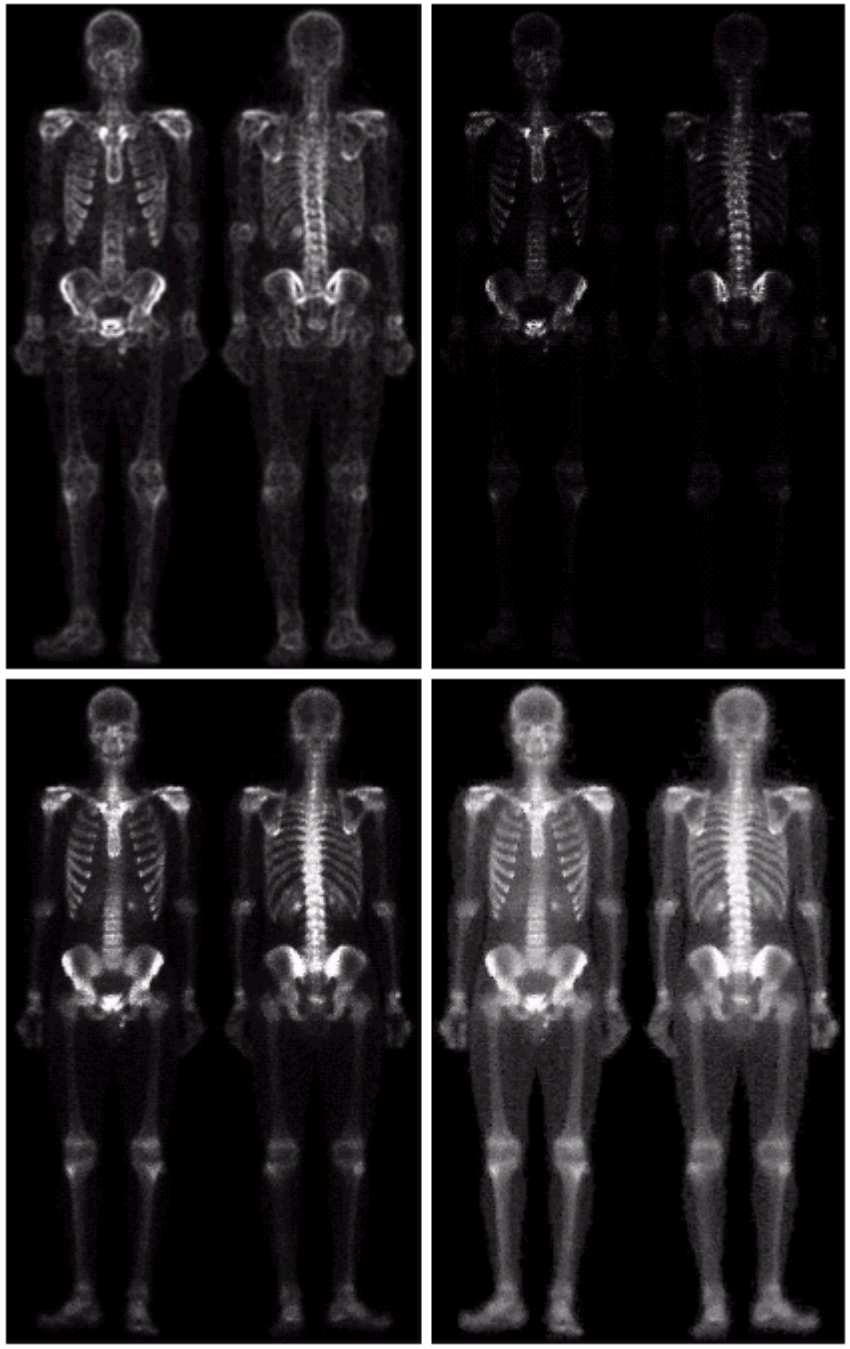

e f
g h

FIGURE 3.46
(Continued)
(e) Sobel image smoothed with a 5×5 averaging filter. (f) Mask image formed by the product of (c) and (e).
(g) Sharpened image obtained by the sum of (a) and (f). (h) Final result obtained by applying a power-law transformation to (g). Compare (g) and (h) with (a). (Original image courtesy of G.E. Medical Systems.)

Frequency Domain

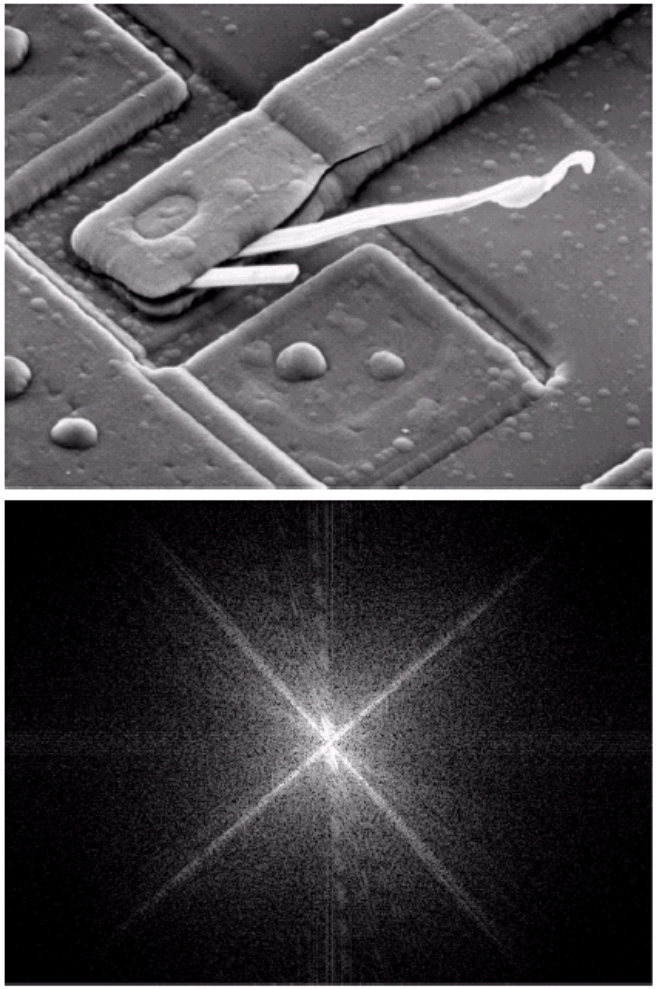

a
b

FIGURE 4.4
(a) SEM image of a damaged integrated circuit. (b) Fourier spectrum of (a). (Original image courtesy of Dr. J. M. Hudak, Brockhouse Institute for Materials Research, McMaster University, Hamilton, Ontario, Canada.)

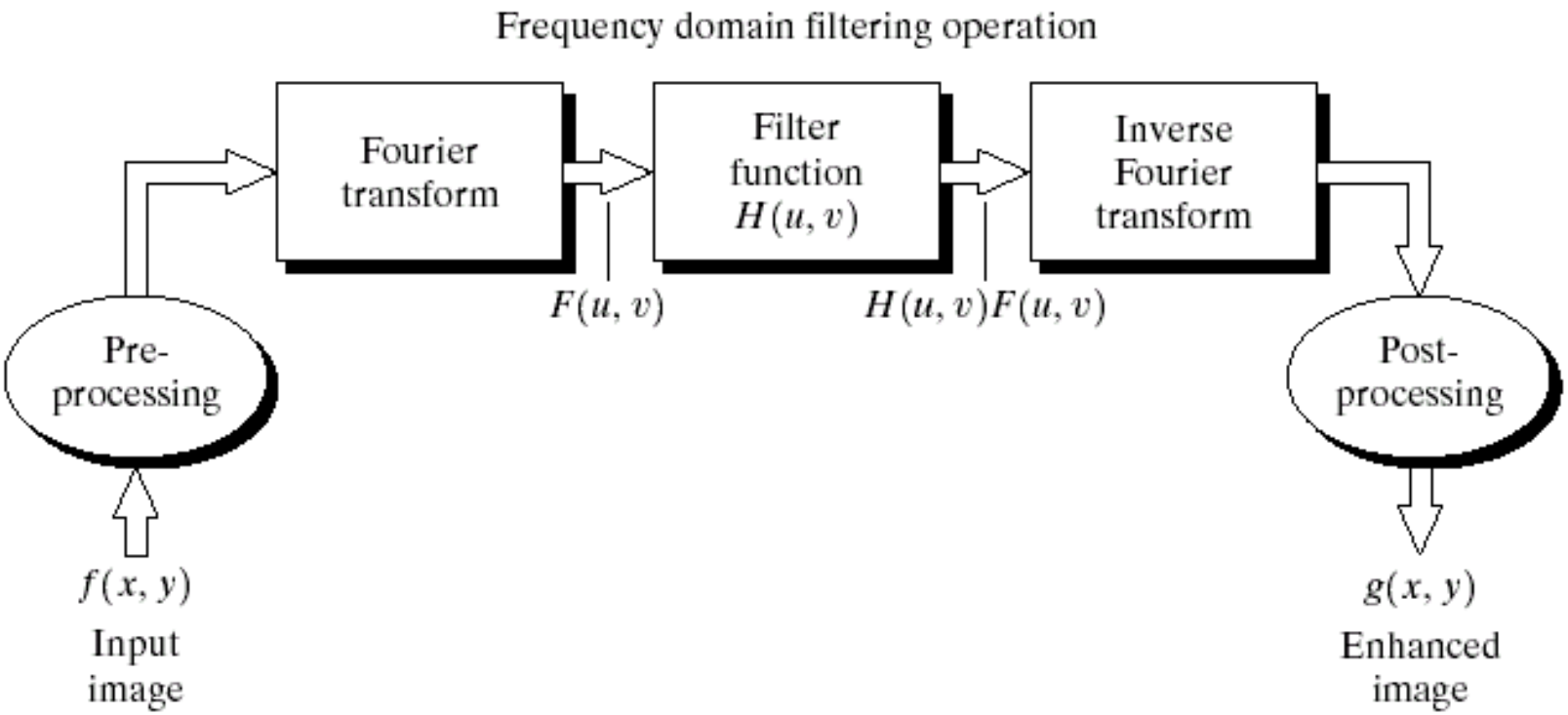

FIGURE 4.5 Basic steps for filtering in the frequency domain.

Lowpass/highpass Filtering

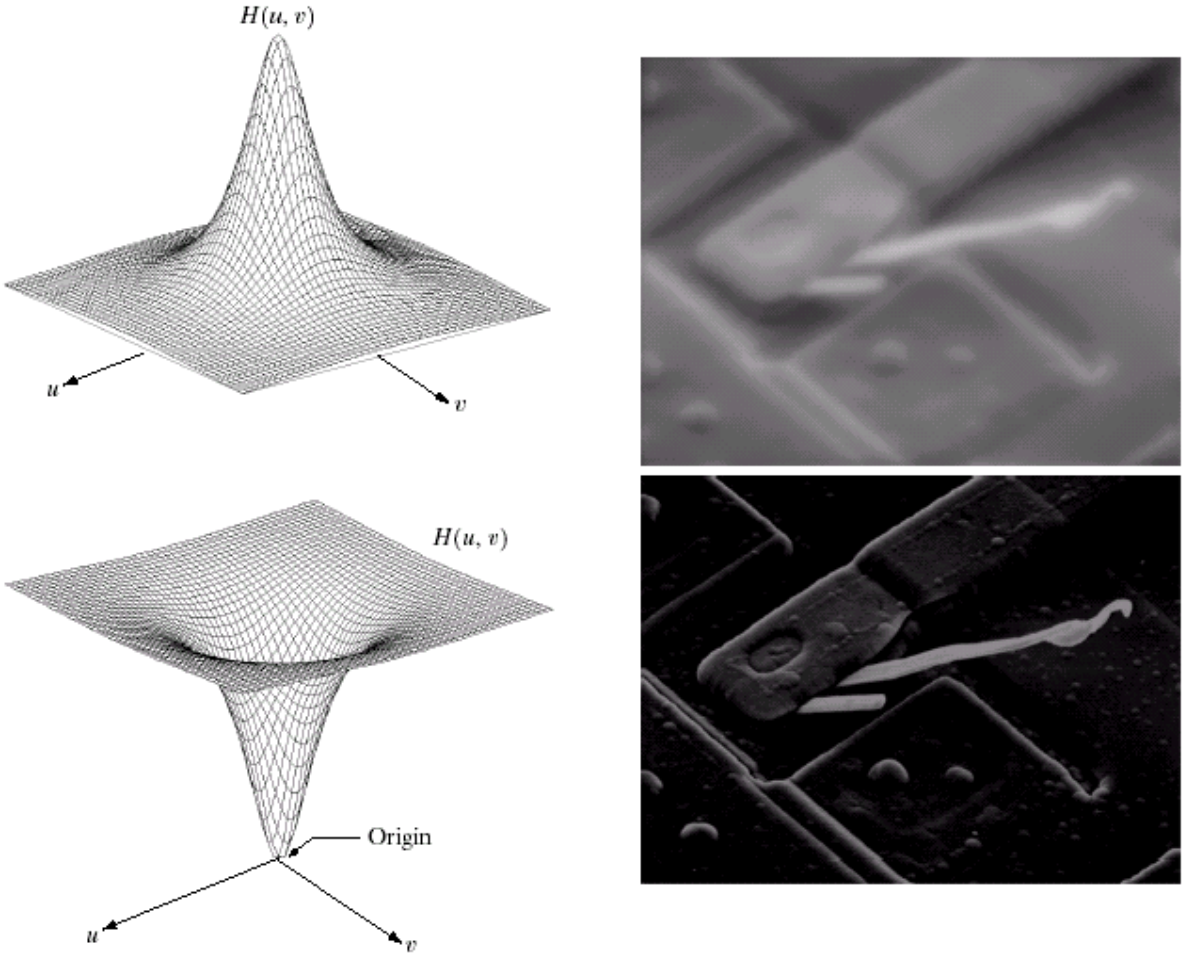

a b
c d

FIGURE 4.7 (a) A two-dimensional lowpass filter function. (b) Result of lowpass filtering the image in Fig. 4.4(a). (c) A two-dimensional highpass filter function. (d) Result of highpass filtering the image in Fig. 4.4(a).

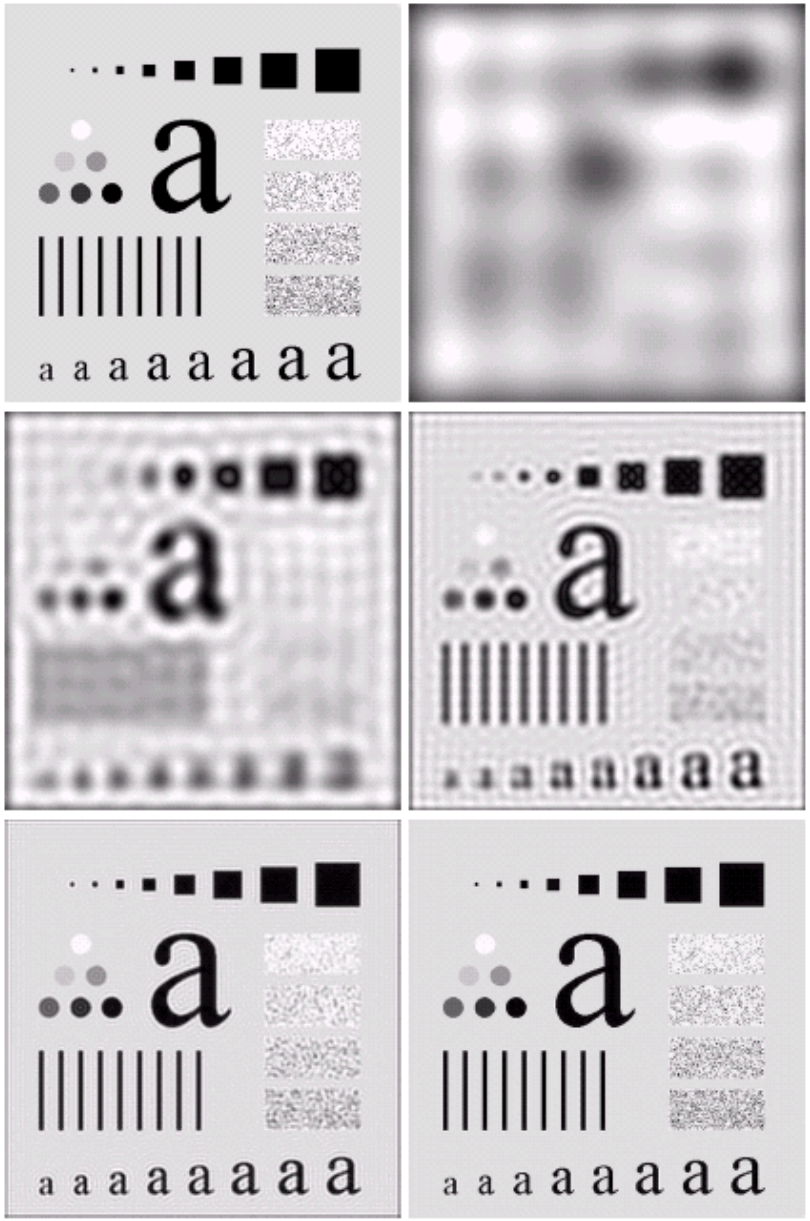

a b
c d
e f

FIGURE 4.12 (a) Original image. (b)–(f) Results of ideal lowpass filtering with cutoff frequencies set at radii values of 5, 15, 30, 80, and 230, as shown in Fig. 4.11(b). The power removed by these filters was 8, 5.4, 3.6, 2, and 0.5% of the total, respectively.

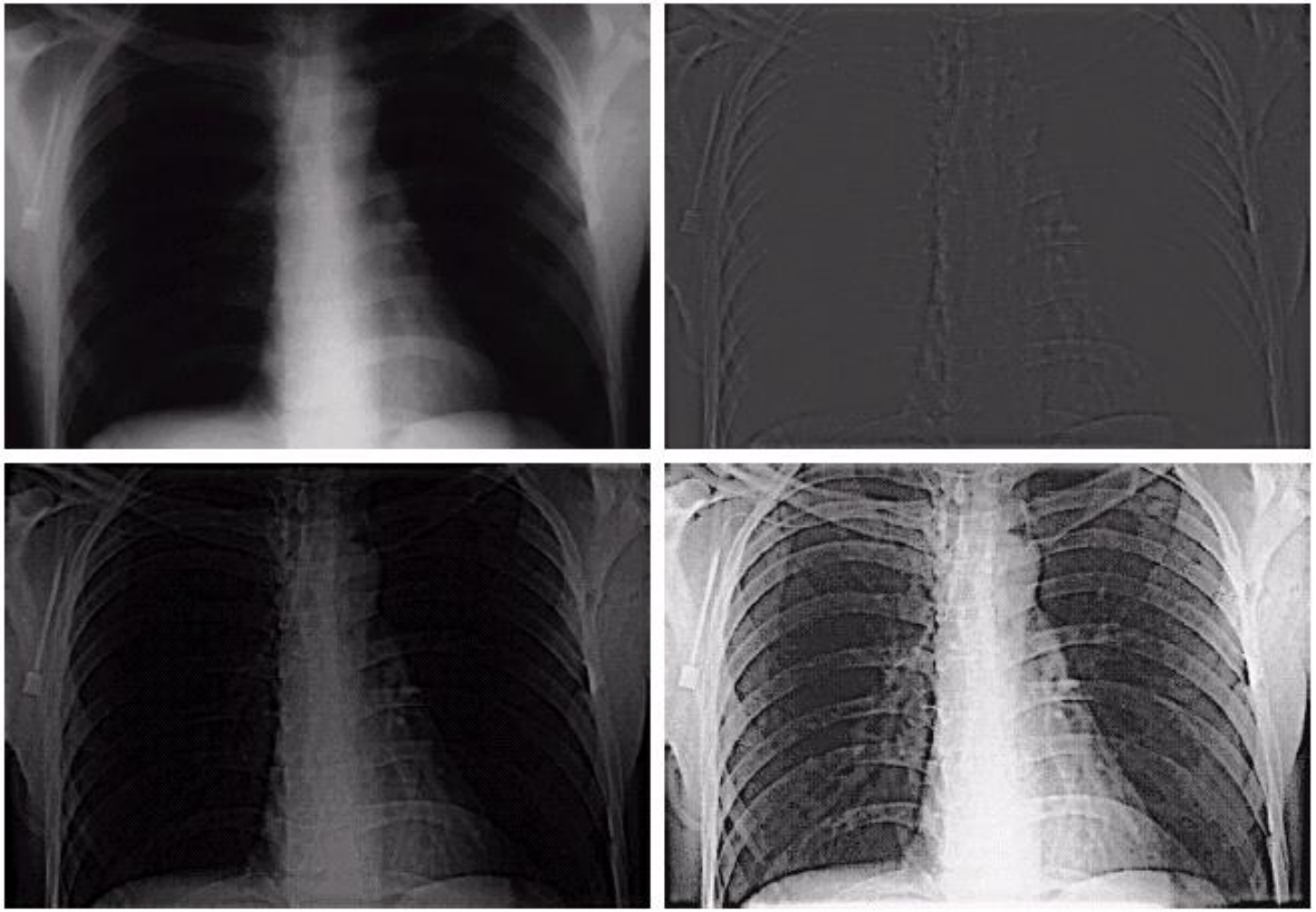

a b
c d

FIGURE 4.30
(a) A chest X-ray image. (b) Result of Butterworth highpass filtering. (c) Result of high-frequency emphasis filtering. (d) Result of performing histogram equalization on (c). (Original image courtesy Dr. Thomas R. Gest, Division of Anatomical Sciences, University of Michigan Medical School.)

Color Images

a
b

FIGURE 6.9
(a) Generating the RGB image of the cross-sectional color plane (127, G, B).
(b) The three hidden surface planes in the color cube of Fig. 6.8.

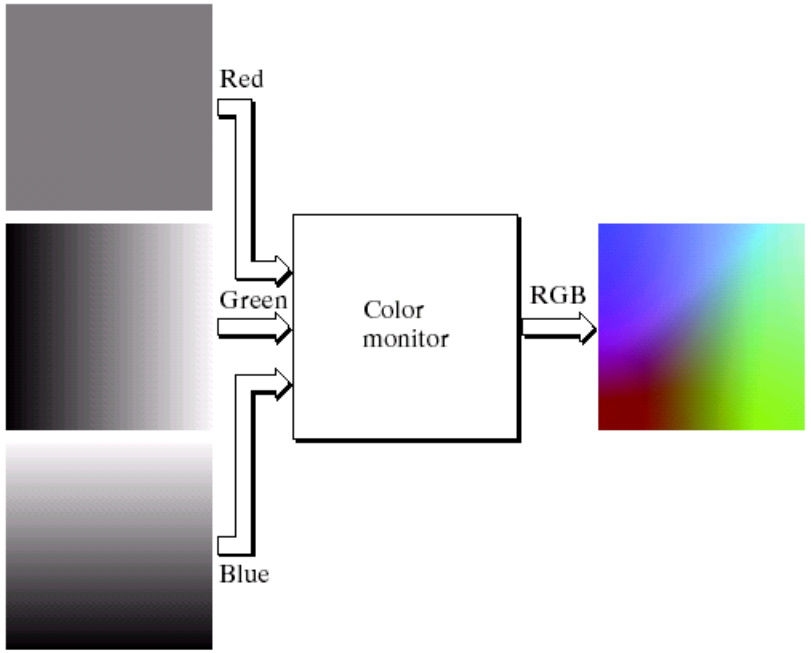

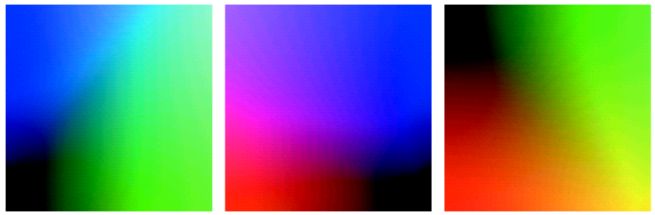

Color Models

- CMY and CMYK Color Models
- HIS Color Model
  - When human view a color object
    - Hue (H)
    - Saturation (S)
    - Brightness or intensity (I)

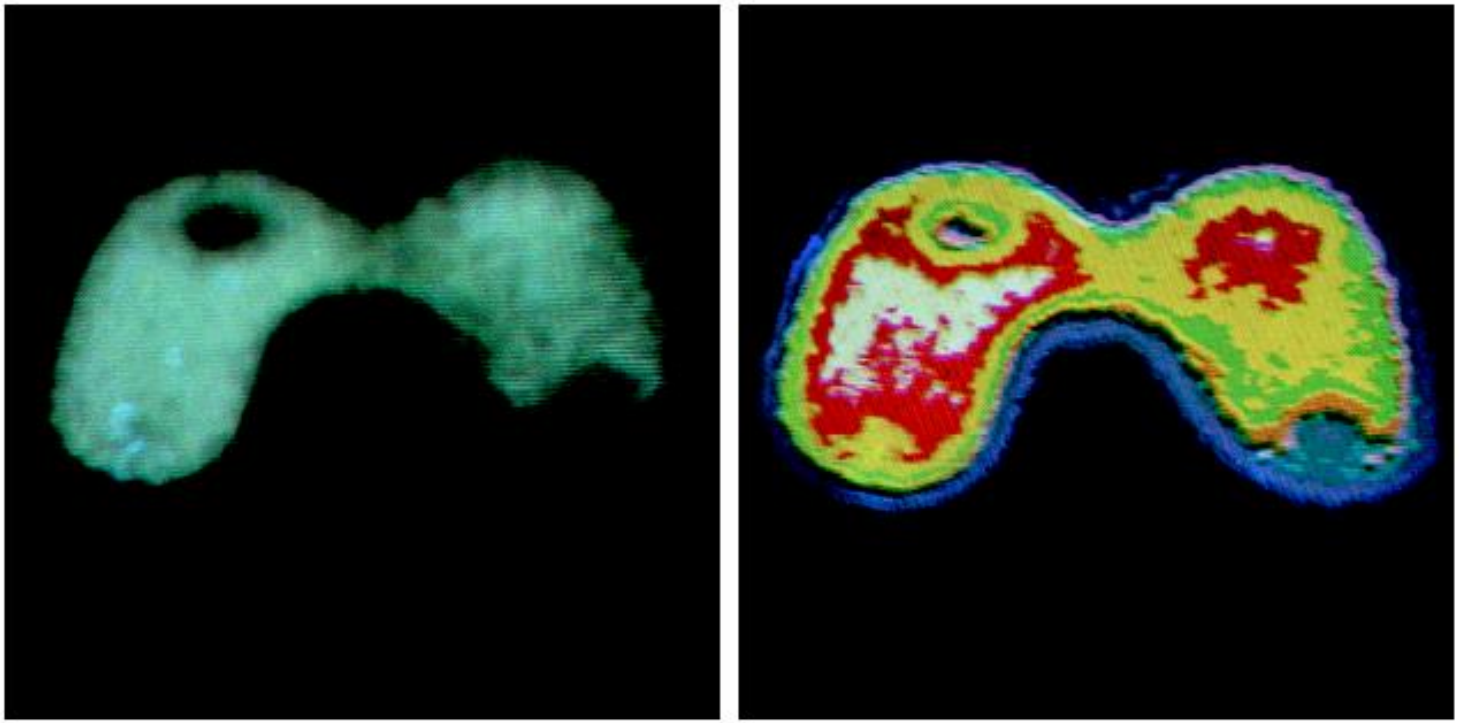

a b

FIGURE 6.20 (a) Monochrome image of the Picker Thyroid Phantom. (b) Result of density slicing into eight colors. (Courtesy of Dr. J. L. Blankenship, Instrumentation and Controls Division, Oak Ridge National Laboratory.)

a
b

FIGURE 6.21
(a) Monochrome X-ray image of a weld. (b) Result of color coding. (Original image courtesy of X-TEK Systems, Ltd.)

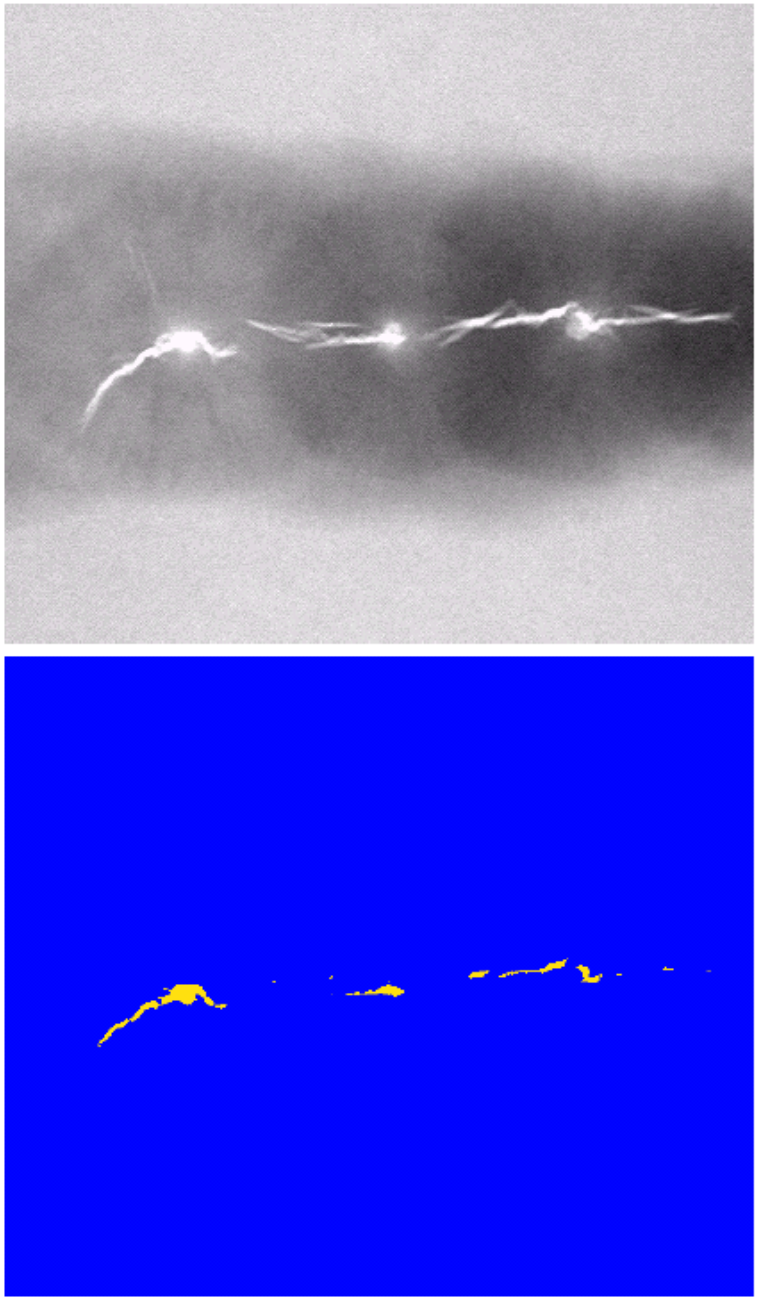

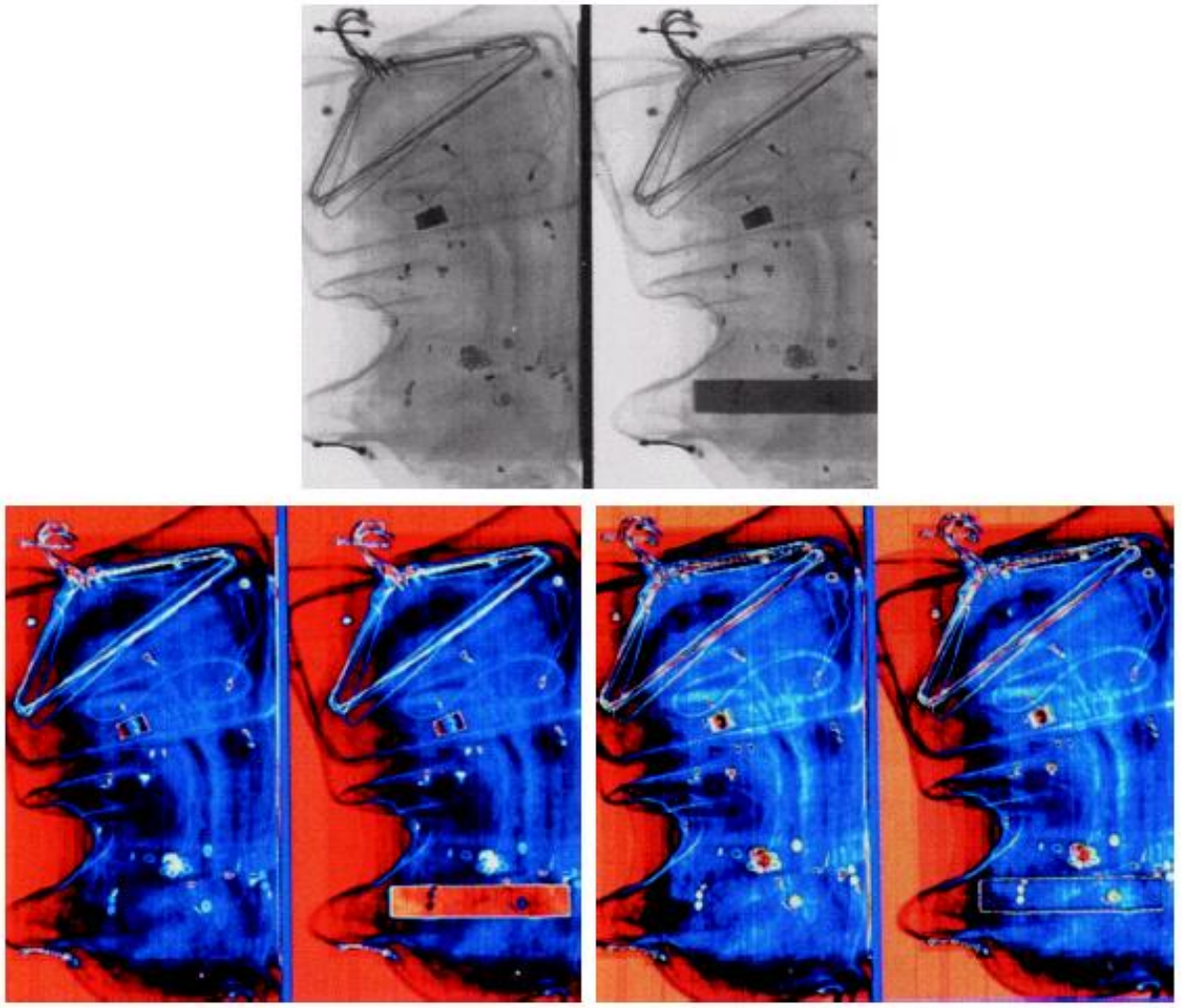

a
b c

FIGURE 6.24 Pseudocolor enhancement by using the gray-level to color transformations in Fig. 6.25. (Original image courtesy of Dr. Mike Hurwitz, Westinghouse.)

Wavelets

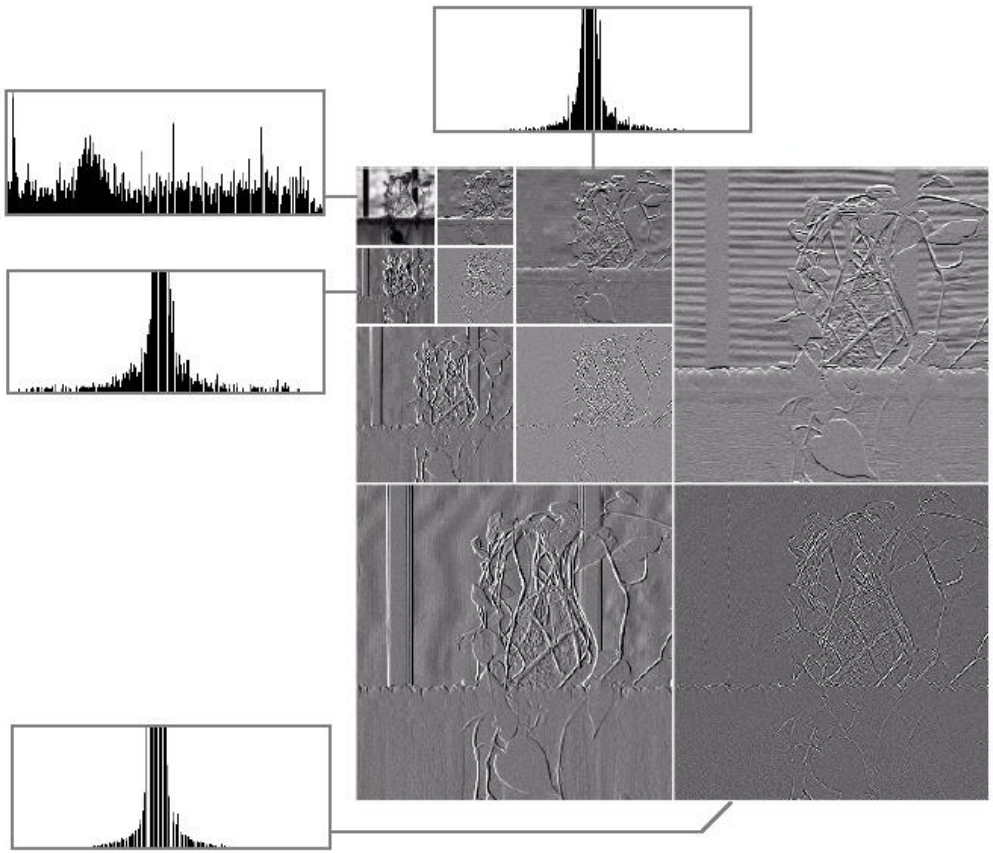

a
b c d

FIGURE 7.8 (a) A discrete wavelet transform using Haar basis functions. Its local histogram variations are also shown; (b)–(d) Several different approximations (64×64, 128×128, and 256×256) that can be obtained from (a).

DWT for Noise Removal

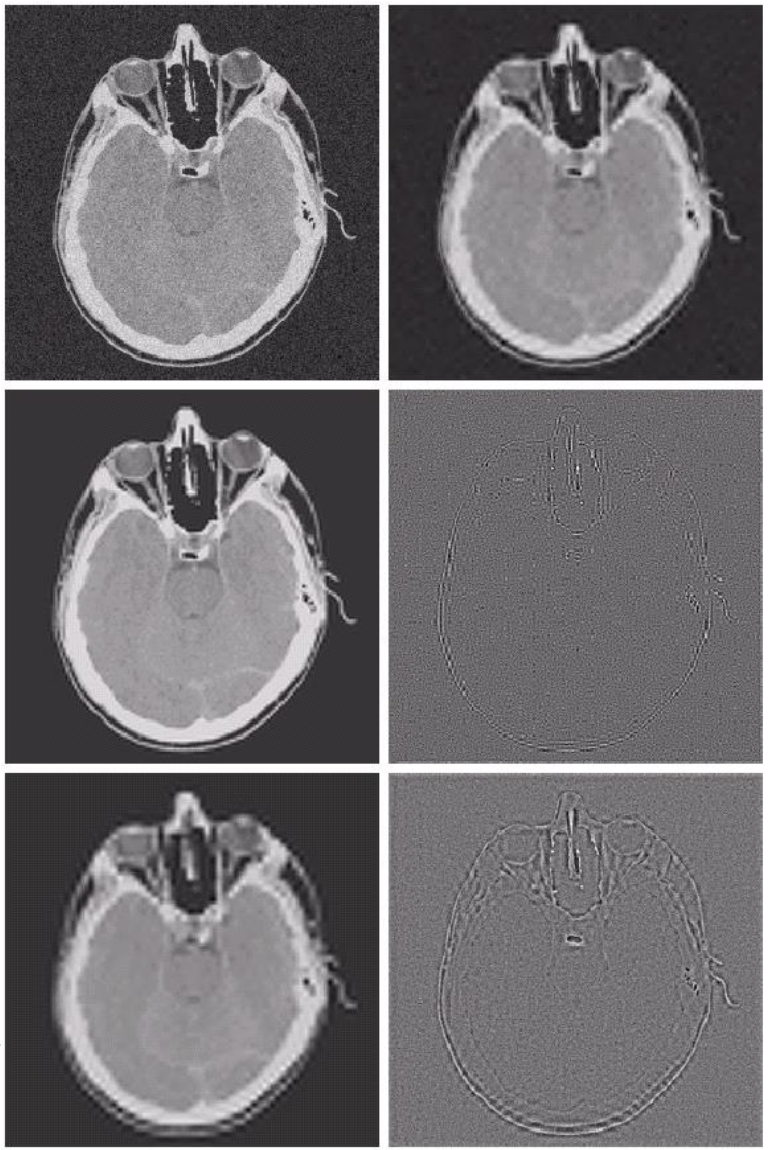

a b
c d
e f

FIGURE 7.26
Modifying a DWT for noise removal: (a) a noisy MRI of a human head; (b), (c) and (e) various reconstructions after thresholding the detail coefficients; (d) and (f) the information removed during the reconstruction of (c) and (e). (Original image courtesy Vanderbuilt University Medical Center.)

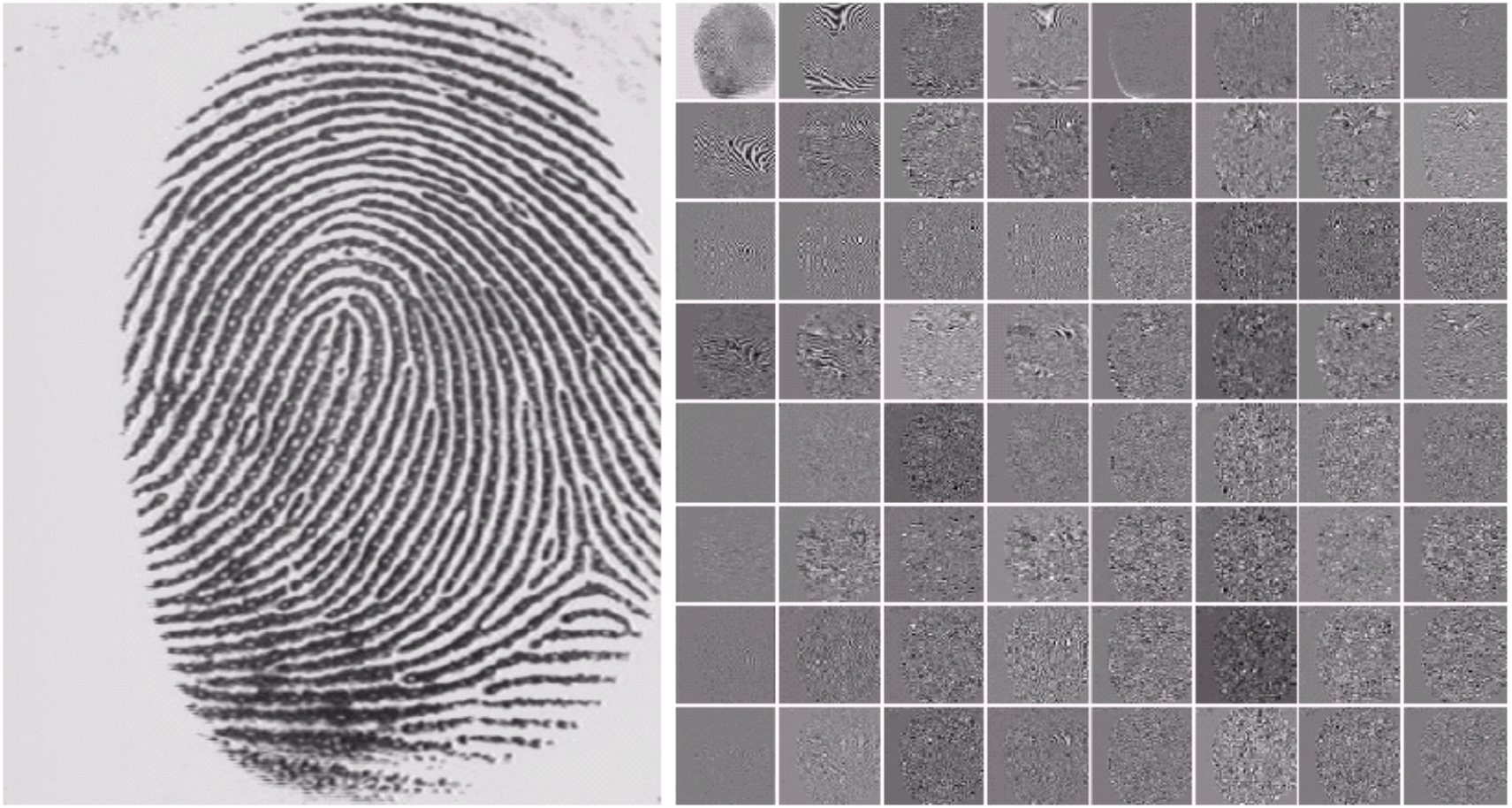

a b

FIGURE 7.34 (a) A scanned fingerprint and (b) its three-scale, full wavelet packet decomposition. (Original image courtesy of the National Institute of Standards and Technology.)

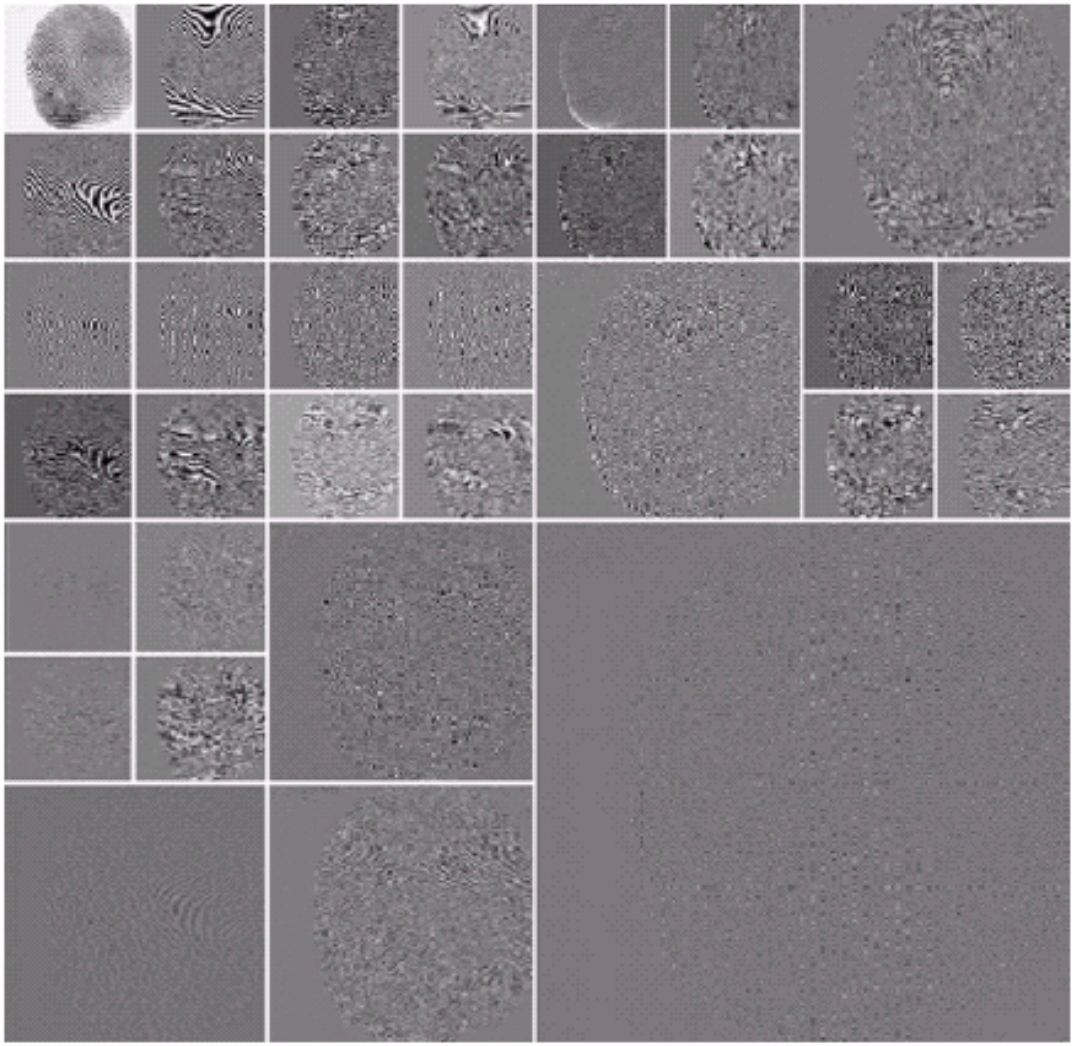

FIGURE 7.35 An optimal wavelet packet decomposition for the fingerprint of Fig. 7.34(a).

Image Compression

- Lossless compression
- Lossy compression

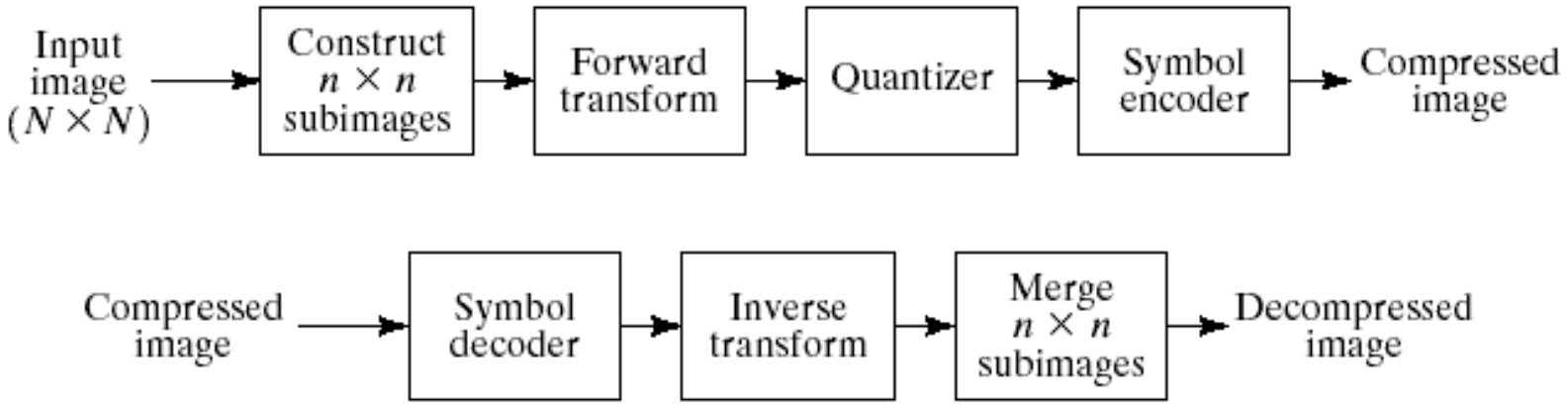

a
b

FIGURE 8.28 A transform coding system: (a) encoder; (b) decoder.

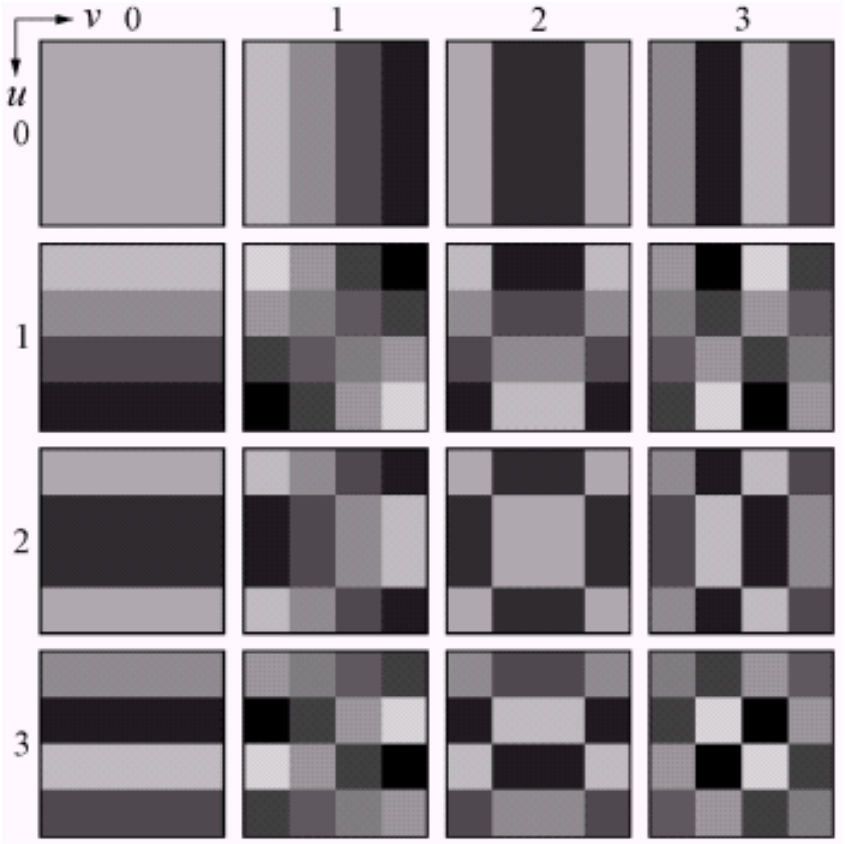

FIGURE 8.30 Discrete-cosine basis functions for $N = 4$. The origin of each block is at its top left.

a b
c d
e f

FIGURE 8.34 Approximations of Fig. 8.23 using 25% of the DCT coefficients: (a) and (b) 8×8 subimage results; (c) zoomed original; (d) 2×2 result; (e) 4×4 result; and (f) 8×8 result.

Wavelet coding

a
b

FIGURE 8.39 A wavelet coding system:
(a) encoder;
(b) decoder.

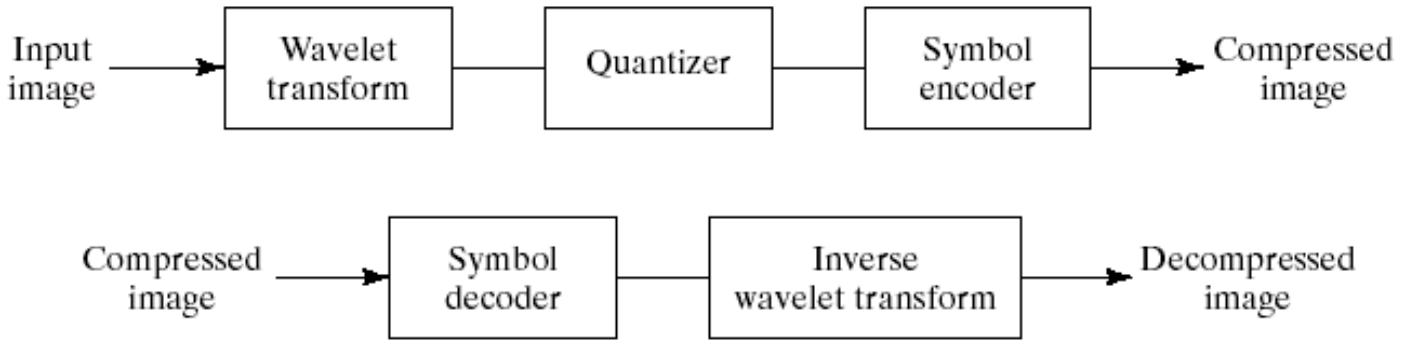

- ***Bilevel (binary) image compression standard***
  - CCITT Group 3 standard - facsimile (FAX) coding
  - CCITT Group 4 standard - facsimile (FAX) coding
  - JBIG - facsimile (FAX) coding

- ***Still-frame monochrome and color image compression***
  - JPEG - still-frame image compression (DCT)
  - JPEG 2000 – using Wavelet transform

- ***Sequential-frame monochrome and color compression***
  - H.261 - video teleconferencing
  - MPEG 1 - "entertainment quality" video compression (e.g., CD-ROM)
  - MPEG 2 - cable TV, narrow-channel satellite broadcasting

Morphological Image Processing

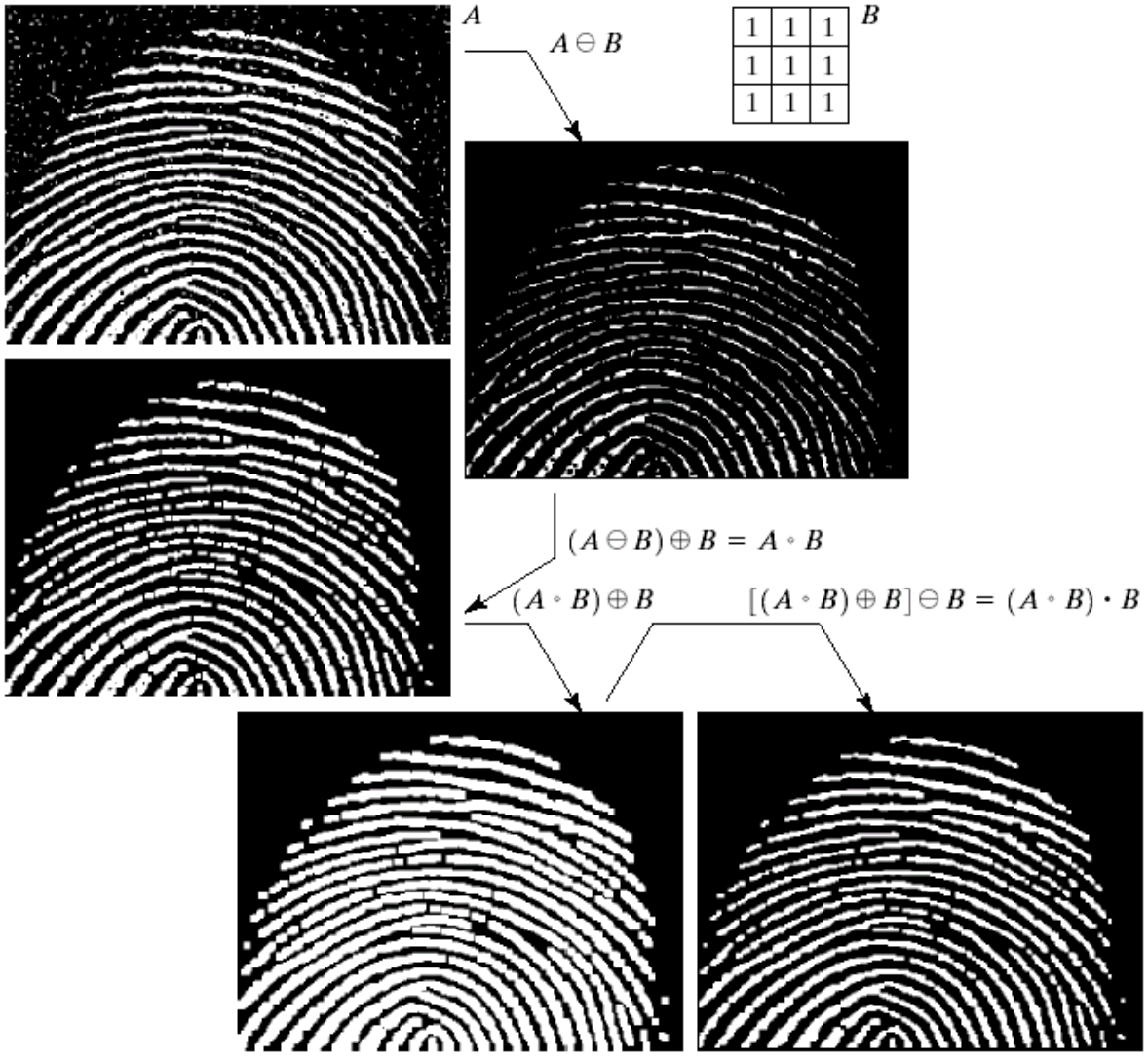

a b
d c
e f

FIGURE 9.11
(a) Noisy image.
(c) Eroded image.
(d) Opening of A.
(d) Dilation of the opening.
(e) Closing of the opening. (Original image for this example courtesy of the National Institute of Standards and Technology.)

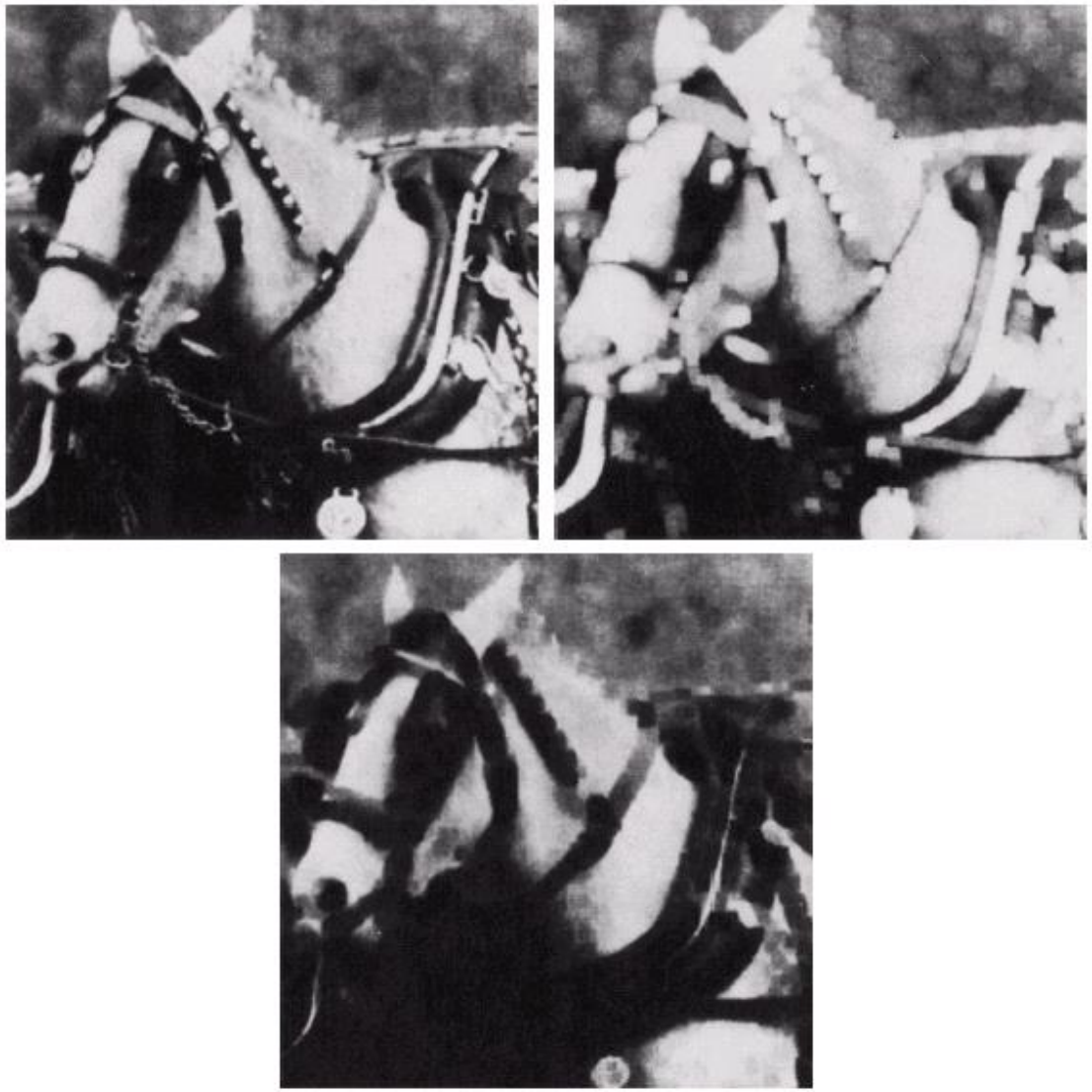

a b
c

FIGURE 9.29
(a) Original image. (b) Result of dilation. (c) Result of erosion. (Courtesy of Mr. A. Morris, Leica Cambridge, Ltd.)

Image Segmentation

- ***Edge Detection***

a
b c
d e
f g

FIGURE 10.8
A 3 × 3 region of an image (the z's are gray-level values) and various masks used to compute the gradient at point labeled z_5.

z_1	z_2	z_3
z_4	z_5	z_6
z_7	z_8	z_9

−1	0	0	−1
0	1	1	0

Roberts

−1	−1	−1	−1	0	1
0	0	0	−1	0	1
1	1	1	−1	0	1

Prewitt

−1	−2	−1	−1	0	1
0	0	0	−2	0	2
1	2	1	−1	0	1

Sobel

a b
c d

FIGURE 10.10
(a) Original image. (b) $|G_x|$, component of the gradient in the x-direction. (c) $|G_y|$, component in the y-direction. (d) Gradient image, $|G_x| + |G_y|$.

a b
c d
e f g

FIGURE 10.15 (a) Original image. (b) Sobel gradient (shown for comparison). (c) Spatial Gaussian smoothing function. (d) Laplacian mask. (e) LoG. (f) Thresholded LoG. (g) Zero crossings. (Original image courtesy of Dr. David R. Pickens, Department of Radiology and Radiological Sciences, Vanderbilt University Medical Center.)

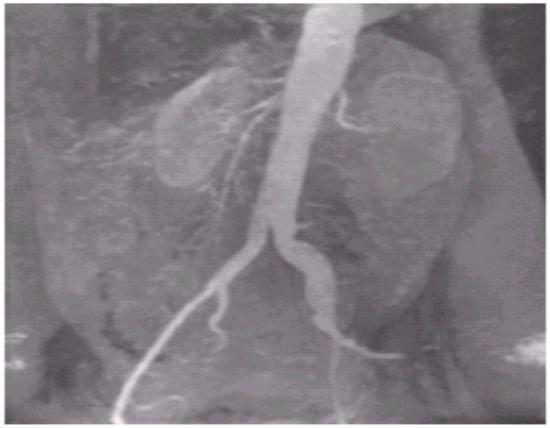

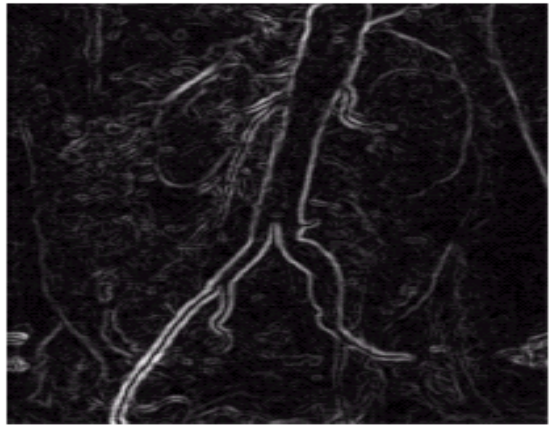

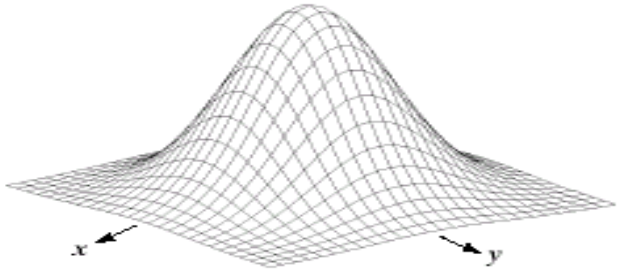

−1	−1	−1
−1	8	−1
−1	−1	−1

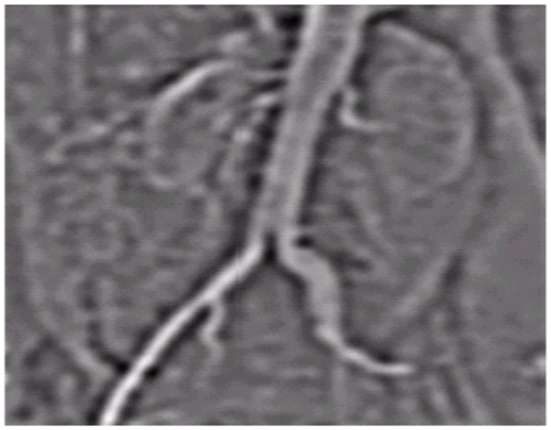

Thresholding

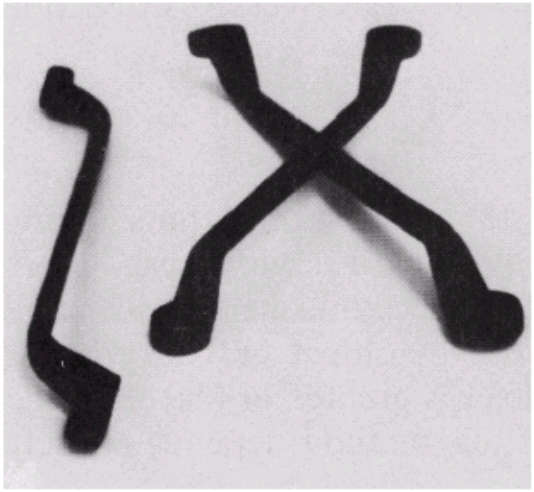

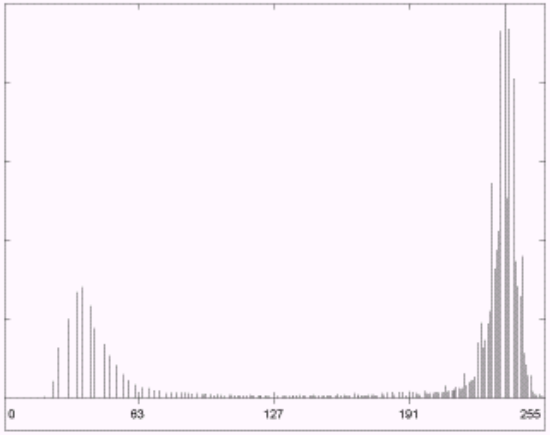

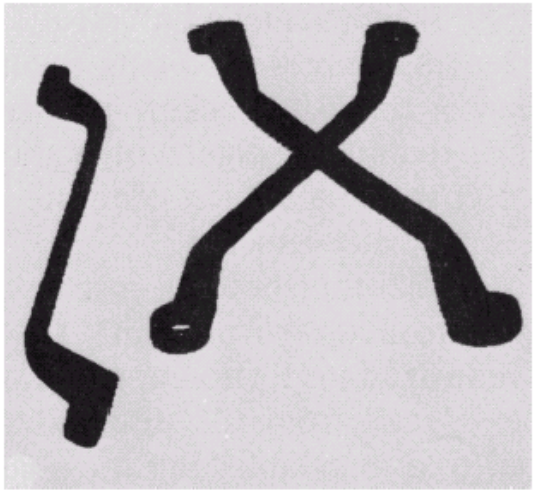

a
b c

FIGURE 10.28
(a) Original image. (b) Image histogram. (c) Result of global thresholding with T midway between the maximum and minimum gray levels.

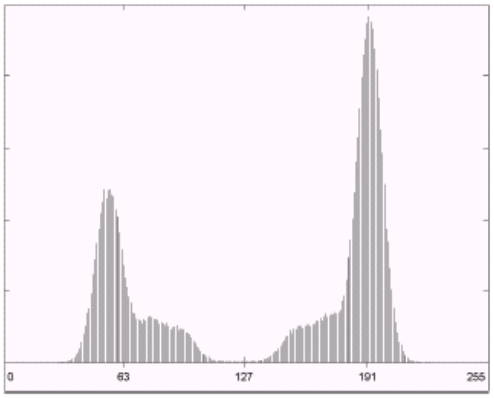

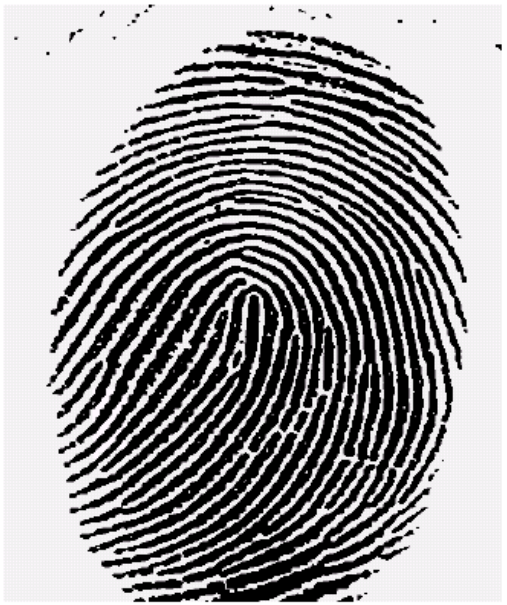

a b
c

FIGURE 10.29
(a) Original image. (b) Image histogram. (c) Result of segmentation with the threshold estimated by iteration. (Original courtesy of the National Institute of Standards and Technology.)

a b

FIGURE 10.33 A cardioangiogram before and after preprocessing. (Chow and Kaneko.)

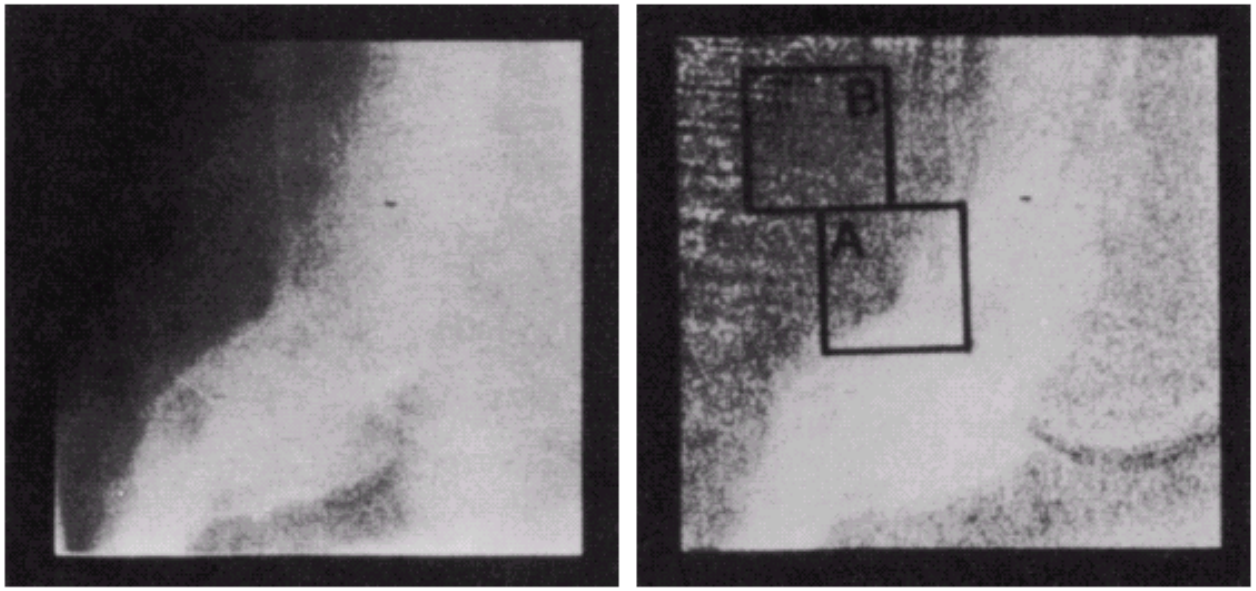

Region Growing

a b
c d

FIGURE 10.40
(a) Image showing defective welds. (b) Seed points. (c) Result of region growing. (d) Boundaries of segmented defective welds (in black). (Original image courtesy of X-TEK Systems, Ltd.).

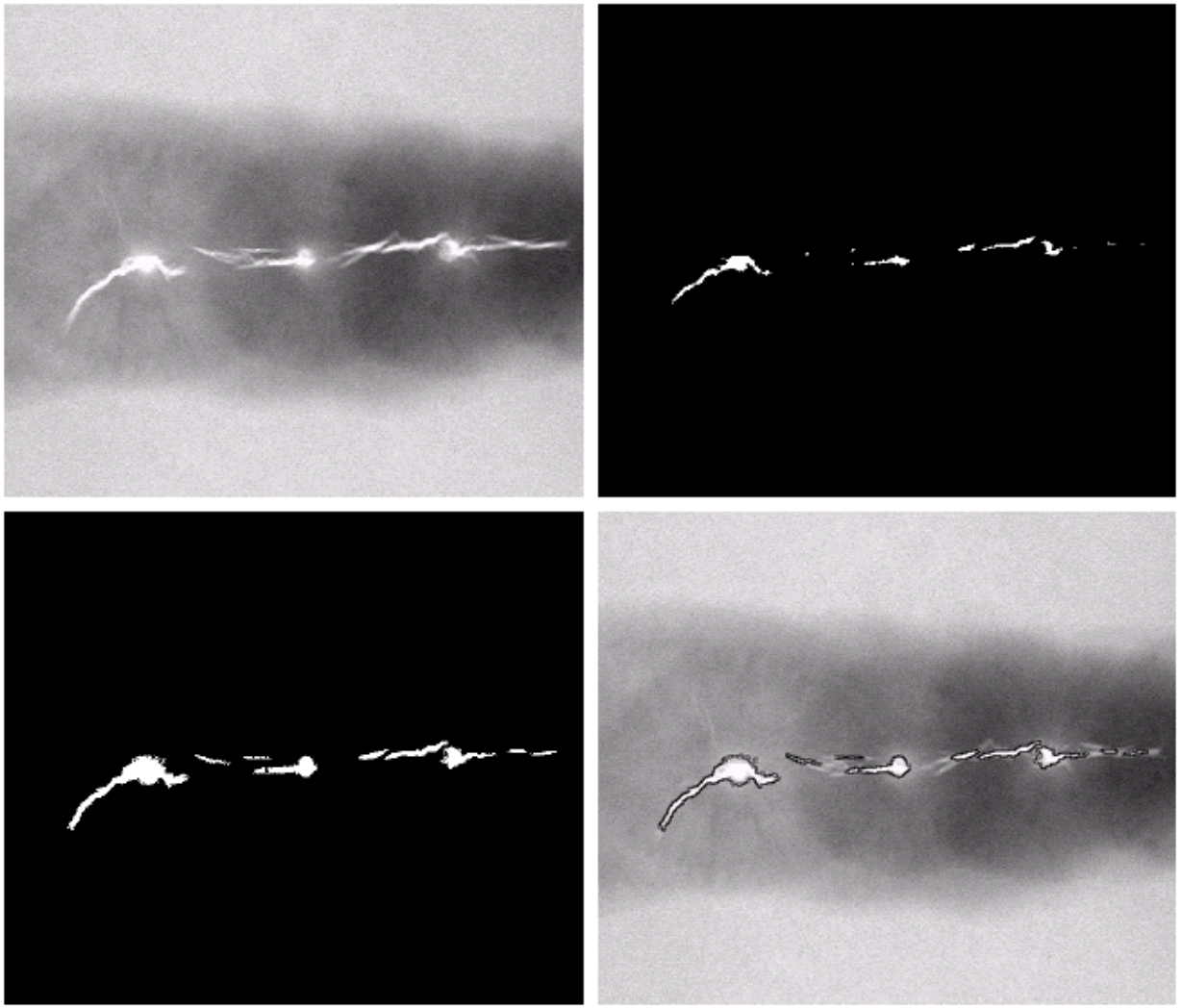

Region Splitting and Merging

a b c

FIGURE 10.43
(a) Original image. (b) Result of split and merge procedure. (c) Result of thresholding (a).

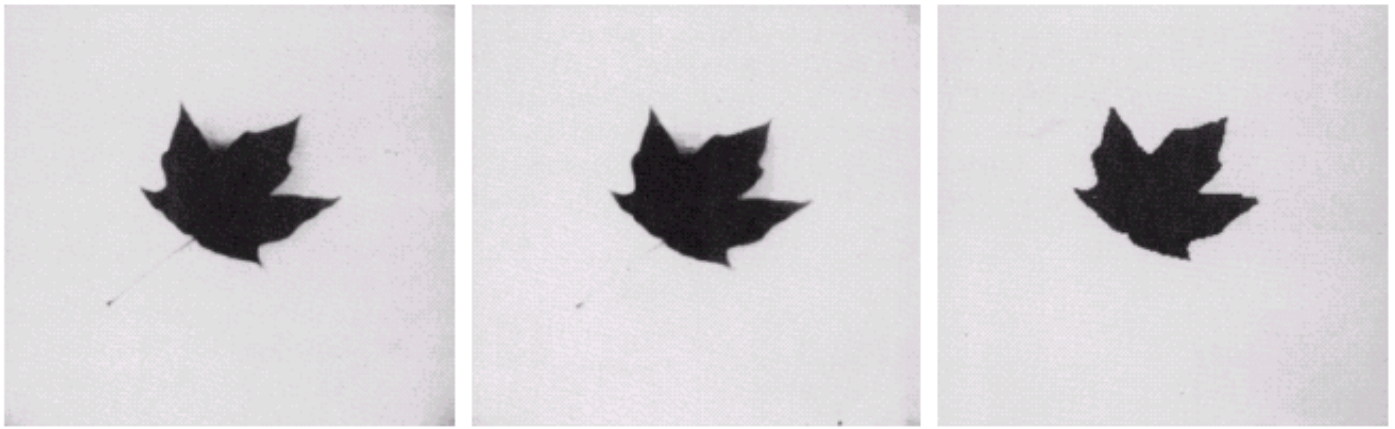

Watersheds

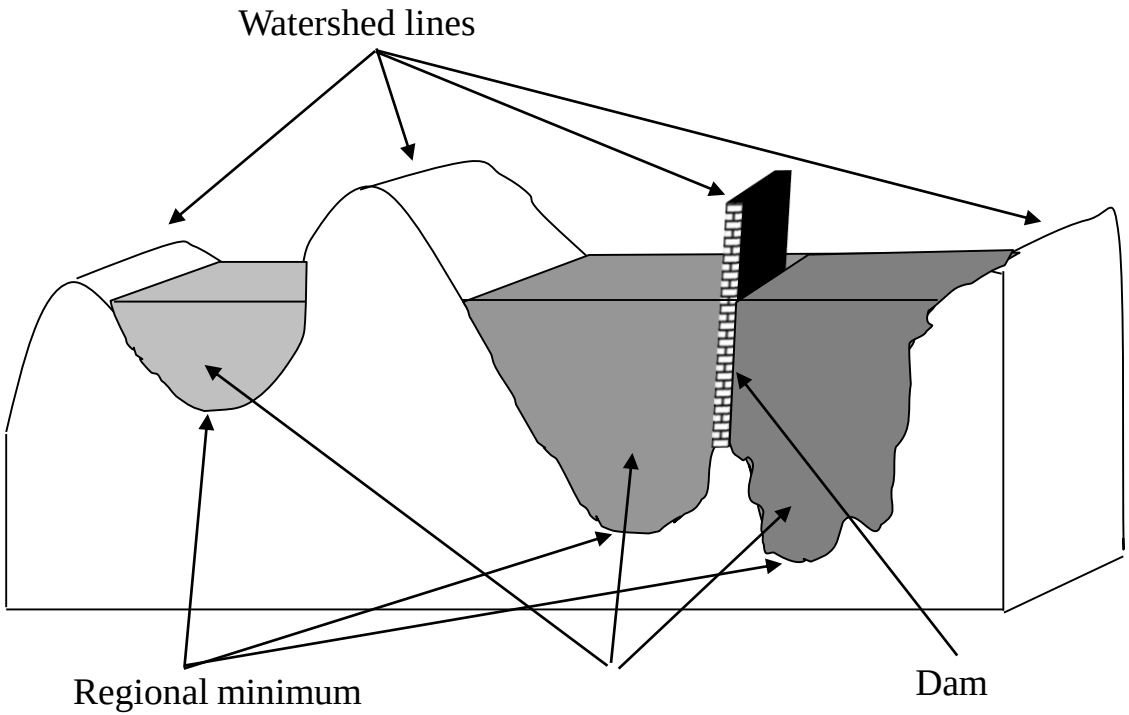

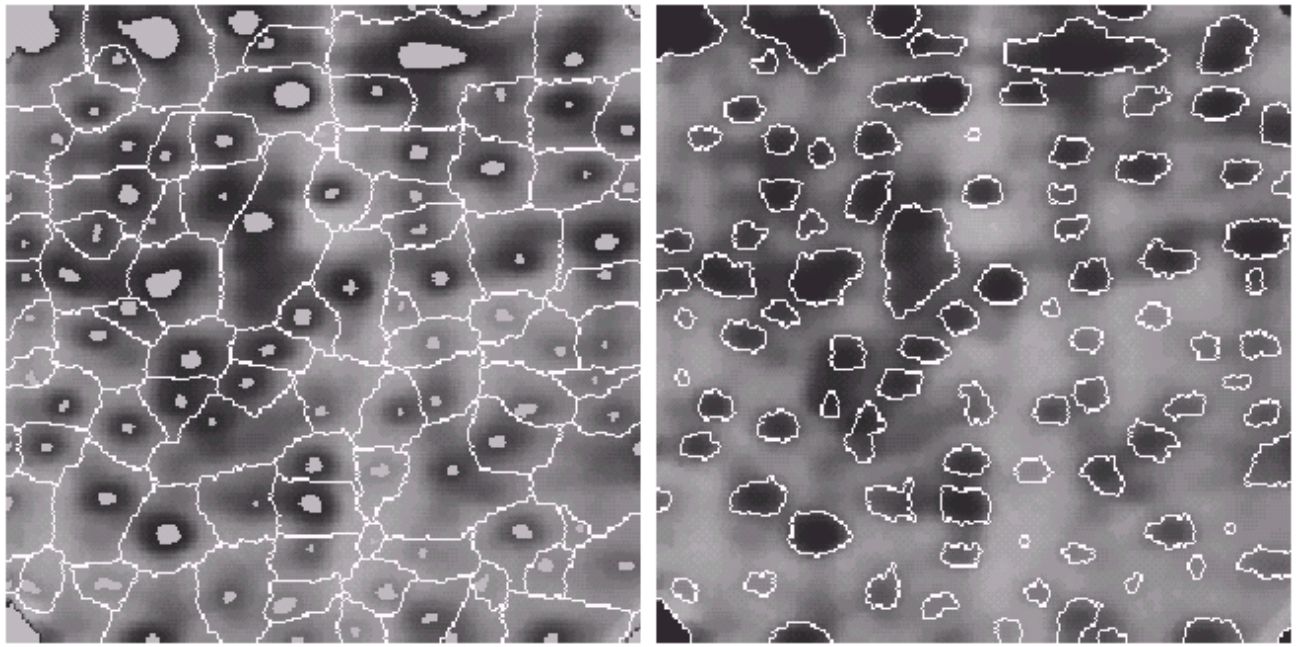

a b

FIGURE 10.48
(a) Image showing internal markers (light gray regions) and external markers (watershed lines). (b) Result of segmentation. Note the improvement over Fig. 10.47(b). (Courtesy of Dr. S. Beucher, CMM/Ecole des Mines de Paris.)

Watersheds Parameters (1)

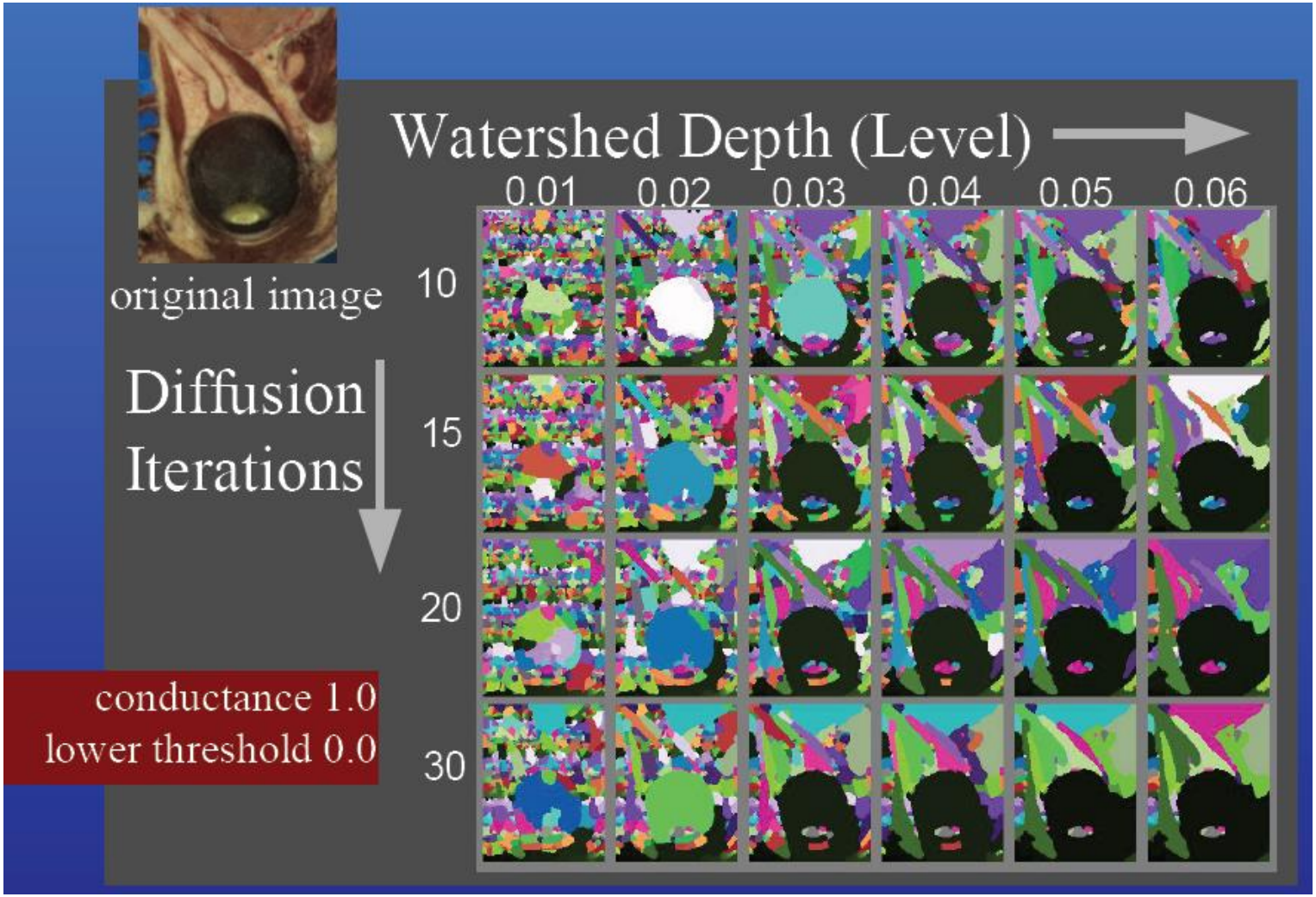

Watersheds Parameters (2)

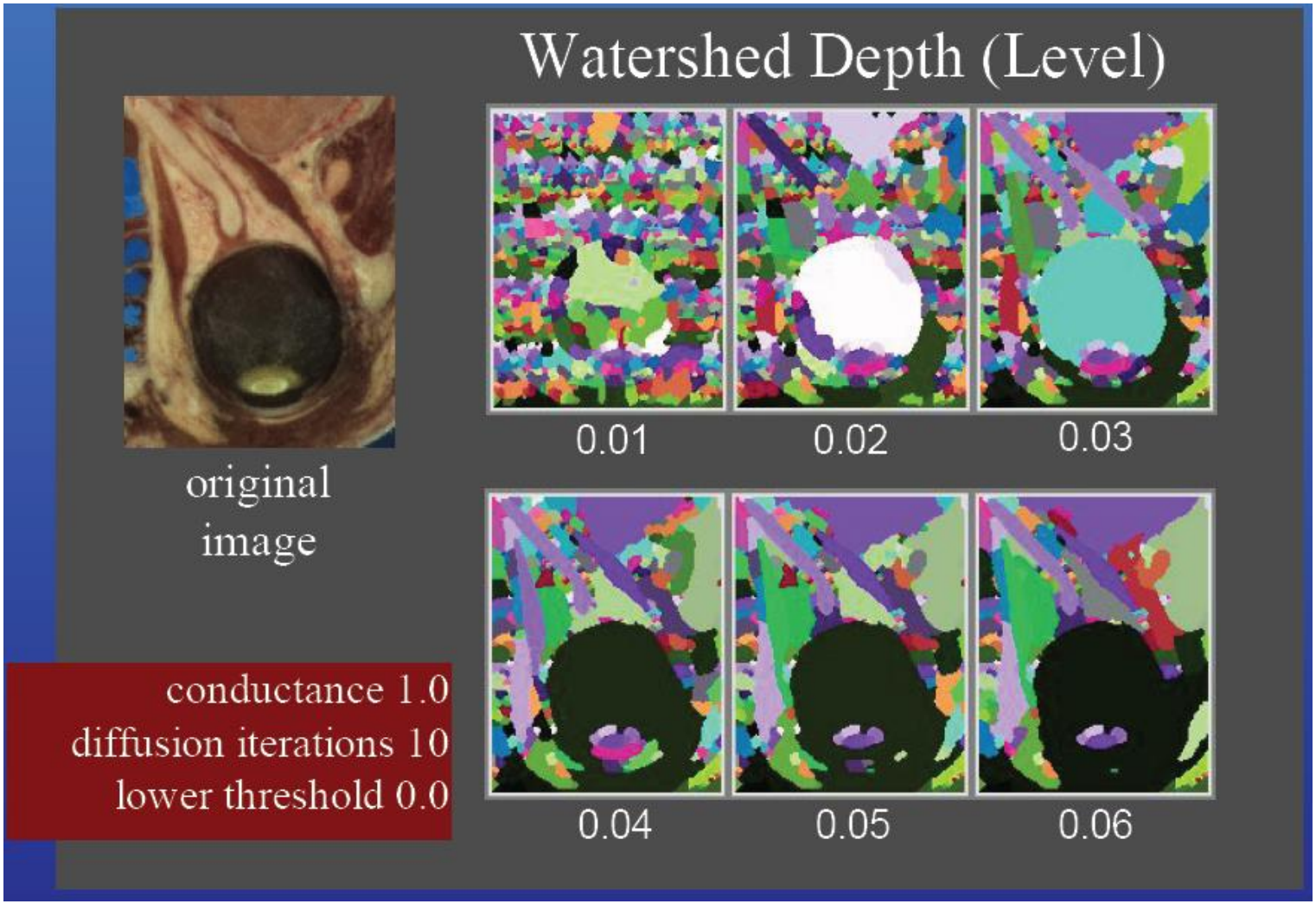

Watersheds Parameters (3)

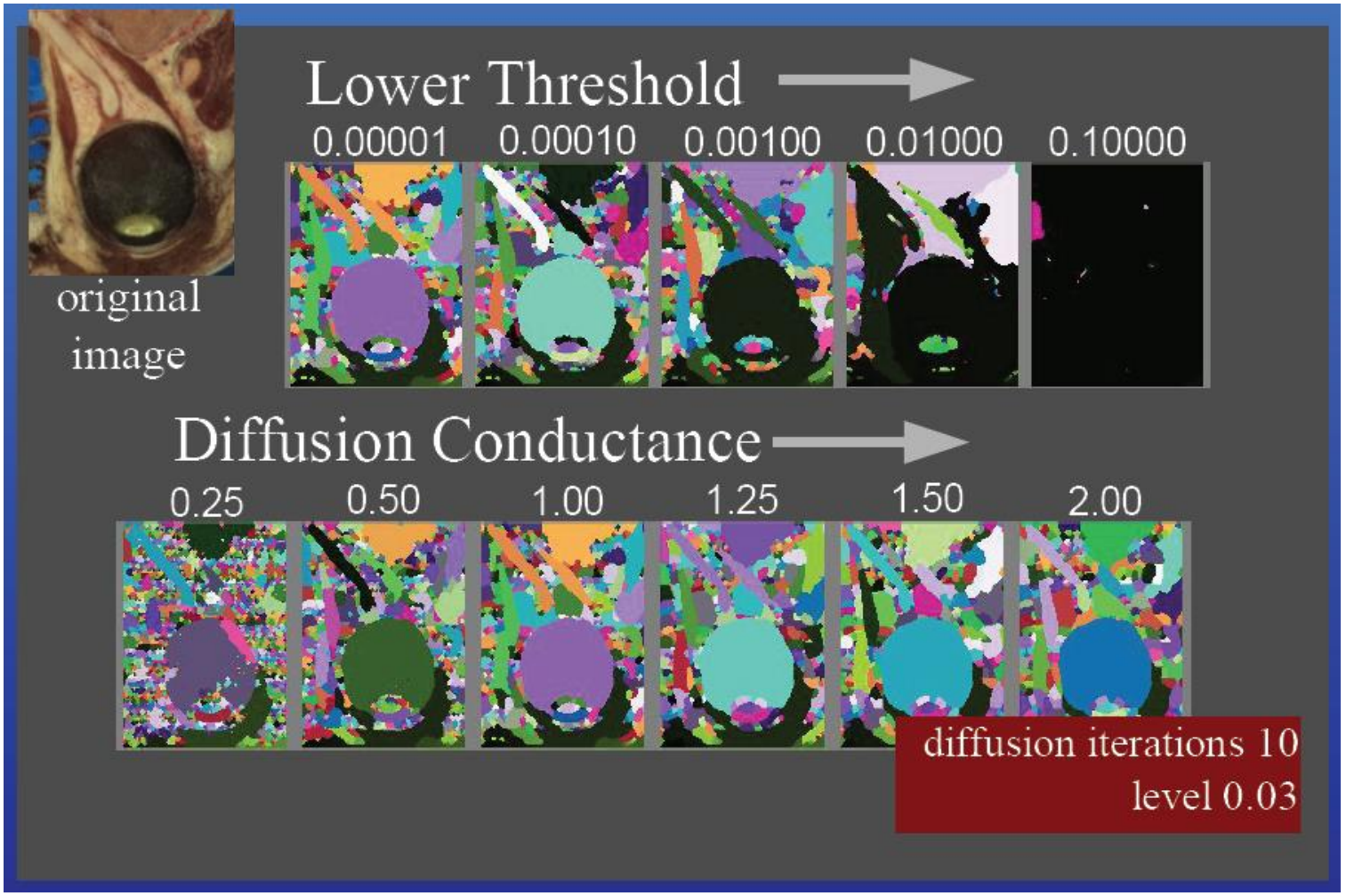

Multiscale 3D Segmentation

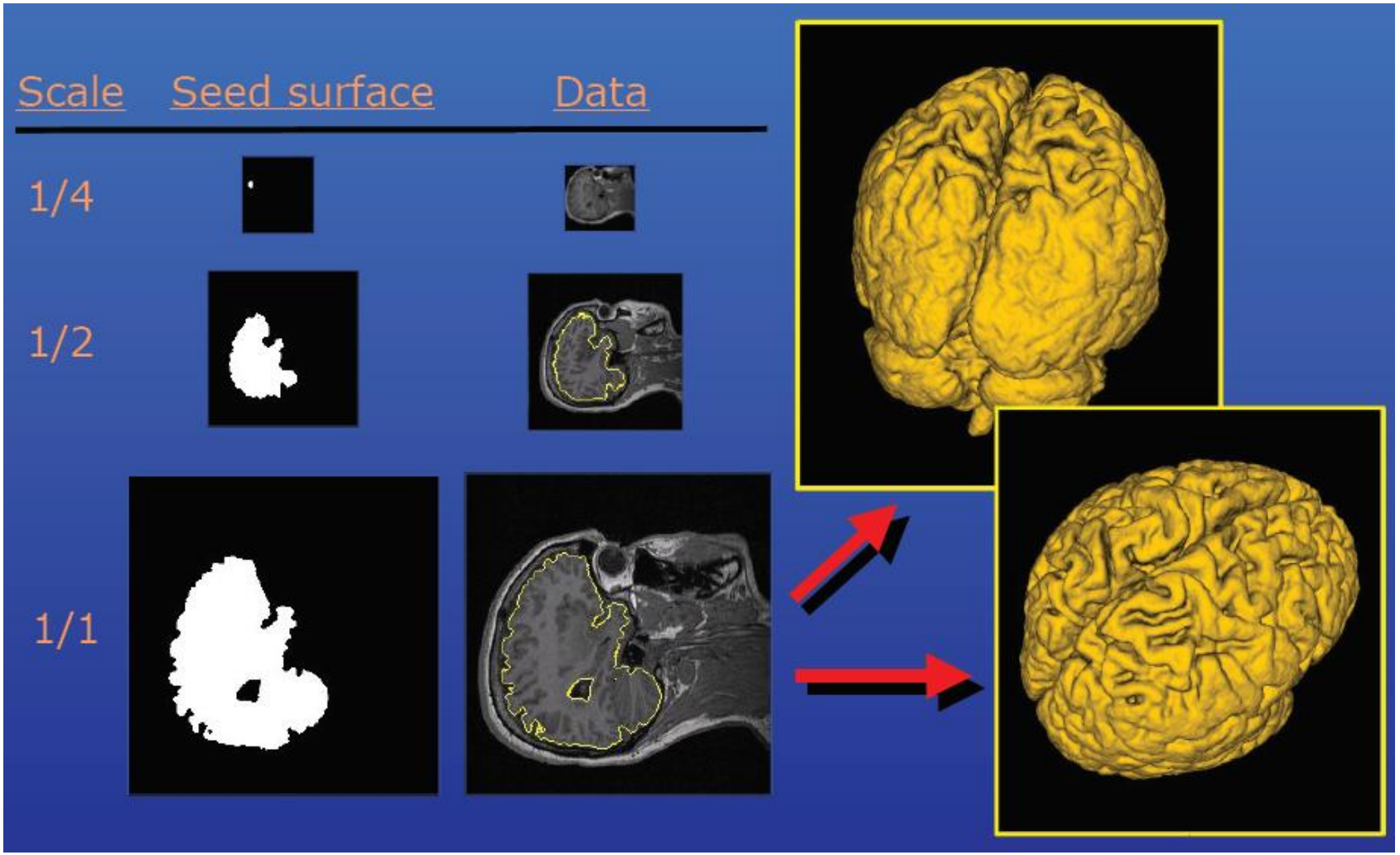

Surface Rendering

- Surface rendering (right) of four anatomical structures in the Visible Female head and neck

Surface Processing

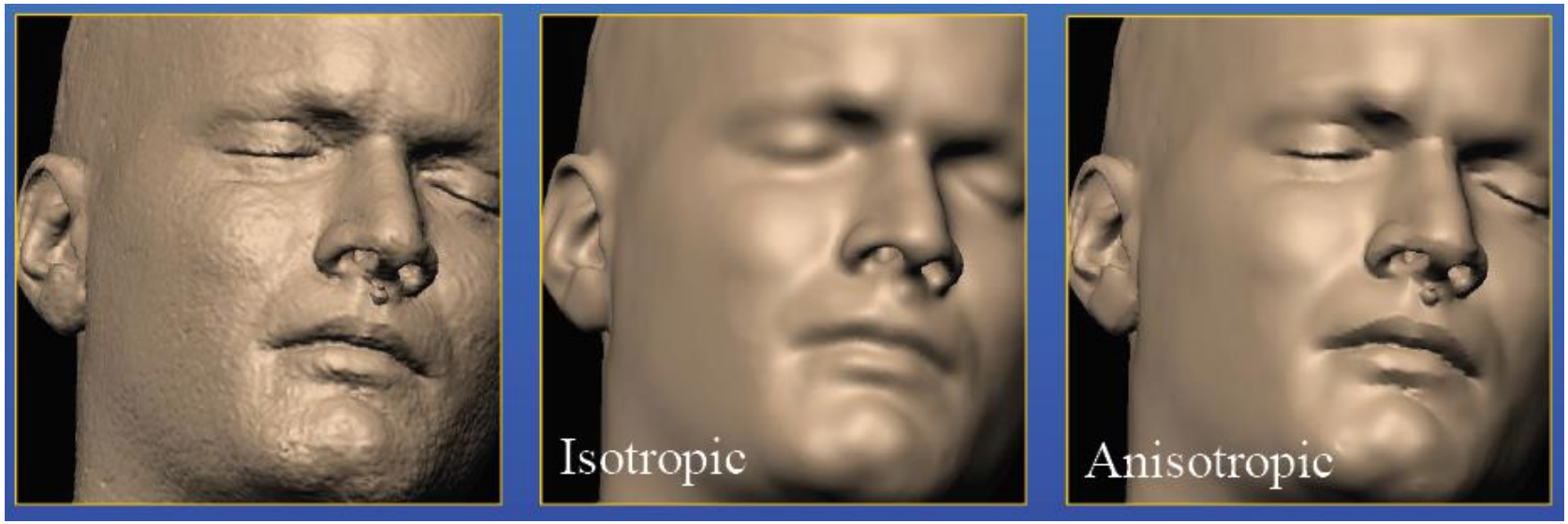

Registration

- 3D CT to MR-T1 Rigid Registration

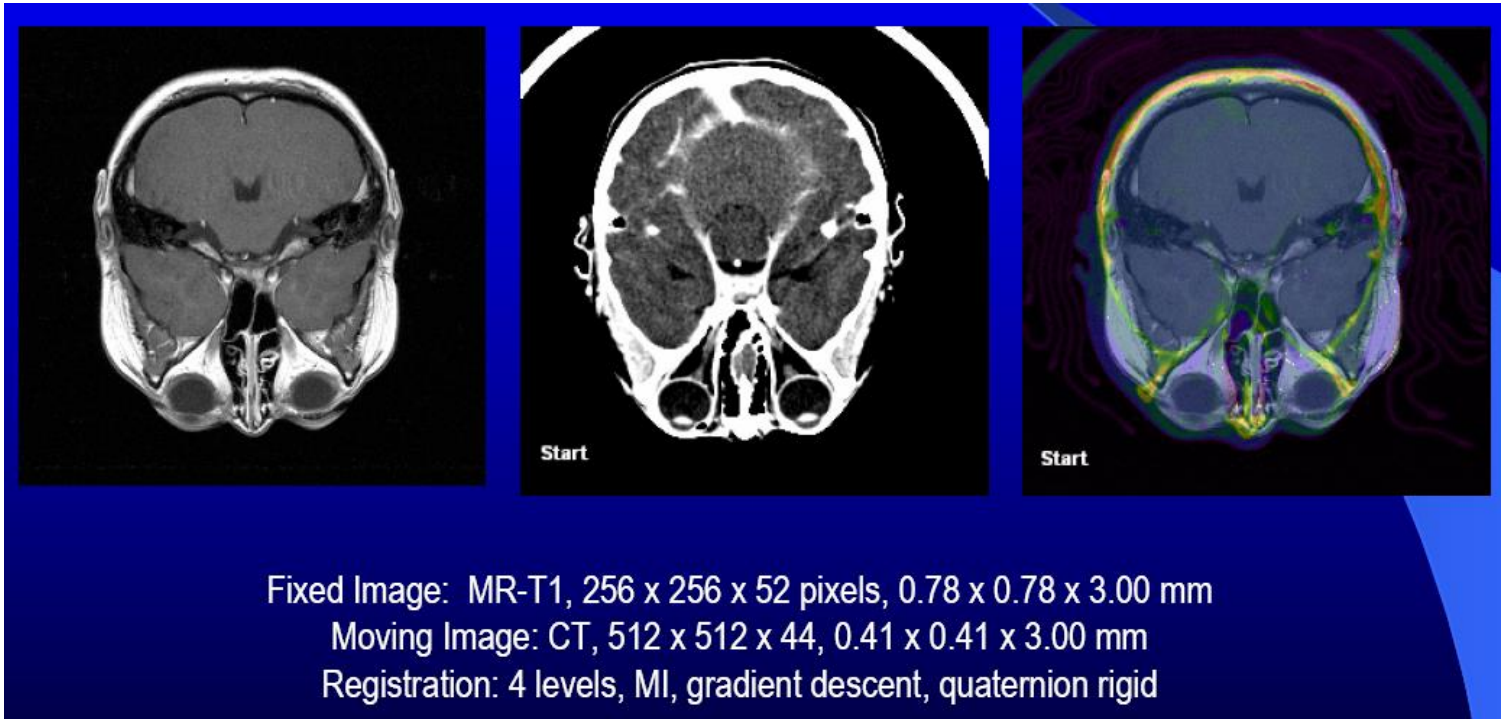

- 3D PET to MR-T2 Rigid Registration

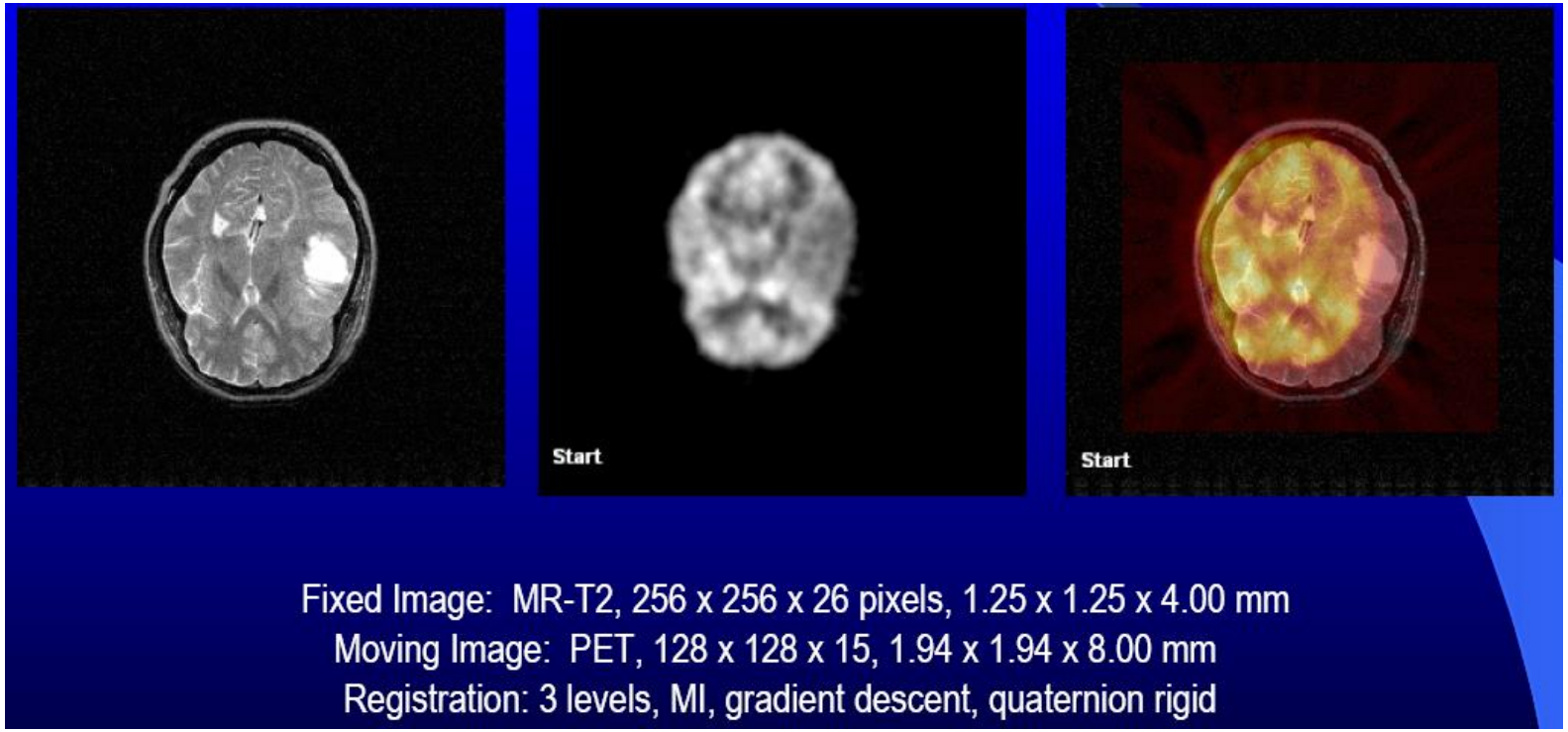

Non-rigid Registration

- 3D Inter-subject MR subject MR-PD Deformable Registration Deformable Registration

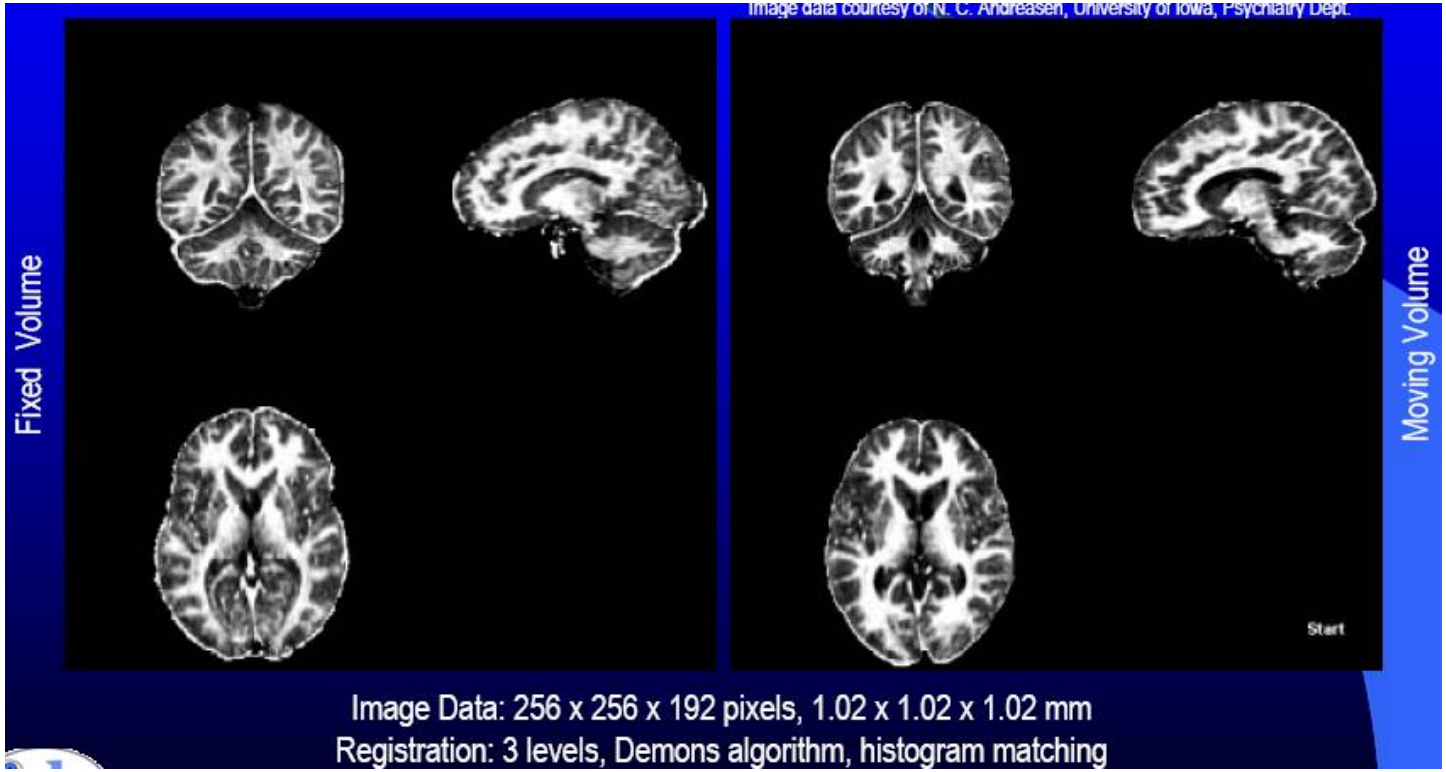

Representation and Description

- **Boundary Descriptor**
- **Regional Descriptor**
- **Texture**
  - Smoothness, coarseness, and regularity

Texture- Smooth, Coarseness, and regular

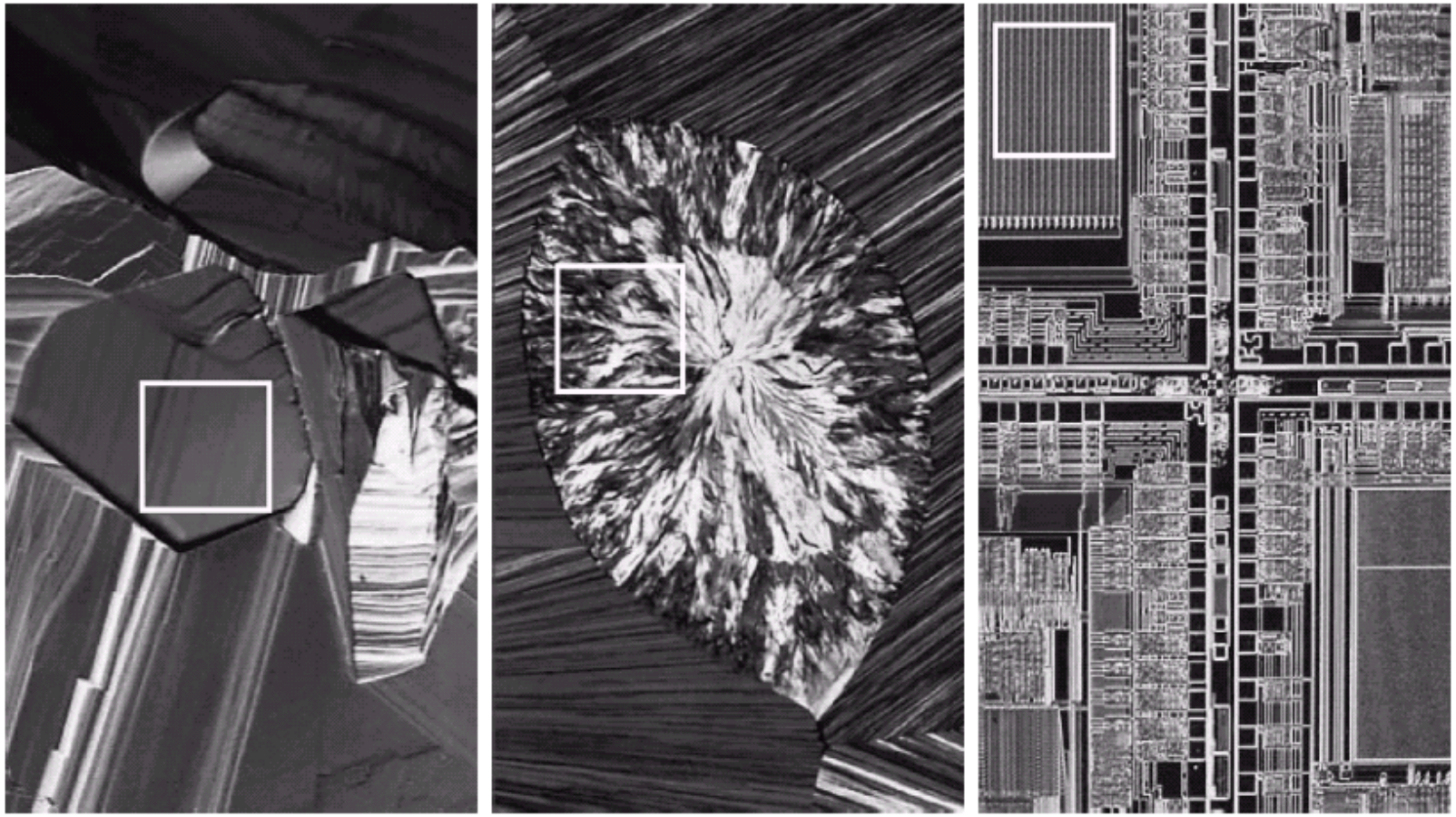

a b c

FIGURE 11.22 The white squares mark, from left to right, smooth, coarse, and regular textures. These are optical microscope images of a superconductor, human cholesterol, and a microprocessor. (Courtesy of Dr. Michael W. Davidson, Florida State University.)

Classification

FIGURE 12.1
Three types of iris flowers described by two measurements.

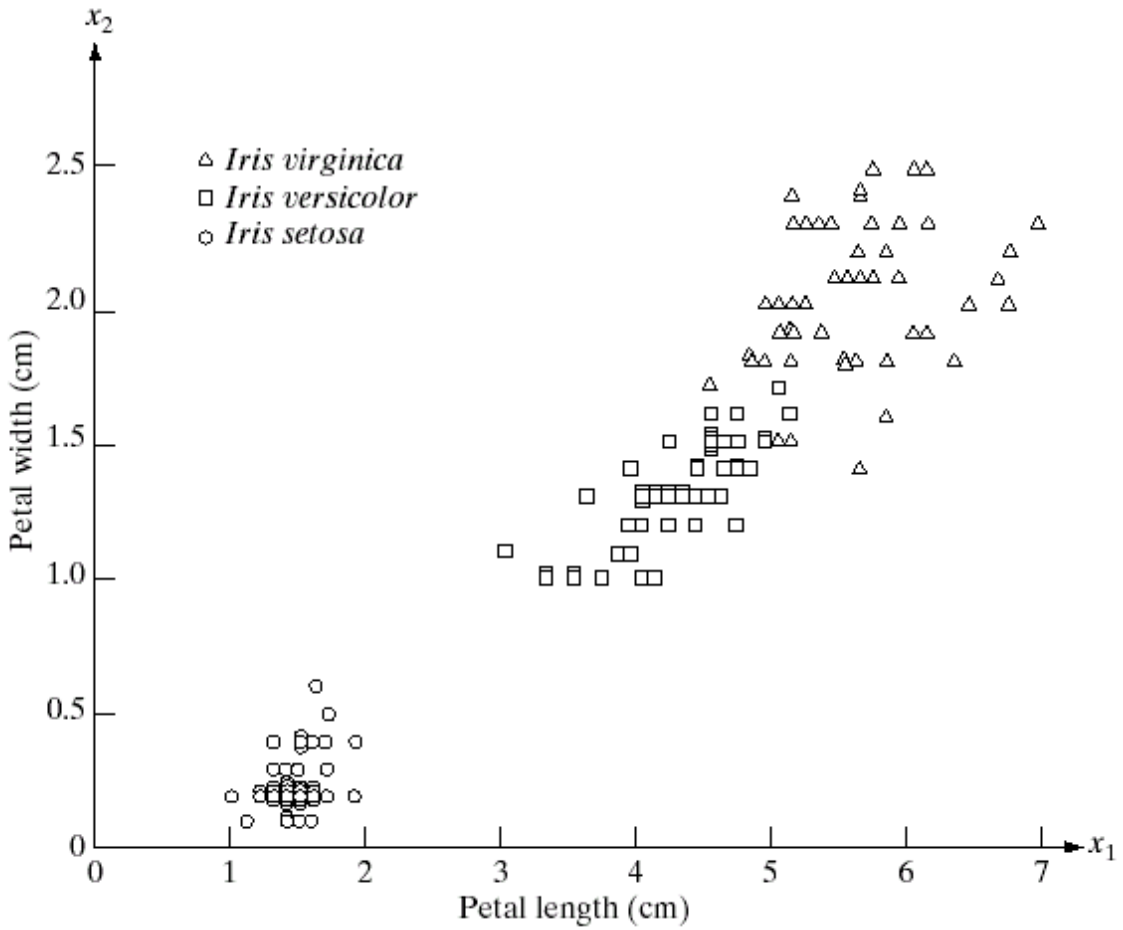

Neural Networks

a
b

FIGURE 12.14
Two equivalent representations of the perceptron model for two pattern classes.

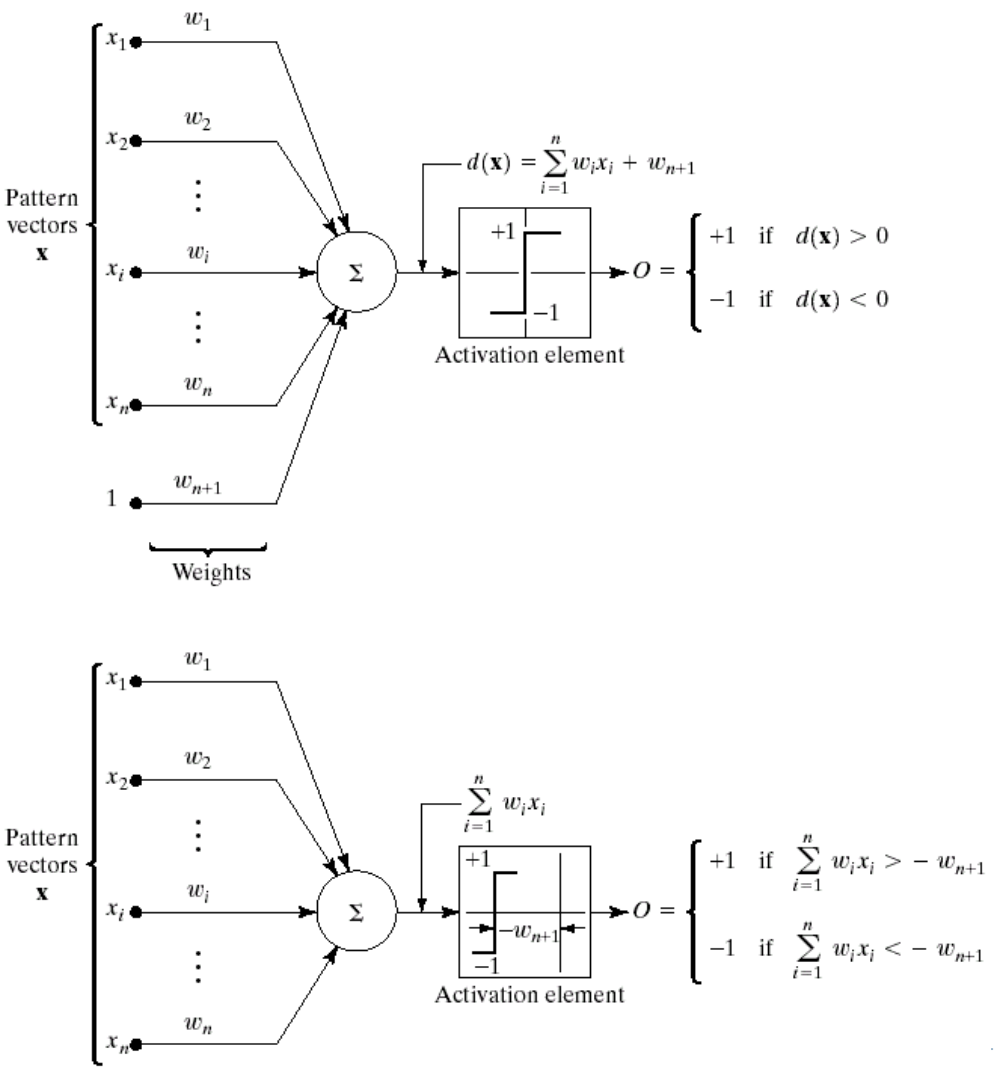

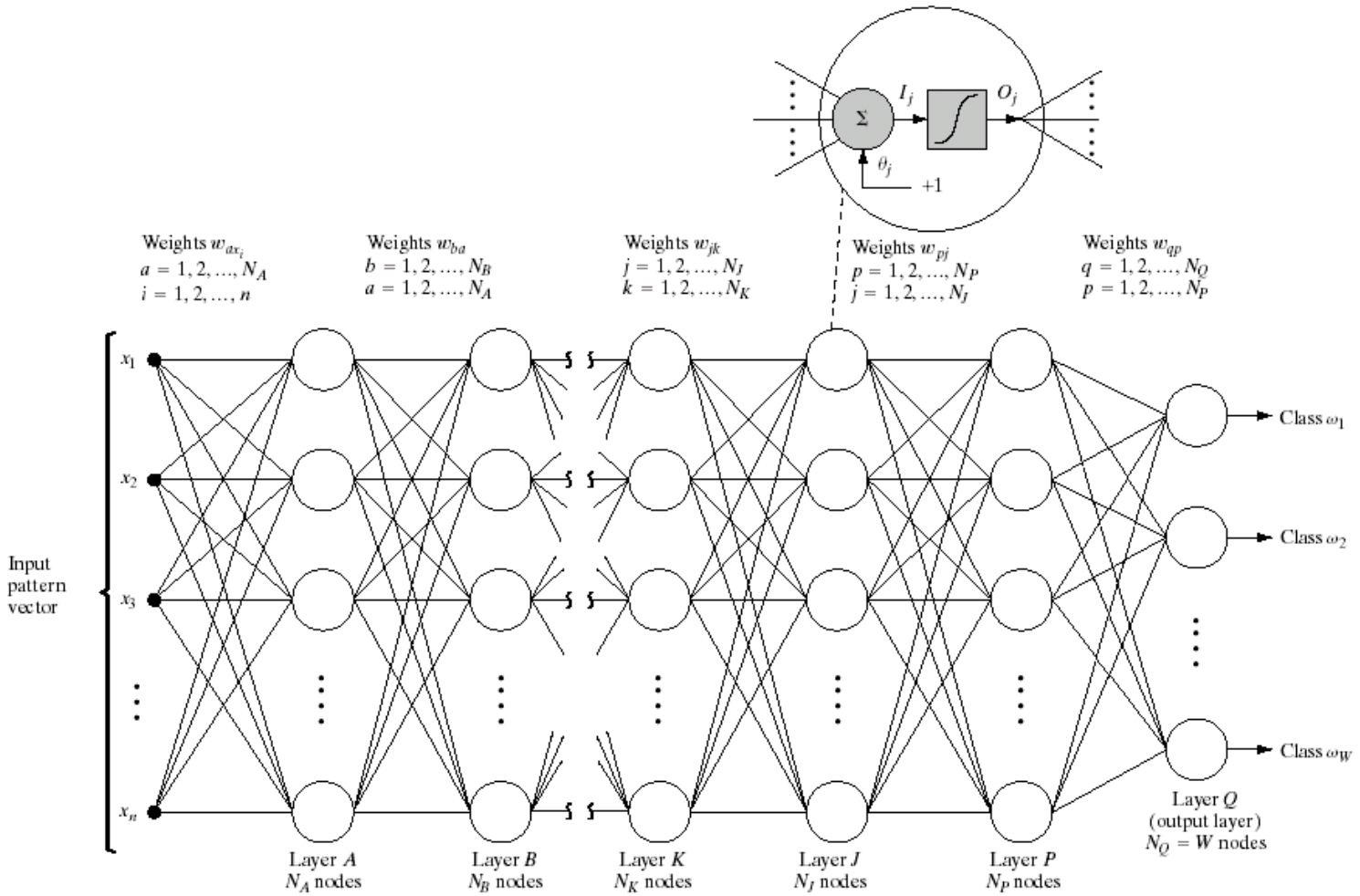

FIGURE 12.16 Multilayer feedforward neural network model. The blowup shows the basic structure of each neuron element throughout the network. The offset, θ_j, is treated as just another weight.

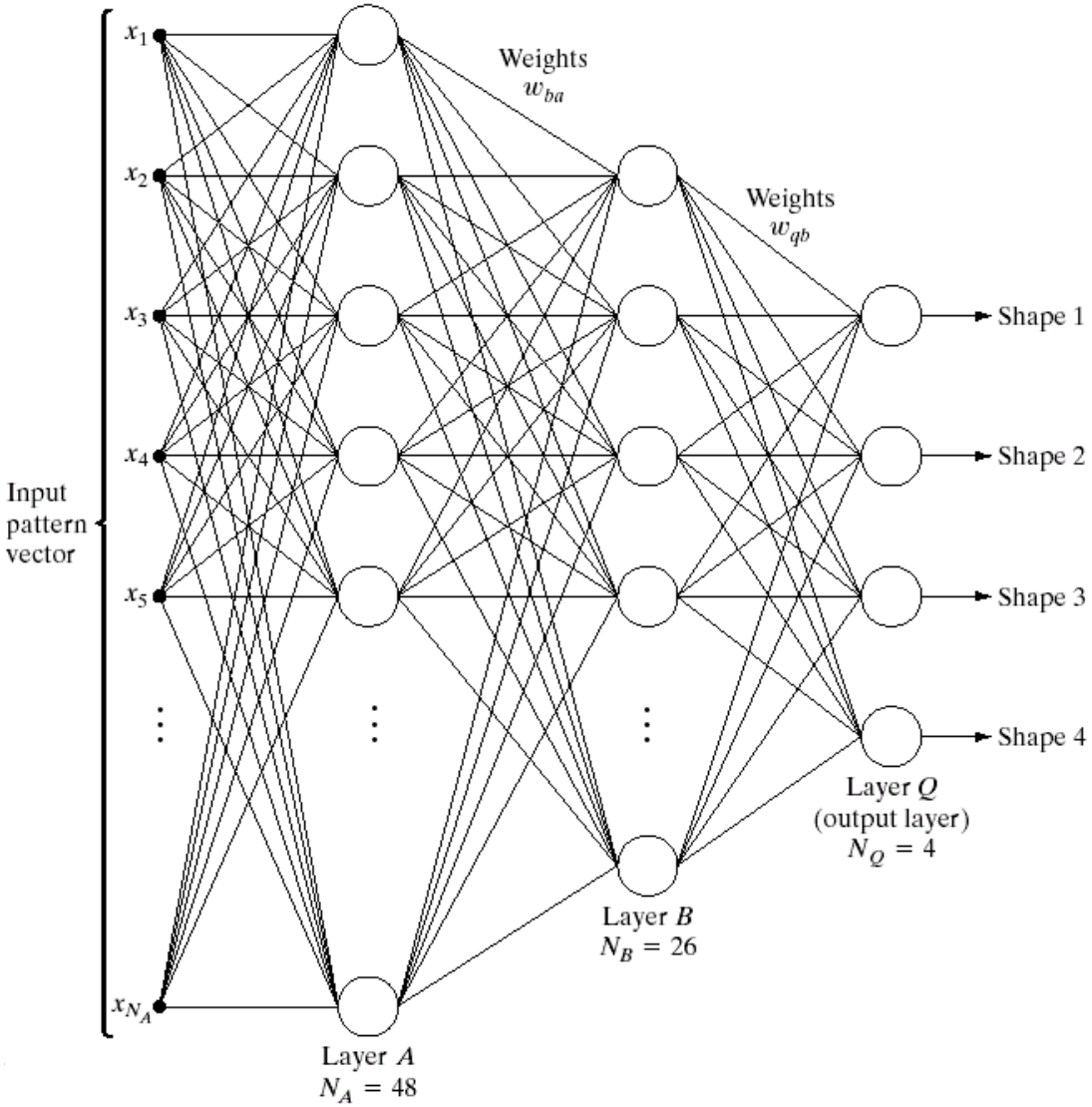

FIGURE 12.19 Three-layer neural network used to recognize the shapes in Fig. 12.18. (Courtesy of Dr. Lalit Gupta, ECE Department, Southern Illinois University.)